

Die approbierte Originalversion dieser Dissertation ist an der Hauptbibliothek der Technischen Universität Wien aufgestellt (<http://www.ub.tuwien.ac.at>).

The approved original version of this thesis is available at the main library of the Vienna University of Technology (<http://www.ub.tuwien.ac.at/englweb/>).

DISSERTATION

**Error Performance
of
Multiple Antenna Systems**

ausgeführt zum Zwecke der Erlangung des akademischen Grades
eines Doktors der technischen Wissenschaften

eingereicht an der Technischen Universität Wien
Fakultät für Elektrotechnik und Informationstechnik

von

Dipl.-Ing. Gerhard Gritsch

Matrikelnummer 9625536

2033 Kammersdorf 49

Wien, im August 2004

unter der Leitung von

Univ. Prof. Dr. Johann Weinrichter

Institut für Nachrichten- und Hochfrequenztechnik
Technischen Universität Wien
Fakultät für Elektrotechnik und Informationstechnik

Univ. Prof. Dr. Ernst Bonek

Institut für Nachrichten- und Hochfrequenztechnik
Technischen Universität Wien
Fakultät für Elektrotechnik und Informationstechnik

Danksagung

Ich möchte allen Personen danken, die mir während meiner Arbeit am Institut und bei meiner Doktorarbeit geholfen haben.

Besonders hervorheben möchte ich Herrn Prof. Weinrichter, der mir jederzeit mit Rat und Tat zur Seite stand.

Weiters bin ich Herrn Prof. Bonek sehr dankbar, weil er mir meine Dissertationsarbeit ermöglicht hat.

Für die äußerst aufschlußreichen wissenschaftlichen Diskussion mit Herrn Prof. Rupp bin ich ebenfalls sehr dankbar.

Ebenfalls bin ich meinem Zimmerkollegen Markus Herdin und meiner Kollegin Biljana Badic zu Dank verpflichtet. Ihre hilfreichen Kommentare und Lösungsvorschläge haben mir sehr geholfen.

Für die Unterstützung privater Natur möchte ich mich bei meiner Familie bedanken, wobei dabei meiner Freundin Daniela besonderer Dank für ihre Geduld gebührt.

Zusammenfassung

In der vorliegenden Arbeit wird das **Bitfehlerverhalten von Mehrantennensystemen** untersucht, wobei der Schwerpunkt der Arbeit auf der **Berechnung von Bitfehlerabschätzungen** liegt. Leider sind die untersuchten Funk-Systeme so komplex, daß geschlossene Ausdrücke für die exakte Bitfehlerrate nicht existieren.

Die Arbeit umfaßt zwei Themenschwerpunkte: **Uncodierte** und **Raum-Zeit codierte Daten-Übertragung** über **räumlich korrelierte, echo-freie Funkkanäle** unter der Verwendung von **optimalen Empfängern**. Die räumliche Korrelation wird mit dem so genannten W-Modell eingebracht, wobei Funkkanal-Meßdaten zur Bestimmung der Modell-Parameter verwendet werden.

Uncodierte Übertragungssysteme: Bereits für die einfacheren, uncodierten Übertragungssysteme ist eine **obere Bitfehler-Schranke** die einzige einfache Möglichkeit, die Bitfehlerrate abzuschätzen. Diese obere Schranke ist einfach die Summe über alle paarweisen Fehlerwahrscheinlichkeiten. Dabei stellt sich heraus, daß das Bitfehlerverhalten mittels einer geringen Anzahl von **Fehlertypen** vollständig beschrieben werden kann. Die abgeleitete obere Schranke wird für verschiedene uncodierte Systeme mit Simulationsergebnissen verglichen. Es zeigt sich, daß die obere Schranke unterhalb einer Bitfehlerwahrscheinlichkeit von zirka 10^{-3} die Simulationsergebnisse sehr genau wiedergibt.

Um die **Diversitätsordnung** und den **Performance-Verlust**, verursacht durch **räumliche Korrelation**, beziffern zu können, wird die obere Schranke für hohes Signal-Rauschleistungs-Verhältnis abgeschätzt. Damit wird eine extrem einfache Beurteilung des Fehlerverhaltens durch Angabe der Steigung und der horizontalen Lage der Bitfehlerratenkurven möglich.

In weiterer Folge wird das **optimale Vorcodierungsfilter** für **minimalen Performance-Verlust** hergeleitet, mit dem der Einfluß der räumlich Korrelation kompensiert werden kann. Das Verhalten des vorcodierten Systems in korrelierten Kanälen kommt dem Systemverhalten ohne Vorcodierung in unkorrelierten Kanälen sehr nahe.

Raum-Zeit codierte Übertragungssysteme: Den zweiten Schwerpunkt bilden Raum-Zeit codierte Übertragungssysteme, wobei in groben Zügen die selben Themenschwerpunkte wie für uncodierte Systeme diskutiert werden. Auch für solche Systeme wird ein **obere Schranke** für die Bitfehlerwahrscheinlichkeit berechnet, die für alle untersuchten Codes und alle Korrelationstypen relativ gut dem simulierten Bitfehlerverhalten entspricht. Mit Hilfe der Signaldistanzen und der oberen Bitfehler-Schranke zeigt sich, daß es Raum-Zeit Block Codes gibt, bei denen das **Fehlerverhalten von Mehrfachsymbolfehlern dominiert wird (MIMO Paradoxon)**. Diese Verhalten steht im diametralen Gegensatz zu den Verhältnissen bei der Datenübertragung in Systemen mit einzelnen Antennen beim Sender und beim Empfänger.

Mittels der Bitfehler-Abschätzung bei hohem Signal-Rauschleistungs-Verhältnis wird die **Diversitätsordnung** und der **Leistungsverlust** infolge räumlicher Korrelation der Antennenfelder quantitativ abgeschätzt.

Ebenso wie für die uncodierten Systeme, wird auch hier ein **optimales Vorcodierungsfilter** hergeleitet, welches die Auswirkungen der räumlichen Korrelation lindert.

Zusätzlich wird eine **untere Schranke** für die Bitfehlerwahrscheinlichkeit hergeleitet, die für alle untersuchten Codes gilt und in unkorrelierten Kanälen fast exakt mit den Simulationsergebnissen übereinstimmt. Im allgemeinen kann damit eine Eingrenzung der Bitfehlerrate von unten und oben her erzielt werden.

Abstract

In this thesis the **error performance of multiple antenna systems** has been investigated. Our focus lies on the **analytical calculation of performance measures**. Unfortunately, due to the difficult framework and the rather unpredictable behavior of the signal distances in randomly varying channels a closed form solution of the exact error performance could not be derived. However, tight performance bounds have been found that can be used to get important performance parameters.

This thesis consists of two main parts concerning the **uncoded** and the **space-time block coded data transmission** over **spatially correlated, frequency flat Multiple Input / Multiple Output (MIMO) channels** using **Maximum Likelihood receivers**. The spatial correlation is modelled by the so-called W-model, where measured data are used to determine the model parameters.

Uncoded MIMO-systems: Even for uncoded systems, the only simple to calculate performance measure is a **union bound**, which is simply the sum over all pairwise error probabilities. In this thesis it is shown that the error performance can be described by a few so called **Error Types (ETs)**. The results of the corresponding union bound are compared with simulation results for different system parameters, i.e., number of transmit antennas, number of receive antennas, modulation formats, and for spatially uncorrelated and correlated MIMO-channels. The derived union bound is tight for Bit Error Ratio (BER) values below 10^{-3} for all systems investigated.

By means of this bound a **high Signal to Noise Ratio (SNR) approximation** for the BER vs. SNR performance is calculated. With this approximation the **diversity order** of the system and a so-called **performance loss** due to fading correlation can be figured out. Especially, the loss due to spatial correlation can be quantified. Using two parameters, the slope and the horizontal position of the BER vs. SNR curves, the error performance can be fully described in the high SNR range.

An **optimal precoder**, which **minimizes the correlation induced power loss**, is presented. For the example discussed in this thesis the error performance applying the optimal precoder in correlated fading is even better than the performance of the standard system in the low SNR range in uncorrelated fading channels.

Space-time block coded MIMO-systems: The second main part of this thesis is devoted to the calculation of performance measures for space-time block coded data transmission. In principle, we follow the same analysis as for uncoded systems. First, it is shown that for some channel types **multiple** instead of single **errors dominate the error performance in MIMO systems (MIMO paradoxon)**. In deriving the **union bound** the ET concept is applied also. The calculated union bounds are compared with simulation results for several codes and several channel correlation types. It turns out that the union bound is tight for BER values of 10^{-3} and below.

Once again, a **high SNR approximation** of the union bound is calculated, to determine the **diversity order** and the **power loss** in case of correlated channels.

An **optimal precoder** for correlated fading is derived. Simulation results show that the precoder effectively mitigates the loss induced by correlated fading.

In addition, an extraordinarily tight **lower bound** of the BER is derived that allows for a two-sided bounding of the BER vs. SNR performance from below and from above. Several code examples assess the tightness of the lower bound, where, for uncorrelated channels, an almost exact performance approximation is achieved.

Contents

1	Introduction	1
2	Transmission System and Channel Model	7
2.1	System Model	7
2.1.1	Uncoded Data Transmission	7
2.1.2	Coded Data Transmission	8
2.2	Channel Model	9
2.2.1	Temporal Channel Modelling	9
2.2.2	Spatial Channel Modelling	9
2.2.2.1	Spatially Uncorrelated Channels	9
2.2.2.2	Spatially Correlated Channels	9
2.3	SNR-Definition	13
3	Uncoded Data Transmission	15
3.1	The Maximum Likelihood Detection Rule	15
3.2	Signal Distance Properties: SISO versus MIMO - Systems	17
3.2.1	Signal Distances in wireless SISO-Systems	17
3.2.2	Signal Distances in MIMO-Systems	17
3.3	Union Bound for the BER	21
3.3.1	Spatially Uncorrelated Channels	22
3.3.2	Spatially Correlated Channels	25
3.3.3	High SNR Approximation of the BER	27
3.3.3.1	Spatially Uncorrelated Channels at high SNR	27
3.3.3.2	Spatially Correlated Channels at high SNR	28
3.3.4	Discussion	29
3.4	Examples and further Discussion	30
3.4.1	Uncoded 4×4 MIMO system with BPSK modulation	30

3.4.1.1	Performance degradation due to spatial correlation	30
3.4.1.2	Tightness of the union bound	31
3.4.2	Uncoded 2×2 MIMO system with 16QAM modulation	33
3.5	Optimal Precoding	34
4	Space-Time Block Coded Data Transmission	37
4.1	Fundamentals of Space-Time Block Codes	37
4.1.1	Space-Time Block Coding Techniques	38
4.1.1.1	Orthogonal Space-Time Block Codes	38
4.1.1.2	Non-Orthogonal Space-Time Block Codes	39
4.1.2	Code Design Criteria	40
4.1.3	Block Coding: SISO vs. MIMO	43
4.1.3.1	Distance Properties	43
4.1.3.2	Dominating Errors	45
4.2	Union Bound of the BER	48
4.2.1	Spatially Uncorrelated Channels	48
4.2.2	Spatially Correlated Channels	51
4.2.3	High SNR Approximation	54
4.2.3.1	Spatially Uncorrelated Channels	54
4.2.3.2	Spatially Correlated Channels	56
4.2.4	Diversity Loss and Loss of Coding Advantage due to Channel Correlation	57
4.2.5	Examples	58
4.2.5.1	Cyclic Code	58
4.2.5.2	Extended Alamouti Code	62
4.2.5.3	Specific Orthogonal Code	66
4.2.5.4	D-STTD Code	68
4.2.6	Optimal Precoding	70
4.3	Lower Bound for the BER in case of STB coded MIMO System	75
4.3.1	Nearest Neighbor Approximation	75
4.3.2	Minimum Distance Lower Bound of the BER	79
4.3.2.1	Fundamentals	79
4.3.2.2	Spatially Uncorrelated Channels	85
4.3.2.3	Spatially Correlated Channels	89
4.3.2.4	Hybrid Method to calculate the MDLB	94
4.3.2.5	Examples and Discussion	95

5 Summary and Conclusions	101
A Notation	105
B Acronyms	107
C Important Variables	109
D Model Parameters	111
E Error Types for Uncoded MIMO Systems	113
F Error Types for the Cyclic STBC	116

Chapter 1

Introduction

In the last decade mobile communication has become a very important part of human life. The demand on having everything mobile has increased substantially. Apart from voice calls, nowadays video streaming, video calls, Internet surfing are mobile too. These applications need high data rates to make them fast and thus comfortable. In the future this trend will go on, and therefore investigating techniques that offer higher data rates is of utmost importance.

One of the most promising new data communication methods makes use of multiple antenna elements at the transmitter and/or at the receiver. In this thesis we focus on such systems, which are called Multiple Input / Multiple Output (MIMO) systems in the literature. In Fig. 1.1 a MIMO system with n_T transmit antennas and n_R receive antennas is shown. $h_{ij}(\tau)$ is the channel impulse response between the j -

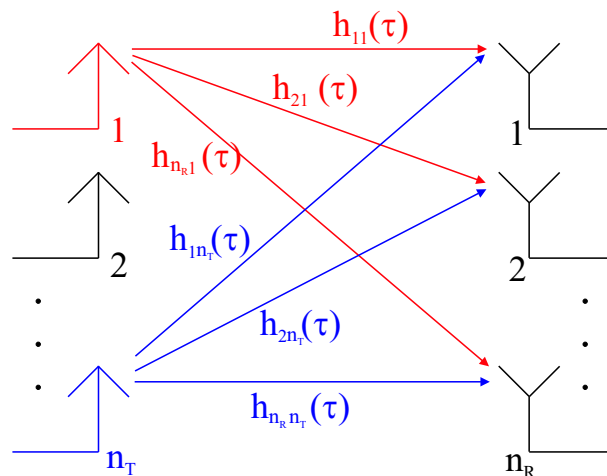


Figure 1.1: MIMO system with n_T transmit antennas and n_R receive antennas.

th transmit antenna and the i -th receive antenna. The enormous research interest in these systems is justified by recently published impressive results on the high channel capacity of such systems [1][2].

MIMO Channel Capacity:

The ergodic (mean) channel capacity [1][2] vs. the mean Signal to Noise Ratio (SNR) for several MIMO systems with 2×2 , 4×4 , 8×8 transmit and receive antennas and a Single Input / Single Output (SISO) system for uncorrelated Rayleigh fading are shown in Fig.1.2. The increase in channel capacity for

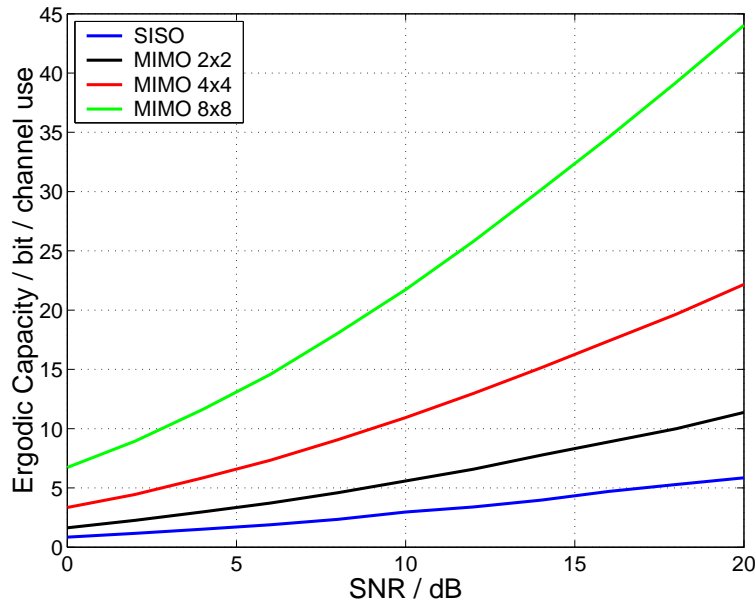


Figure 1.2: Ergodic channel capacity vs. mean SNR for several MIMO systems (2×2 , 4×4 , 8×8) and a SISO system for uncorrelated Rayleigh fading.

MIMO systems compared to a SISO system is quite impressive. The channel capacity for the SISO system at SNR=10dB is approximately 2.95 bit /channel use. A 2×2 MIMO system almost doubles the capacity (5.6 bit / channel use), a 4×4 MIMO system obtains more than 10.9 bit / channel use and a 8×8 MIMO system promises the seven fold capacity (21.7 bit / channel use) at the same SNR value. These improvements have attracted a lot of research interest in the last years, due to the huge increase in the MIMO capacity compared to a SISO system. One of the most important field in the research area of MIMO systems is how to exploit this promised increase in channel capacity in an efficient way. There are a lot of approaches, which can mainly be subdivided into investigations concerning uncoded and coded MIMO systems.

Uncoded MIMO Systems:

Uncoded MIMO transmission systems are also called systems with “Spatial Multiplexing”. “BLAST” [4], is the most prominent realization of an uncoded MIMO system. The acronym BLAST stands for **B**ell **L**Ayered **S**pace **T**ime. It is an efficient method to transmit uncoded symbols from each of the n_T transmit antennas. As shown in Fig. 1.3, *independent* data streams are transmitted over each transmit antenna. The MIMO channel delivers a superposition of the transmit signals to the receiver. As it can already be seen in Fig. 1.3, the transmitter complexity is very low and the main part of the signal processing has to be done at the receiver. The receiver has to regain the transmitted symbols from the mixed received symbols. The maximum symbol rate of $R_S = n_T$ symbols per channel use is achieved and the transmitter is very simple to implement. The main disadvantage is its limited performance, which strongly depends on the utilized receiver. Several receiver strategies can be applied:

-) ML - detection,
-) MMSE -, ZF - detection,
-) BLAST nulling and canceling.

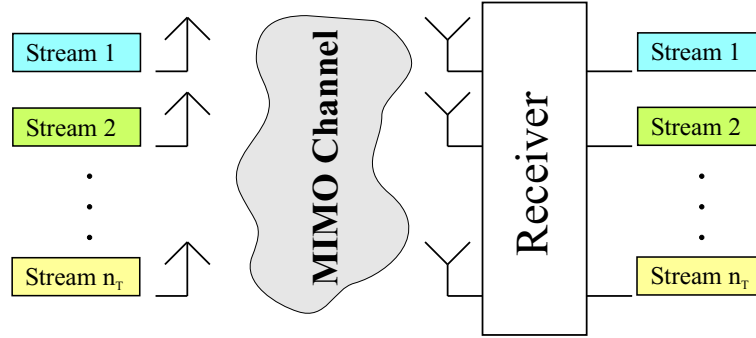


Figure 1.3: Uncoded MIMO transmission system with n_T independent data streams.

The ML (Maximum Likelihood) receiver (Sec. 3) achieves the best performance, but needs the most complex detection algorithm. A maximum diversity order of $D = n_R$ can be achieved. Obviously, in uncoded MIMO systems the transmit diversity is only $D_T = 1$ and thus the total diversity D is equal to the receive diversity D_R , which is at most n_R for spatially uncorrelated channels (Sec. 2.2).

Assuming full knowledge of the MIMO channel at the receiver, the ML receiver calculates all possible noiseless receive signals by transforming all possible transmit signals by the known MIMO channel transfer matrix \mathbf{H} . Then the receiver searches for that signal calculated in advance, which minimizes the Euclidean distance to the actually received signal. The undisturbed transmit signal that leads to this minimum distance is considered as the most likely transmit signal. Note that the above described detection process is optimum for white Gaussian noise.

Due to the exhaustive search within the complete signal alphabet, this receiver is very complex. There exist approximate receive strategies, which achieve almost ML performance and need only a fraction of the ML complexity [9] [8] [7].

MMSE (Minimum Mean Square Error) and ZF (Zero Forcing) [4] receiver strategies belong to the group of linear receivers. The ZF receiver completely nulls out the influence of the interference from signals coming from other transmit antennas. Then each data stream is separately detected. The detection (quantization) is performed in the same way as in SISO systems. The disadvantage of this approach is that due to canceling the influence of the signals from other transmit antennas, the noise may be strongly increased and thus the performance may heavily degrade. Due to the separate decision of each data stream, the complexity of this algorithm is much lower than in case of an ML receiver. The diversity order for ZF receivers in spatially uncorrelated channels is only $D = n_R - n_T + 1$ [10].

The MMSE receiver compromises between noise and signal interference and minimizes the mean squared error between the really transmitted symbol and the detected symbol. Thus the results of the MMSE equalization are the transmitted data streams plus some residual interference and noise. After MMSE equalization each data stream is separately detected (quantized) in the same way as in the ZF case. The complexity is almost equal to the complexity of ZF receivers, but the performance is better.

BLAST receivers apply a “Nulling and Canceling” or a “Decision Feedback” strategy. Such receivers are similar to the “Nulling and Canceling” multiuser detectors explained in [3] or to “Decision Feedback” equalizers in frequency selective fading SISO channels [27]. In principle, all received symbols are equalized according to the ZF approach (“Nulling”) and afterwards the symbol with the highest SNR (that can easily be calculated with the knowledge of the MIMO channel) is detected by a grid decision. The detected symbol is assumed to be correct and its influence on the received symbol vector is subtracted (“Canceling”). This procedure is iterated until all symbols are detected. Instead of the ZF “Nulling” approach also an MMSE equalizer can be used. Then the term “Nulling” is not quite adequate. The complexity of such receivers is higher than in case of ZF or MMSE receivers, but still much lower than

in case of ML receivers. The performance of these nulling and canceling receivers lies in between the performance of linear receivers (ZF and MMSE) and ML receivers.

Coded MIMO Systems:

Another transmission strategy is based on Space Time Coding (STC) [56] [57] [58], which is a more elaborate and thus also more complex way to perform reliable data transmission over wireless MIMO links. STC is especially useful if the channel is only known at the receiver and not at the transmitter. STC is understood as a redundant transmission of symbols that are correlated (repeated) in time and/or in space over several transmit antennas. Hence, redundancy is introduced in space and time and therefore the information symbol rate of such systems is lower than in uncoded systems but the error performance is better. The loss in symbol rate R_S can be compensated by using a higher modulation format (transmitting more bits per symbol) and thus the same bit rate as for uncoded systems can be achieved, which is actually the adequate performance measure. In spite of the higher modulation format, the performance of coded systems is usually better than for uncoded systems!

There are several approaches to implement STCs: Space Time Trellis Codes (STTCs), Space Time Block Codes (STBCs), Space Time Turbo Codes and so on. A space time trellis encoder with 3 input bit streams I_1 , I_2 and I_3 , two transmit antennas and at least one delay element per bit stream is shown in Fig. 1.4. The coefficients a_i^j , b_i^j and c_i^j shown in Fig. 1.4 determine the performance of the coded

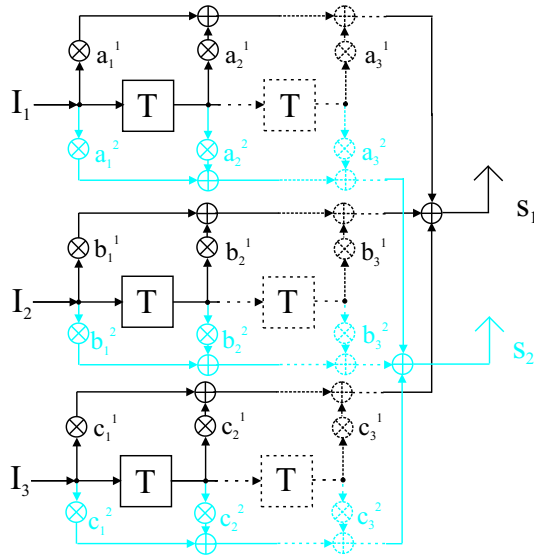


Figure 1.4: Space time trellis encoder.

system. Therefore, these coefficients have to be chosen in an optimal way. Considering only the first input bit stream I_1 in Fig. 1.4 for example, it can be seen that the corresponding preprocessing is actually a convolutional encoder as used in a SISO system. However, in MIMO systems the information of input stream I_1 is distributed over all (in this case 2) transmit antennas and over more than one time slot. Due to this spreading of the input information in the spatial and temporal domain, such systems achieve high diversity and good performance. The main disadvantage of such systems is the high receiver complexity. The optimal receiver for such a code is the well known Vector Viterbi decoder [27]. For low data rates and few delay elements the receiver complexity is not too high, but if the information bit rate and/or the encoder memory grows, the number of trellis states increases exponentially and thus the complexity reaches the limits of nowadays processors very soon. An alternative are STBCs, that need a much lower decoding complexity compared to STTC. More about STTCs can be found in [5] [6].

A very simple space time block coding system is shown in Fig. 1.5. Here, the space time block encoder

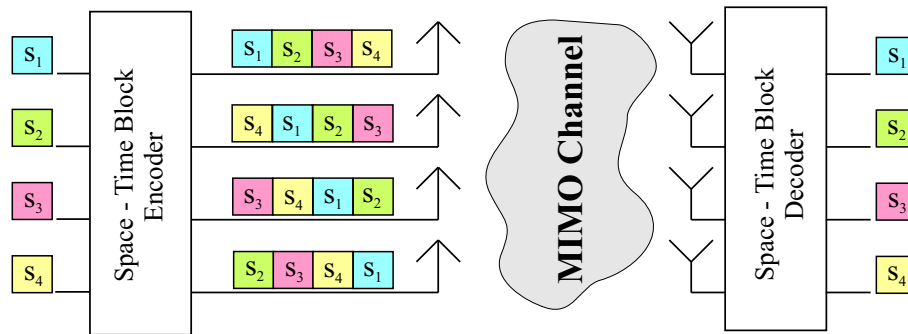


Figure 1.5: Space time block coding system for 4 transmit and 4 receive antennas.

is rather a signal mapping than an encoding. Therefore, the input symbols are not that widely spread over the spatial and temporal domain as in the case of STTCs. However, the encoder and decoder complexity is much lower than with STTCs. In general all receivers (ML, ZF, MMSE, ...) that are used in uncoded systems can also be used for STBCs with some modifications. For a special case of STBCs, namely the orthogonal STBCs [51] [49], even a matched filter and a separate “grid decision” afterwards, which is easy to implement, leads to the optimum performance. There is a lot of literature on the topic of space time block coding and a lot of different code-design strategies have been proposed.

Scope of this Thesis:

Apart from complexity, a very important characteristic of a system is its Bit Error Ratio (BER) performance. Frequently, performance evaluations are done by simulations, which are very time consuming at high SNR values. For this reason and to get more insight into the behavior of MIMO systems, analytical performance approximation or bounds of the resulting BER values are of great interest.

The aim of this thesis is to provide an analytical expression of error bounds and to get BER approximations for uncoded and space time block coded MIMO systems utilizing ML receivers for frequency flat MIMO channels.

The analysis of the BER performance helps to understand, which system parameters influence the system performance essentially and which parameters are of minor importance. With this knowledge some important conclusions for an optimum design strategy can be drawn.

The rest of this thesis is organized as follows: The system model and the essential properties of the MIMO channel are presented in Chapter 2. Additionally, the SNR definition used in this thesis is explained in some detail.

Chapter 3 covers uncoded MIMO systems. A union bound for the BER vs. SNR performance is derived for spatially uncorrelated and correlated MIMO channels using ML receivers. A high SNR approximation of the union bound is derived, which helps to specify the diversity order and allows a simple comparison of the error performance achievable in uncorrelated and correlated channels. The simulated performance is compared to the derived union bound and to the high SNR approximation for several MIMO systems with different modulation formats. The diversity loss and the power loss due to spatial channel correlation is specified. Additionally an optimal precoding filter is derived that improves the error performance in correlated fading.

Chapter 4 deals with space-time block coded MIMO systems. A union bound for the BER vs. SNR performance is derived for spatially uncorrelated and correlated MIMO channels using ML receivers. A high SNR approximation of the union bound is derived, which helps to specify the diversity order and allows a simple comparison of the error performance in uncorrelated and correlated channels. The simulated performance is compared to the derived union bound and to the high SNR approximation for

several codes with different modulation formats. The diversity loss and the power loss due to spatial channel correlation is also specified. An optimal precoding filter is derived in order to improve the performance in correlated fading. Additionally, a lower bound for the BER is calculated. This lower bound is an extraordinary tight performance measure in case of uncorrelated channels. Together with the calculated union bound a new joint bounding technique of the BER from below and from above is derived.

Essential insights and important conclusions are summarized in Chapter 5.

Some supplements and details can be found in the Appendix.

Chapter 2

Transmission System and Channel Model

2.1 System Model

2.1.1 Uncoded Data Transmission

The system model for uncoded data transmission is shown in Fig. 2.1

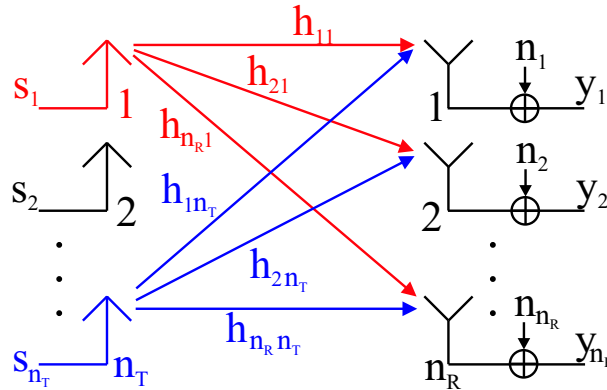


Figure 2.1: System model for uncoded transmission over frequency flat MIMO channels.

and can be described mathematically by:

$$\mathbf{y} = \mathbf{H}\mathbf{s} + \mathbf{n} . \quad (2.1)$$

$\mathbf{y} = (y_1 \ y_2 \ \dots \ y_{n_R})^T$ is the receive symbol vector, \mathbf{H} is the MIMO channel transfer matrix, $\mathbf{s} = (s_1 \ s_2 \ \dots \ s_{n_T})^T$ is the transmit symbol vector and $\mathbf{n} = (n_1 \ n_2 \ \dots \ n_{n_R})^T$ is the additive noise vector. Note that the system model implicitly assumes a flat fading MIMO channel, i.e., the channel impulse response between transmit antenna j and receive antenna i $h_{ij}(\tau) = h_{ij}\delta(\tau)$ and thus the transfer function $H_{ij}(j\omega)$ is frequency flat. $\delta(\tau)$ denotes a Dirac impulse. Therefore, in the following the delay variable τ is omitted and the complex-valued flat fading channel coefficients are denoted by h_{ij} . The MIMO channel matrix \mathbf{H} consists of $n_R \cdot n_T$ channel coefficients h_{ij} . The way in which the realizations of the channel matrix \mathbf{H} are modeled, is discussed in Sec. 2.2.

Throughout this thesis, it is assumed that the transmit symbol vectors are uncorrelated: $E\{\mathbf{s}\mathbf{s}^H\} = P_s\mathbf{I}$, where P_s denotes the mean signal power of the used modulation format at each transmit antenna. This implies that modulation formats with identical mean power on all transmit antennas are considered. The

entries of the noise vector \mathbf{n} are independent identically complex Gaussian distributed random variables with zero mean and variance σ_n^2 :

$$\mathbf{n} \sim \mathcal{N}_C^{n_R \times 1}(0, \sigma_n^2) \quad (2.2)$$

2.1.2 Coded Data Transmission

The system model for space-time block coded transmission is similar to the model for uncoded transmission shown in Fig. 2.1 and can be described by:

$$\mathbf{Y} = \mathbf{H}\mathbf{S} + \mathbf{N}. \quad (2.3)$$

$\mathbf{Y} = (\mathbf{y}_1 \mathbf{y}_2 \dots \mathbf{y}_{n_{OTS}})$ is the receive symbol matrix, $\mathbf{S} = (\mathbf{s}_1 \mathbf{s}_2 \dots \mathbf{s}_{n_{OTS}})$ is the transmit symbol matrix or space-time block code matrix and $\mathbf{N} = (\mathbf{n}_1 \mathbf{n}_2 \dots \mathbf{n}_{n_{OTS}})$ is the additive noise matrix. n_{OTS} denotes the **N**umber of **O**ccupied **T**ime **S**lots of the code matrix \mathbf{S} . The setup of the space-time block code matrix can be seen in Fig. 2.2. In principle, here the system model for uncoded transmission is

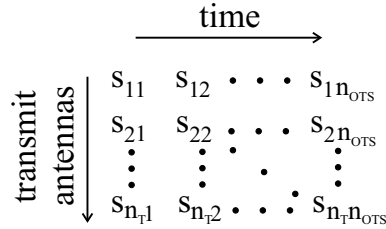


Figure 2.2: Setup of the space-time block code matrix \mathbf{S} .

extended to more than one time slot. The properties of \mathbf{s}_i and \mathbf{n}_i for coded transmission are the same as for \mathbf{s} and \mathbf{n} for uncoded transmission. Note that \mathbf{n}_i is independent from \mathbf{n}_j for all $i \neq j$. In contrast, \mathbf{s}_i is **not** independent from \mathbf{s}_j . This is obvious, because in general codes incorporate correlation between the transmit symbols, e.g. by calculating parity symbols. Summarizing, within one transmit symbol vector \mathbf{s}_i the symbols are uncorrelated, but different symbol vectors of the code matrix are strongly correlated.

2.2 Channel Model

In order to get practically useful results in Sec. 3 and Sec. 4, a realistic channel model has to be used. There are a lot of possibilities to model the MIMO channel in the temporal and in the spatial domain. In the following, the models used in this thesis are explained.

2.2.1 Temporal Channel Modelling

The temporal behavior of the channel is very important for a reliable transmission schemes. For example, Closed Loop Schemes (CLS) [25] [26] [22] [23] rely on more or less slowly fading channels, because the feedback information is no more reliable if the channel changes too fast and thus the transmitter cannot be informed about the actual channel parameters.

However, for analytical error performance bounds, the temporal model is not that important. The emphasis here lies on spatial correlation of the channel coefficients. Nevertheless some specifications are necessary. The temporal behavior of the MIMO channel is modeled by block fading. The channel is assumed to be constant for the duration of the transmission of one data symbol. After each transmission of a data symbol, the channel changes arbitrarily. A data symbol is a single symbol vector for uncoded transmission and a code matrix for space-time block coded transmission. This temporal behavior is called block fading or quasi static fading [29]. It is an appropriate approximation of a slow fading channel using some form of frequency hopping or time interleaving. More about the temporal behavior of MIMO channels can be found in [12].

2.2.2 Spatial Channel Modelling

In this thesis, two different spatial channel models are of interest. In general, we can distinguish between spatially uncorrelated and spatially correlated channels.

2.2.2.1 Spatially Uncorrelated Channels

Spatially uncorrelated channels are modeled by a random matrix \mathbf{H} with independent identically distributed (i.i.d.) complex Gaussian entries with zero mean and unit variance:

$$\mathbf{H} \sim \mathcal{N}_C^{n_R \times n_T}(0, 1) \quad (2.4)$$

This frequently used model is called i.i.d. model, first mentioned in [1] [2].

Such a MIMO channel can be observed in scenarios, where the antenna elements are located far apart from each other and a lot of scatterers surround the antenna arrays at both sides of the link. Due to the limited space at the mobile station, the antenna elements are often densely spaced and thus, in realistic MIMO transmission systems, i.i.d. channels might rarely be observed even in indoor environments. For this reason it is necessary to use correlation models.

2.2.2.2 Spatially Correlated Channels

In most cases, the MIMO channel transfer coefficients are correlated. The antenna array at the Base Station (BS) is quite often mounted above rooftop and therefore the number of scatterers around it is small. Therefore, there are only some distinct waves impinging at the antenna array and thus the received signals at the various receive antennas at the BS are highly correlated.

In principle, correlated MIMO channels can be modeled in two ways. There are geometrically-based [30] [20] and statistically-based [19] [28] channel models. In this thesis the focus lies on statistical models. A very simple and appropriate approach is to assume the entries of the channel matrix \mathbf{H} to be complex Gaussian distributed with zero mean and unit variance with complex correlations between all entries h_{ij} [19]. The full correlation matrix can then be defined as:

$$\mathbf{R}_{\mathbf{H}} = \mathbb{E} \left\{ \begin{array}{cccc} \mathbf{h}_1 \mathbf{h}_1^H & \mathbf{h}_1 \mathbf{h}_2^H & \dots & \mathbf{h}_1 \mathbf{h}_{n_T}^H \\ \mathbf{h}_2 \mathbf{h}_1^H & \mathbf{h}_2 \mathbf{h}_2^H & \dots & \mathbf{h}_2 \mathbf{h}_{n_T}^H \\ \vdots & \vdots & \ddots & \vdots \\ \mathbf{h}_{n_T} \mathbf{h}_1^H & \mathbf{h}_{n_T} \mathbf{h}_2^H & \dots & \mathbf{h}_{n_T} \mathbf{h}_{n_T}^H \end{array} \right\}, \quad (2.5)$$

where \mathbf{h}_i denotes the i -th column vector of the channel matrix \mathbf{H} . Knowing all complex correlation coefficients, the actual channel matrix \mathbf{H} can be modeled as:

$$\mathbf{H} = (\mathbf{h}_1 \ \mathbf{h}_2 \ \dots \ \mathbf{h}_{n_T}) \quad \text{with} \quad (\mathbf{h}_1^T \ \mathbf{h}_2^T \ \dots \ \mathbf{h}_{n_T}^T)^T = (\mathbf{R}_{\mathbf{H}})^{\frac{1}{2}} \mathbf{g}. \quad (2.6)$$

\mathbf{g} is an i.i.d. $(n_R \cdot n_T) \times 1$ random vector with complex Gaussian distributed entries with zero mean and unit variance. In the following this model is called *full correlation model*. The big disadvantage of this model is the huge number of parameters necessary to describe and generate correlated channel matrices \mathbf{H} . The number of parameters is $(n_R \cdot n_T)^2$.

Due to the drawback of a huge number of parameters, another correlation model has been introduced, namely the so-called Kronecker model [14] [15] [16] [19]. In this model it is assumed that the transmit correlation and the receive correlation can be separated and characterized by the transmit correlation matrix

$$\mathbf{R}_T = \mathbb{E}_{\mathbf{H}} \left\{ \mathbf{H}^T \mathbf{H}^* \right\}, \quad (2.7)$$

and the receive correlation matrix

$$\mathbf{R}_R = \mathbb{E}_{\mathbf{H}} \left\{ \mathbf{H} \mathbf{H}^H \right\}. \quad (2.8)$$

Accordingly, correlated MIMO channel matrices \mathbf{H} are generated as:

$$\mathbf{H} = \frac{1}{\sqrt{\text{tr}(\mathbf{R}_R)}} \mathbf{R}_R^{1/2} \mathbf{G} \left(\mathbf{R}_T^{1/2} \right)^T, \quad (2.9)$$

where the matrix \mathbf{G} is an i.i.d. random matrix with complex Gaussian entries with zero mean and unit variance. With this approach the large number of model parameters is dramatically reduced, namely to $n_R^2 + n_T^2$. The full correlation matrix simplifies to $\mathbf{R}_{\mathbf{H},Kron} = \mathbf{R}_T \otimes \mathbf{R}_R$ (Eqn. 2.5), and therefore this model is called Kronecker model. A big disadvantage of this correlation model is that MIMO channels with relatively high spatial correlation cannot be modeled adequately, due to the limiting heuristic assumption $\mathbf{R}_{\mathbf{H},Kron} = \mathbf{R}_T \otimes \mathbf{R}_R$. Further details, on this topic can be found in [21], [28] and [11].

This deficiency of the Kronecker model led to a novel channel model invented by Werner Weichselberger [28] [11]. In the following this novel approach is called W-model. The advantage of this method is that the number of parameters is not too much increased compared to the Kronecker model (in fact $n_R^2 + n_R \cdot n_T + n_T^2$), but the modeling error with respect to measured channel characteristics is substantially decreased [28]. MIMO channel realizations according to the W-model are calculated as:

$$\mathbf{H} = \mathbf{U}_R \left(\tilde{\boldsymbol{\Omega}} \odot \mathbf{G} \right) \mathbf{U}_T^T. \quad (2.10)$$

\odot denotes the element wise product of matrix elements. \mathbf{U}_R and \mathbf{U}_T are the receiver and transmitter eigenbasis, which can be interpreted as a characteristic of the structure of scatterers around the receive and the transmit antenna array. $\tilde{\boldsymbol{\Omega}}$ denotes the element wise square root of $\boldsymbol{\Omega}$, $\boldsymbol{\Omega}$ being a power coupling matrix, which describes the average coupling between the receiver and the transmitter eigenbasis. The

entries of $\mathbf{\Omega}$ can easily be estimated from MIMO measurements [11]. The matrix \mathbf{G} is an i.i.d. random matrix with complex Gaussian distributed entries with zero mean and unit variance. In contrast to the Kronecker model, in the W-model only the eigenbasis of the transmit (receive) correlation matrix \mathbf{U}_T (\mathbf{U}_R) is assumed to be independent of the receive (transmit) antenna weights.

Note that this model is a generalization of the Kronecker model. Thus, a Kronecker modeling of MIMO channels can also be done with this model by specializing $\mathbf{\Omega}$. In this case, the power coupling matrix $\mathbf{\Omega}$ of the W-model can be calculated from the parameters of the Kronecker model by:

$$\mathbf{\Omega} = \frac{1}{\sqrt{\sum_{i=1}^{n_R} \lambda_{R,i}}} \begin{pmatrix} \lambda_{R,1} \cdot \lambda_{T,1} & \lambda_{R,1} \cdot \lambda_{T,2} & \dots & \lambda_{R,1} \cdot \lambda_{T,n_T} \\ \lambda_{R,2} \cdot \lambda_{T,1} & \lambda_{R,2} \cdot \lambda_{T,2} & \dots & \lambda_{R,2} \cdot \lambda_{T,n_T} \\ \vdots & \vdots & \ddots & \vdots \\ \lambda_{R,n_R} \cdot \lambda_{T,1} & \lambda_{R,n_R} \cdot \lambda_{T,2} & \dots & \lambda_{R,n_R} \cdot \lambda_{T,n_T} \end{pmatrix}. \quad (2.11)$$

Here, $\lambda_{R,i}$ and $\lambda_{T,i}$ denote the eigenvalues of the (measured) receive correlation matrix \mathbf{R}_R and the transmit correlation matrix \mathbf{R}_T defined in Eqn. (2.7) and Eqn. (2.8).

Note that for all spatial models the same normalization is used:

$$\mathbb{E}_{\mathbf{H}} \left\{ \text{tr} \left(\mathbf{H}^H \mathbf{H} \right) \right\} = \sum_{i=1}^{n_R} \sum_{j=1}^{n_T} \mathbb{E}_{\mathbf{H}} \left\{ |h_{ij}|^2 \right\} = n_R n_T. \quad (2.12)$$

Therefore, the correlation matrix $\mathbf{R}_{\mathbf{H}}$ for the full correlation model, the correlation matrices \mathbf{R}_R and \mathbf{R}_T for the Kronecker model and the power coupling matrix $\mathbf{\Omega}$ have to be normalized appropriately.

Because of the essential advantages of the W-model discussed in detail in [28] and the fact that this model is also capable to realize Kronecker MIMO channels, it is the preferred channel model in this thesis.

In Sec. 3 and Sec. 4, correlated MIMO channels are used to investigate the performance of various systems. Therefore practically relevant model parameters are needed. In order to use realistic channel parameters, model parameters are extracted from MIMO channel measurements, which have been performed at our Institute. In the following important measurement parameters are listed:

carrier frequency	5.2 GHz
bandwidth	120 MHz
transmit antenna array	virtual 20×10 antenna array with 0.5λ inter element spacing
receive antenna array	8 element Uniform Linear Array (ULA) with 0.4λ inter element spacing

More details about the measurements can be found in [24] [13]. Some measurements have been performed at the 3rd floor of our Institute, where a lot of scenarios has been investigated. A detailed map of the 3rd floor of our Institute is shown in Fig. 2.3. As can be seen in Fig. 2.3 the position of the 20×10 virtual transmit antenna array denoted by TX has been fixed for all measurements. Several positions of the receive antenna array have been considered and are denoted by RX. At each RX position three distinct measurements have been performed, where the 8 element receive ULA has been looking in three different directions. These directions are indicated by three arrows labeled with D1, D2 and D3 at the left hand side of Fig. 2.3. An example for the notation of a measurement scenario is “14D3”. 14 stands for RX position 14 and D3 denotes that the receive arrays broadside is looking in direction 3.

In the following it is explained how the model parameters are extracted from the measurement data. The channel transfer coefficients have been measured between the virtual 20×10 transmit array and the 8 element ULA at the receiver at 193 frequency values. With the large virtual transmit array, it is possible to find 130 distinct realizations of an 8 element transmit array. For example, one realization is produced

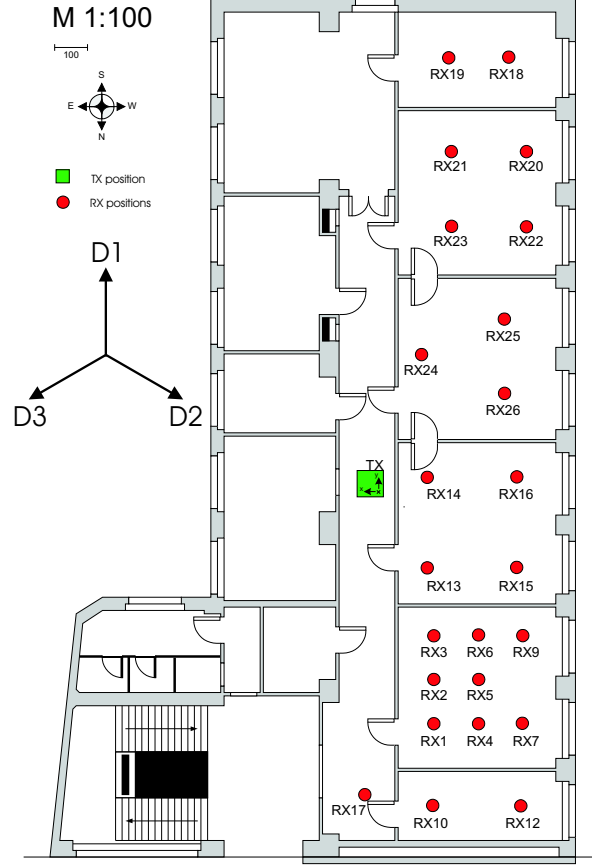


Figure 2.3: Detailed map of the 3rd floor of the Institute of Communications and Radio-Frequency Engineering.

by taking the 1st to the 8th element of the first row (out of 10 rows) from the virtual transmit antenna array. The second realization refers to the positions 2 to 9 of the first row and so on. Taking into account all rows, 130 so-called spatially distinct realizations can be found. Note that the inter element spacing is 0.5λ for each realization. Taking into account the 8 element ULA at the receiver, 130 realizations of an 8×8 indoor MIMO channel matrix can be obtained for every frequency bin. 193 so-called frequency realizations for each spatial realization are available and thus in total $130 \cdot 193 = 25.090$ realizations of an 8×8 MIMO channel matrix are obtained, which is considered to be a sufficiently large ensemble.

Extracting the channel parameters for a 4×4 MIMO channel, only the first four rows of the 8×8 channel matrix discussed above are considered. Each of these rows consists of 8 elements, where again only the first four are used. Thus, a distinct 4×4 matrix out of each 8×8 matrix is extracted. In order to obtain the model parameters for the W-model, the correlation matrices \mathbf{R}_R and \mathbf{R}_T have to be calculated according to Eqn. (2.7) and Eqn. (2.8) by averaging over all realizations of \mathbf{H} at a specific receiver location. Applying an eigenvalue decomposition to the correlation matrices \mathbf{R}_R and \mathbf{R}_T , the eigenbases \mathbf{U}_R and \mathbf{U}_T are obtained. Having calculated the eigenbases, the power coupling matrix is obtained by [31]:

$$\mathbf{\Omega} = E_{\mathbf{H}} \left\{ (\mathbf{U}_R^H \mathbf{H} \mathbf{U}_T) \odot (\mathbf{U}_R^T \mathbf{H}^* \mathbf{U}_T^*) \right\} \quad (2.13)$$

For the investigations in Sec. 3 and Sec. 4, moderately and strongly correlated 4×4 MIMO channels are of primary interest. For this reason, the scenarios 14D3 and 1D3 were chosen to extract the model parameters corresponding to strongly correlated and moderately correlated MIMO channels. The model parameters in case of moderate correlation (scenario 1D3) and strong correlation (scenario 14D3) are provided in Appendix D.

2.3 SNR-Definition

In this thesis the error performance of uncoded and coded transmission is investigated in terms of BER vs. SNR. Therefore, it is worth to say a few words about the SNR definition. It is reasonable to define the mean SNR as the ratio of the **total received signal power to the total noise power**:

$$\text{SNR} = E_{\mathbf{H}, \mathbf{s}, \mathbf{n}} \left\{ \frac{\|\mathbf{y}\|_2^2}{\|\mathbf{n}\|_2^2} \right\}. \quad (2.14)$$

$\|\cdot\|_2$ denotes the l2-norm operator. The expectation is with respect to the channel matrix \mathbf{H} , the noise \mathbf{n} and the transmit symbol vector \mathbf{s} . Due to the independence of \mathbf{y} and \mathbf{n} , Eqn. (2.14) is equivalent to

$$\text{SNR} = \frac{E_{\mathbf{H}, \mathbf{s}} \left\{ \|\mathbf{H}\mathbf{s}\|_2^2 \right\}}{E_{\mathbf{n}} \left\{ \|\mathbf{n}\|_2^2 \right\}} = \frac{E_{\mathbf{H}, \mathbf{s}} \left\{ \sum_{i=1}^{n_R} \left| \sum_{j=1}^{n_T} h_{ij} s_j \right|^2 \right\}}{E_{\mathbf{n}} \left\{ \sum_{i=1}^{n_R} |n_i|^2 \right\}}. \quad (2.15)$$

The last step in the numerator expansion holds, because of the independence of \mathbf{H} from \mathbf{s} and because the vector symbols \mathbf{s} are assumed to be independent as mentioned in Sec. 2.1. Due to the assumption of white noise (Sec. 2.1), the denominator is equivalent to $n_R \sigma_n^2$ and thus we get:

$$\text{SNR} = \frac{\sum_{i=1}^{n_R} \sum_{j=1}^{n_T} E_{\mathbf{H}} \left\{ |h_{ij}|^2 \right\} P_s}{n_R \sigma_n^2}. \quad (2.16)$$

P_s denotes the mean signal power of the used modulation format at each transmit antenna. With the normalization of the MIMO channel matrix defined in Sec. (2.2.2.2), the final result for the mean SNR is obtained:

$$\text{SNR} = \frac{n_R n_T P_s}{n_R \sigma_n^2} = \frac{n_T P_s}{\sigma_n^2}. \quad (2.17)$$

Note that the SNR definition is symbol based. Other authors [18] prefer bit based definitions:

$$\text{SNR}_{bit} = \frac{\text{SNR}}{\text{ld}(|\mathcal{A}|)}, \quad (2.18)$$

where $|\mathcal{A}|$ denotes the size of the symbol alphabet of the modulation format.

Chapter 3

Uncoded Data Transmission

In this section the error performance of uncoded MIMO transmission systems is investigated. Only optimal ML receivers are considered.

3.1 The Maximum Likelihood Detection Rule

Let's remember the detection rule of an ML receiver:

$$\hat{\mathbf{s}}_{ML} = \operatorname{argmin}_i \left\{ \|\mathbf{y} - \mathbf{H}\mathbf{s}_i\|_2^2 \right\}, \quad (3.1)$$

i.e., the ML receiver performs an exhaustive search for that vector symbol \mathbf{s}_i , which leads to the smallest distance between the received symbol vector \mathbf{y} and $\mathbf{H}\mathbf{s}_i$. Exhaustive search means that the whole symbol alphabet \mathcal{A}^{n_T} has to be checked. In order to perform this search, the channel matrix \mathbf{H} has to be known. In practical systems the channel matrix \mathbf{H} has to be estimated [38][39][40][41]. Throughout this thesis perfect channel knowledge at the receiver is assumed.

Now, consider the case, when \mathbf{s}_i is sent and the ML detector decides in favor of the erroneous symbol \mathbf{s}_j . The probability for this erroneous decision (Pairwise Error Probability - PEP) can be calculated as:

$$P(\mathbf{s}_i \rightarrow \mathbf{s}_j) = P(\|\mathbf{y} - \mathbf{H}\mathbf{s}_i\|_2^2 > \|\mathbf{y} - \mathbf{H}\mathbf{s}_j\|_2^2). \quad (3.2)$$

Inserting $\mathbf{y} = \mathbf{H}\mathbf{s}_i + \mathbf{n}$ yields:

$$\begin{aligned} P(\mathbf{s}_i \rightarrow \mathbf{s}_j) &= P(\|\mathbf{H}\mathbf{s}_i + \mathbf{n} - \mathbf{H}\mathbf{s}_i\|_2^2 > \|\mathbf{H}\mathbf{s}_i + \mathbf{n} - \mathbf{H}\mathbf{s}_j\|_2^2) \\ &= P(\|\mathbf{n}\|_2^2 > \|\underbrace{\mathbf{H}(\mathbf{s}_i - \mathbf{s}_j)}_{\mathbf{b}_{i,j}} + \mathbf{n}\|_2^2), \end{aligned} \quad (3.3)$$

where $\mathbf{b}_{i,j}$ is called the symbol difference vector. This inequality can be further simplified to:

$$\begin{aligned} \|\mathbf{n}\|_2^2 &> \|\mathbf{H}\mathbf{b}_{i,j} + \mathbf{n}\|_2^2 \\ \mathbf{n}^H \mathbf{n} &> (\mathbf{b}_{i,j}^H \mathbf{H}^H + \mathbf{n}^H)(\mathbf{H}\mathbf{b}_{i,j} + \mathbf{n}) \\ \mathbf{n}^H \mathbf{n} &> \mathbf{b}_{i,j}^H \mathbf{H}^H \mathbf{H} \mathbf{b}_{i,j} + \mathbf{n}^H \mathbf{H} \mathbf{b}_{i,j} + \mathbf{b}_{i,j}^H \mathbf{H}^H \mathbf{n} + \mathbf{n}^H \mathbf{n} \\ -\mathbf{b}_{i,j}^H \mathbf{H}^H \mathbf{H} \mathbf{b}_{i,j} &> \underbrace{2 \operatorname{Re} \left\{ \mathbf{n}^H \mathbf{H} \mathbf{b}_{i,j} \right\}}_{z_{i,j}} \end{aligned} \quad (3.4)$$

The next step in this derivation is to determine the statistics of $z_{i,j}$. \mathbf{n} is a random vector with i.i.d. complex Gaussian entries (see Sec. 2.1). \mathbf{n} is linearly transformed by the matrix \mathbf{H} and the vector $\mathbf{b}_{i,j}$.

A linear transformation does not change the Gaussian distribution and therefore $\mathbf{n}^H \mathbf{H} \mathbf{b}_{i,j}$ is complex Gaussian too. Then, the real part operation turns the complex Gaussian distribution into a real Gaussian distribution. The mean $\mu_{z_{i,j}}$ of $z_{i,j}$ is:

$$\mu_{z_{i,j}} = E_{\mathbf{n}} \left\{ 2 \operatorname{Re} \left\{ \mathbf{n}^H \mathbf{H} \mathbf{b}_{i,j} \right\} \right\} = 0 \quad (3.5)$$

and the variance of $z_{i,j}$ is

$$\sigma_{z_{i,j}}^2 = E_{\mathbf{n}} \left\{ 2 \operatorname{Re} \left\{ \mathbf{b}_{i,j}^H \mathbf{H}^H \mathbf{n} \right\} 2 \operatorname{Re} \left\{ \mathbf{n}^H \mathbf{H} \mathbf{b}_{i,j} \right\} \right\} = \dots = 2 \sigma_n^2 \mathbf{b}_{i,j}^H \mathbf{H}^H \mathbf{H} \mathbf{b}_{i,j} . \quad (3.6)$$

The dots indicate that the derivation is quite lengthy but straight forward. Now, the complete statistics of $z_{i,j}$ is known and therefore the so-called Pairwise Error Probability (PEP) can be calculated:

$$\begin{aligned} P(\mathbf{s}_i \rightarrow \mathbf{s}_j) &= P(z_{i,j} < -\mathbf{b}_{i,j}^H \mathbf{H}^H \mathbf{H} \mathbf{b}_{i,j}) = \frac{1}{\sqrt{2\pi\sigma_{z_{i,j}}^2}} \int_{-\infty}^{-\mathbf{b}_{i,j}^H \mathbf{H}^H \mathbf{H} \mathbf{b}_{i,j}} e^{-\frac{1}{2} \left(\frac{\xi}{\sigma_{z_{i,j}}} \right)^2} d\xi \\ &= \frac{1}{\sqrt{2\pi\sigma_{z_{i,j}}^2}} \int_{\mathbf{b}_{i,j}^H \mathbf{H}^H \mathbf{H} \mathbf{b}_{i,j}}^{\infty} e^{-\frac{1}{2} \left(\frac{\xi}{\sigma_{z_{i,j}}} \right)^2} d\xi = \frac{1}{\sqrt{2\pi}} \int_{\frac{\mathbf{b}_{i,j}^H \mathbf{H}^H \mathbf{H} \mathbf{b}_{i,j}}{\sigma_{z_{i,j}}}}^{\infty} e^{-\frac{1}{2} \alpha^2} d\alpha \\ &= Q \left(\frac{\mathbf{b}_{i,j}^H \mathbf{H}^H \mathbf{H} \mathbf{b}_{i,j}}{\sigma_{z_{i,j}}} \right) = Q \left(\frac{\mathbf{b}_{i,j}^H \mathbf{H}^H \mathbf{H} \mathbf{b}_{i,j}}{\sqrt{2\sigma_n^2 \mathbf{b}_{i,j}^H \mathbf{H}^H \mathbf{H} \mathbf{b}_{i,j}}} \right) \\ &= Q \left(\sqrt{\frac{\mathbf{b}_{i,j}^H \mathbf{H}^H \mathbf{H} \mathbf{b}_{i,j}}{2\sigma_n^2}} \right) = Q \left(\sqrt{\frac{d_{Ri,j}^2}{2\sigma_n^2}} \right) = \operatorname{PEP}_{i,j} \end{aligned} \quad (3.7)$$

This derivation leads to the very important definition of the Euclidean distance between the images of the symbol vectors \mathbf{s}_i and \mathbf{s}_j observed at the receiver:

$$d_{Ri,j}^2 = \mathbf{b}_{i,j}^H \mathbf{H}^H \mathbf{H} \mathbf{b}_{i,j} = |\mathbf{H} \mathbf{b}_{i,j}|_2^2 = (\mathbf{s}_i - \mathbf{s}_j)^H \mathbf{H}^H \mathbf{H} (\mathbf{s}_i - \mathbf{s}_j) . \quad (3.8)$$

The subscript R at $d_{Ri,j}^2$ indicates that the distance of the vectors is considered at the receiver. The distance of signal vectors at the transmitter is defined as:

$$d_{Ti,j}^2 = \mathbf{b}_{i,j}^H \mathbf{b}_{i,j} = |\mathbf{b}_{i,j}|_2^2 = (\mathbf{s}_i - \mathbf{s}_j)^H (\mathbf{s}_i - \mathbf{s}_j) . \quad (3.9)$$

As can be seen in Eqn. (3.7) the Euclidean distance at the receiver governs the statistic of the PEP. For this reason in the following section, the distance properties of receive signals stemming from different transmit vectors are investigated.

3.2 Signal Distance Properties: SISO versus MIMO - Systems

In this section important differences in the behavior of MIMO systems compared to SISO (Single Input Single Output) systems with respect to signal distance characteristics are discussed.

3.2.1 Signal Distances in wireless SISO-Systems

The system model for uncoded wireless MIMO systems (shown in Sec. 2.1) can be easily adapted to describe SISO systems by using scalars instead of vectors and matrices¹. In the SISO-case the system is described by

$$y = h s + n . \quad (3.10)$$

Applying the framework derived above, the distance at the receiver results in:

$$d_{Ri,j}^2 = (s - \tilde{s})^* h^* h (s - \tilde{s}) = |h|^2 |s - \tilde{s}|^2 = |h|^2 d_{Ti,j}^2 . \quad (3.11)$$

This implies that the squared distances between all signal points at the receiver are only scaled values of the squared distances at the transmitter. Actually, the channel only rotates and scales the signal configuration. The following conclusions can be drawn:

-) The smallest (largest) distance of distinct signals at the transmitter leads to the smallest (largest) distance at the receiver.
-) The distance of different signals at the receiver is zero, only if either the distance at the transmitter is zero or the channel coefficient vanishes, that is $|h|^2 = 0$.

The first property is very important for the calculation of the total error performance (BER vs. SNR curve) of SISO systems. Due to the non-linear Gaussian Q-function only the signal points with the smallest distance values determine the error performance at high SNR. Contributions of distances that are approximately twice the smallest distance can be neglected completely. Therefore, only the signal point configuration at the transmitter has to be investigated to find a very good performance approximation. These ideas lead to the very famous Nearest Neighbor Approximation (NNA) [27]. For this approximation only the distances to the nearest neighboring signal points $d_{R,NN}^2$ and the average number of nearest neighbors \bar{n}_{NN} are of essential interest:

$$P_\varepsilon \approx \bar{n}_{NN} Q \left(\sqrt{\frac{d_{R,NN}^2}{2 \sigma_n^2}} \right) . \quad (3.12)$$

P_ε is the approximate symbol error probability of a SISO-system.

Unfortunately, matters are much more complicated in MIMO systems.

3.2.2 Signal Distances in MIMO-Systems

Here, the distance properties of uncoded MIMO systems are analyzed, which are extremely different compared to the SISO case. The difficulties arising in MIMO systems can be easily and illustratively explained by an example. In order to operate with two-dimensional plots, some restrictions have to be made. In the following, a 2×2 ($n_R = 2$ and $n_T = 2$) MIMO system with BPSK modulation (+1,-1) is considered. Nevertheless, the distance properties observed in this special case, also apply to all uncoded MIMO systems of any dimension. Note that the channel coefficients of the channel matrix \mathbf{H} in this

¹As mentioned in Sec. 2.1 only flat fading channels are considered.

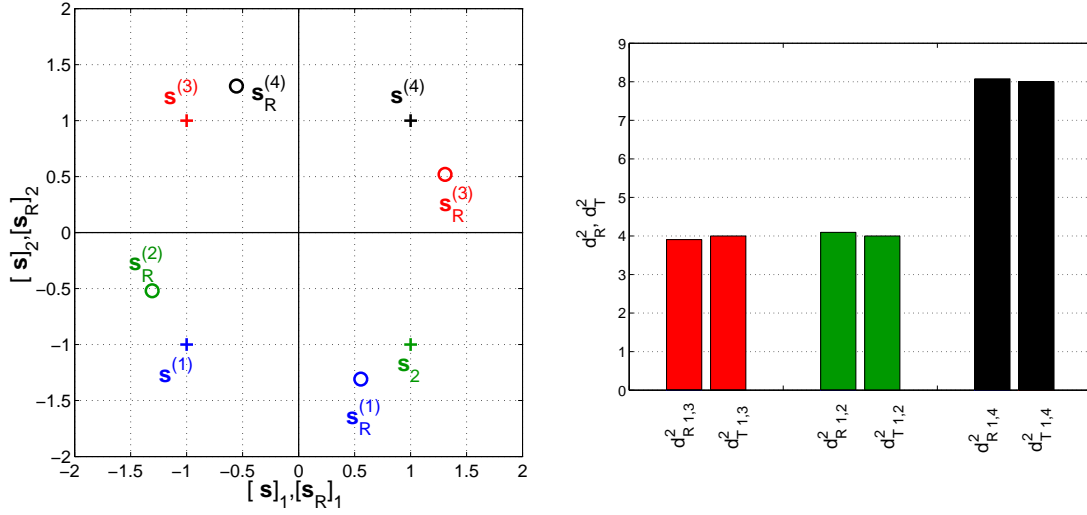


Figure 3.1: Signal distortion and the corresponding distances for uncoded MIMO systems (\mathbf{H}_1).

example are real-valued. In the following, three figures show the behavior of the distances at the receiver for different channel realization \mathbf{H}_k , where each channel is normalized to $\text{tr}(\mathbf{H}_k^H \mathbf{H}_k) = 2$. In the left plot of each figure, all (four) transmit symbol vectors $\mathbf{s}^{(i)}$ ² (labeled by “+”-marker) and the modified symbol vectors $\mathbf{s}_R^{(i)} = \mathbf{H}_k \mathbf{s}^{(i)}$ at the receiver (labeled by “o”-marker) can be seen. In the right plot of each figure the squared distances at the receiver $d_{R1,2}^2$, $d_{R1,3}^2$ and $d_{R1,4}^2$ for the transmit symbols $\mathbf{s}^{(1)} = (-1 -1)$, $\mathbf{s}^{(2)} = (1 -1)$, $\mathbf{s}^{(3)} = (-1 1)$ and $\mathbf{s}^{(4)} = (1 1)$ are compared to corresponding distances at the transmitter ($d_{T1,2}^2 = 4$, $d_{T1,3}^2 = 4$ and $d_{T1,4}^2 = 8$). Note that the subscripts 1 (2) at $[s_R]$ at the vertical (horizontal) axis of the left plot of each figure denotes the first (second) symbol of the vector \mathbf{s}_R . This is also true for $[s_1]$ and $[s_2]$. Actually, $[s_1] = s_1$ and $[s_2] = s_2$.

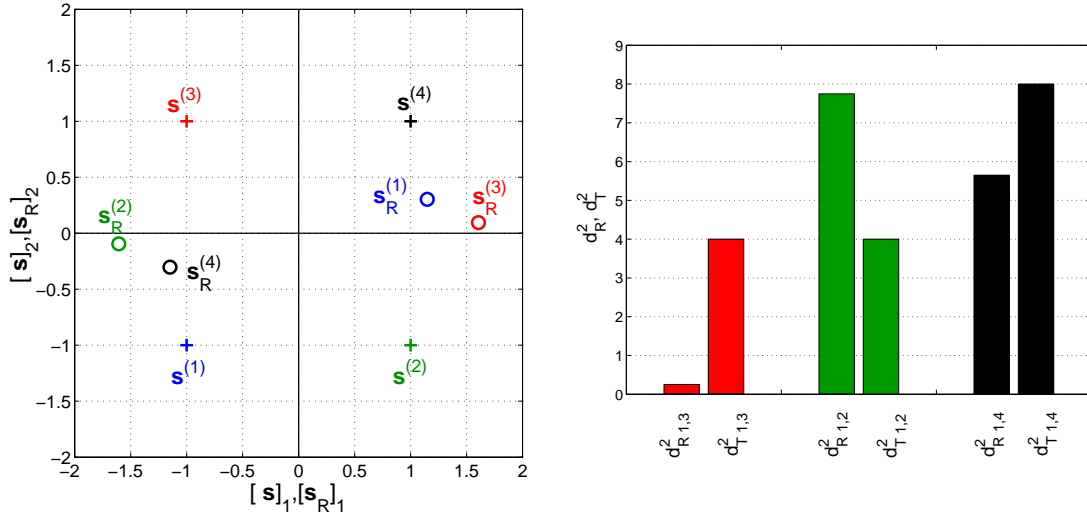


Figure 3.2: Signal distortion and the corresponding distances for uncoded MIMO systems (\mathbf{H}_2).

²Note that $\mathbf{s}^{(i)} = \mathbf{s}_i$. This is only an alternative notation in order to improve the readability in the presented figures in Section 3.2.

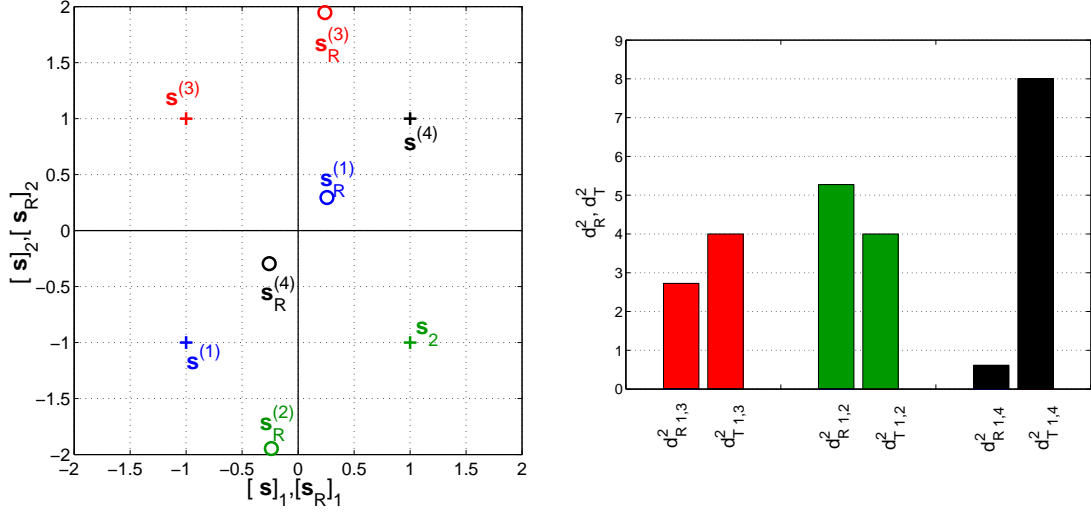


Figure 3.3: Signal distortion and the corresponding distances for uncoded MIMO systems (\mathbf{H}_3).

The three different channel matrices are chosen as:

$$\mathbf{H}_1 = \begin{pmatrix} -0.9317 & 0.3763 \\ 0.3942 & 0.9138 \end{pmatrix} \quad \mathbf{H}_2 = \begin{pmatrix} -1.3775 & 0.2283 \\ -0.1989 & -0.1038 \end{pmatrix} \quad \mathbf{H}_3 = \begin{pmatrix} -0.2484 & -0.0095 \\ -1.1211 & 0.8255 \end{pmatrix}$$

Fig. 3.1 shows the signal constellations at the transmitter $\mathbf{s}^{(i)}$ (labeled by “+”-marker) and at the receiver $\mathbf{s}_R^{(i)} = \mathbf{H}_1 \mathbf{s}^{(i)}$ (labeled by “o”-marker) in the left plot. In the right plot three groups of bars can be seen: The right bar in each group indicates the squared distances at the transmitter and the left bar in each group shows the squared distances at the receiver. Both plots are drawn for the channel matrix \mathbf{H}_1 . As can be seen in Fig. 3.1, \mathbf{H}_1 is a well behaved channel since the distances at the transmitter and the receiver are almost equal. The signal constellation map is only rotated by the MIMO channel. This special MIMO channel behaves very similar to a SISO channel. Examples for well behaved MIMO channels are:

-) $\mathbf{H} = \mathbf{I}$: The signal constellation diagram remains unchanged: $\mathbf{y} = \mathbf{H}\mathbf{s} + \mathbf{n} = \mathbf{s} + \mathbf{n}$.
-) The channel matrix is a unitary matrix $\mathbf{H} = \mathbf{U}$: The signal constellation diagram is rotated, but the distances remain unchanged. Note that the channel used in Fig. 3.1 is almost unitary: $\mathbf{H}_1^H \mathbf{H}_1 \approx \mathbf{I}$. Then, the distance at the receiver results in: $d_{R,i,j}^2 = \mathbf{b}_{i,j}^H \mathbf{H}^H \mathbf{H} \mathbf{b}_{i,j} = \mathbf{b}_{i,j}^H \mathbf{U}^H \mathbf{U} \mathbf{b}_{i,j} = \mathbf{b}_{i,j}^H \mathbf{b}_{i,j} = d_{T,i,j}^2$.

Fig. 3.2 shows the signal constellations at the transmitter $\mathbf{s}^{(i)}$ (labeled by “+”-marker) and at the receiver $\mathbf{s}_R^{(i)} = \mathbf{H}_2 \mathbf{s}^{(i)}$ (labeled by “o”-marker) in the left plot. In the right plot three groups of bars can be seen. The right bar in each group indicates the squared distances at the transmitter and the left bar in each group shows the squared distances at the receiver. Both plots are drawn for the channel matrix \mathbf{H}_2 . In Fig. 3.2, it can be seen that due to the influence of the specific channel matrix \mathbf{H}_2 the signal constellation diagram is extremely distorted. The signal map is not only a rotation and scaling like in the SISO case. The signal configuration is completely changed. All transmit signal distances transfer to completely different distance values at the receiver! For example, the distance between the symbols $\mathbf{s}^{(1)}$ and $\mathbf{s}^{(4)}$ can even become zero, if two of the four channel coefficients vanish:

$$d_{R,1,2}^2 = \mathbf{b}_{1,2}^H \mathbf{H}^H \mathbf{H} \mathbf{b}_{1,2} = (0 \ 2)^* \mathbf{H}^H \mathbf{H} (0 \ 2)^T = 4(|h_{21}|^2 + |h_{22}|^2) = 0. \quad (3.13)$$

Due to the small values of h_{21} and h_{22} in the channel matrix \mathbf{H}_2 , the distance $d_{R,1,2}^2$ becomes very small: $d_{R,1,2}^2 = 4(|0.1989|^2 + |0.1038|^2) = 0.2013$ (see Fig. 3.2).

Fig. 3.3 shows the signal constellations at the transmitter $\mathbf{s}^{(i)}$ (labeled by “+”-marker) and at the receiver $\mathbf{s}_R^{(i)} = \mathbf{H}_3 \mathbf{s}^{(i)}$ (labeled by “o”-marker) in the left plot. In the right plot three groups of bars can be seen. The right bar in each group indicates the squared distances at the transmitter and the left bar in each group shows the squared distances at the receiver. Both plots are drawn for the channel matrix \mathbf{H}_3 . Interestingly, the largest distance at the transmitter (between $\mathbf{s}^{(1)}$ and $\mathbf{s}^{(4)}$, $d_{T,1,4}^2 = 8$), becomes the smallest distance at the receiver! This is an important peculiarity of the MIMO channel. Even worse, both entries of the symbol vectors $\mathbf{s}^{(1)}$ and $\mathbf{s}^{(4)}$ are different from each other, therefore this crossover event ($\mathbf{s}^{(1)} \rightarrow \mathbf{s}^{(4)}$) corresponds to a double error. For such double errors the distance between two signals at the receiver may even vanish, in spite of the fact that the power of every channel coefficient is far away from zero! It is sufficient that

$$d_{R,1,4}^2 = \mathbf{b}_{1,4}^H \mathbf{H}^H \mathbf{H} \mathbf{b}_{1,4} = (-2 \ -2)^* \mathbf{H}^H \mathbf{H} (-2 \ -2)^T = 4(|h_{11} + h_{12}|^2 + |h_{21} + h_{22}|^2) = 0, \quad (3.14)$$

such that this system shows catastrophic error performance! It is easy to see, how the channel coefficients have to be set up, in order to get zero distance $d_{R,1,4}^2$, namely: $h_{11} - h_{12} = 0$ and $h_{21} - h_{22} = 0$.

Summarizing the MIMO distance properties:

-) The signal constellation diagram may be heavily distorted, due to the matrix multiplication of the transmit signal vector with the channel matrix \mathbf{H} .
-) The largest distance at the transmitter may become the smallest distance at the receiver.
-) The distance at the receiver can be zero, even if the power of every channel coefficient is far away from zero.

Due to these facts a simple NNA is hard to derive and therefore in the following a simpler performance measure namely a union bound is derived.

3.3 Union Bound for the BER

In this section we focus on the derivation of a tight union bound for the BER in spatially uncorrelated and correlated MIMO channels. The essential derivations have already been published in [35]. First, we treat the general case and then an illustrative example will show some interesting details.

The union bound for the BER is simply calculated by summing up all PEPs. If the symbol vector \mathbf{s}_i is transmitted all crossover events are taken into account and thus the probability of deciding on an erroneous symbol vector can be upper bounded by:

$$P_\varepsilon(\mathbf{s} = \mathbf{s}_i) \leq \sum_{\substack{j=1 \\ j \neq i}}^{|\mathcal{A}|^{n_T}} \text{PEP}_{i,j}. \quad (3.15)$$

Actually, we are interested in the mean performance and not only in the performance if \mathbf{s}_i is transmitted. Averaging over all possible transmit symbols \mathbf{s}_i (Eqn. (3.15)) leads to:

$$\begin{aligned} P_\varepsilon &= \mathbb{E}_i \{P_\varepsilon(\mathbf{s} = \mathbf{s}_i)\} = \sum_{i=1}^{|\mathcal{A}|^{n_T}} P_\varepsilon(\mathbf{s} = \mathbf{s}_i) P(\mathbf{s}_i) = \frac{1}{|\mathcal{A}|^{n_T}} \sum_{i=1}^{|\mathcal{A}|^{n_T}} P_\varepsilon(\mathbf{s} = \mathbf{s}_i) \\ &\leq \frac{1}{|\mathcal{A}|^{n_T}} \sum_{i=1}^{|\mathcal{A}|^{n_T}} \sum_{\substack{j=1 \\ j \neq i}}^{|\mathcal{A}|^{n_T}} \text{PEP}_{i,j}. \end{aligned} \quad (3.16)$$

Note that Eqn. (3.16) implicitly assumes that the transmit symbol vectors occur equally likely ($P(\mathbf{s}_i) = 1/|\mathcal{A}|^{n_T}$). The right hand side of Eqn. (3.16) is the union bound for the vector symbol error probability. For arriving at the union bound for the BER, a further derivation step is necessary. For each crossover event $\mathbf{s}_i \rightarrow \mathbf{s}_j$ a different number of scalar symbols (note the difference to vector symbols) and thus a different number of information bits is erroneous. For this reason, a so-called weighting factor $\tilde{w}_{i,j}$ is introduced. This factor turns the vector symbol error probability into the BER, by counting the number of erroneous bits $n_{BE\ i,j}$ in the numerator and the number of transmitted bits per symbol vector $\text{ld}(|\mathcal{A}|) n_T$ in the denominator:

$$\tilde{w}_{i,j} = \frac{n_{BE\ i,j}}{\text{ld}(|\mathcal{A}|) n_T}. \quad (3.17)$$

Therefore, we get:

$$\text{BER} \leq \frac{1}{|\mathcal{A}|^{n_T}} \sum_{i=1}^{|\mathcal{A}|^{n_T}} \sum_{\substack{j=1 \\ j \neq i}}^{|\mathcal{A}|^{n_T}} \tilde{w}_{i,j} \text{PEP}_{i,j}. \quad (3.18)$$

The final essential task that is still to do, is the calculation of the $\text{PEP}_{i,j}$. As can be seen in Eqn. (3.7), the PEP is governed by the Euclidean distance at the receiver $d_{R\ i,j}^2$. Therefore, the statistics of the distance has to be calculated and then we average over the Gaussian Q-function with respect to the distance. To this end, a new random vector is defined:

$$\mathbf{u}_{i,j} = \mathbf{H}\mathbf{b}_{i,j}. \quad (3.19)$$

A linear transformation of a complex Gaussian random vector / matrix results again in a complex Gaussian random vector / matrix and therefore the random vector $\mathbf{u}_{i,j}$ is complex Gaussian distributed with the following first and second order moment:

$$\begin{aligned} \boldsymbol{\mu}_{\mathbf{u}_{i,j}} &= \mathbb{E}_{\mathbf{H}} \{\mathbf{H}\mathbf{b}_{i,j}\} = \mathbf{0}, \\ \mathbf{R}_{\mathbf{u}_{i,j}} &= \mathbb{E}_{\mathbf{H}} \{\mathbf{H}\mathbf{b}_{i,j}\mathbf{b}_{i,j}^H \mathbf{H}^H\}. \end{aligned} \quad (3.20)$$

Therefore, $\mathbf{u}_{i,j}$ can be modeled as:

$$\mathbf{u}_{i,j} = \sqrt{\mathbf{R}_{\mathbf{u}_{i,j}}} \mathbf{g}, \quad (3.21)$$

where \mathbf{g} is an independent complex Gaussian distributed vector of entries with zero mean and unit variance and $\mathbf{R}_{\mathbf{u}_{i,j}}$ reflects the spatial correlation of the channel matrix \mathbf{H} . Then $d_{R i,j}^2$ can be written as:

$$d_{R i,j}^2 = \mathbf{u}_{i,j}^H \mathbf{u}_{i,j} = \mathbf{g}^H \mathbf{R}_{\mathbf{u}_{i,j}} \mathbf{g}. \quad (3.22)$$

In the following case spatially uncorrelated MIMO channels and spatially correlated MIMO channels are considered separately.

3.3.1 Spatially Uncorrelated Channels

For uncorrelated channels, $\mathbf{R}_{\mathbf{u}_{i,j}}$ degenerates to a scaled unity matrix:

$$\mathbf{R}_{\mathbf{u}_{i,j}} = \mathbf{b}_{i,j} \mathbf{b}_{i,j}^H \mathbf{I}_{n_R}, \quad (3.23)$$

where \mathbf{I}_{n_R} is the unity matrix of dimension n_R . Hence, Eqn. (3.22) simplifies to:

$$d_{R i,j}^2 = d_T^2 i,j \left(|g_1|^2 + |g_2|^2 + \dots + |g_{n_R}|^2 \right). \quad (3.24)$$

The sum over n_R squared magnitudes of independent complex Gaussian random variables with the same variance $d_T^2 i,j$ is a new χ^2 distributed random variable with $2n_R$ degrees of freedom. Thus, the Probability Density Function (PDF) of $d_{R i,j}^2$ is:

$$p_{d_{R i,j}^2}(\xi) = \frac{\xi^{n_R-1}}{(d_T^2 i,j)^{n_R} \Gamma(n_R)} e^{-\frac{\xi}{d_T^2 i,j}}. \quad (3.25)$$

Now, we know the PDF of the squared Euclidean distance $d_{R i,j}^2$ at the receiver, but actually we are interested in the mean error performance. The mean PEP is calculated as:

$$\begin{aligned} \text{PEP}_{i,j}^{\text{i.i.d.}} &= \mathbb{E}_{\mathbf{H}} \left\{ Q \left(\sqrt{\frac{d_{R i,j}^2}{2\sigma_n^2}} \right) \right\} = \int_0^\infty Q \left(\sqrt{\frac{\xi}{2\sigma_n^2}} \right) \frac{\xi^{n_R-1}}{(d_T^2 i,j)^{n_R} \Gamma(n_R)} e^{-\frac{\xi}{d_T^2 i,j}} d\xi \\ &= \left(\frac{1 - \mu_{i,j}}{2} \right)^{n_R} \sum_{k=0}^{n_R-1} \binom{n_R-1+k}{k} \left(\frac{1 + \mu_{i,j}}{2} \right)^k \quad \text{with} \quad \mu_{i,j} = \sqrt{\frac{d_T^2 i,j}{4\sigma_n^2 + d_T^2 i,j}}. \end{aligned} \quad (3.26)$$

The superscript i.i.d. is used to distinguish the PEPs for uncorrelated and correlated channels. The integral is taken from [36]. As it can be seen in Eqn. (3.26), apart from n_R , the only essential parameter, which determines the PEP is $d_T^2 i,j$. Investigating $d_T^2 i,j$ for all crossover events can help to simplify the summation in Eqn. (3.18).

Definition 3.1 A so-called Error Type (ET) is defined as the set of all crossover events of transmit vectors, which have the same key-parameters. Key-parameters are entities, which fully describe the properties of crossover events and thus the corresponding ET. The key-parameters of an ET are $d_T^2 i,j$ and $n_{BE i,j}^2$ for the uncorrelated case. (The key-parameter for the correlated case are the set of eigenvalues $\lambda_m^{(i,j)}$ and $n_{BE i,j}^2$ (defined further ahead).) Therefore an ET is fully described by these two parameters and they do not depend on the crossover event itself. Therefore, new indices are introduced for each ET indexed by k : d_k^2 and $n_{BE k}^2$. The number of crossover events belonging to the ET k , which fulfill the conditions $d_k^2 = d_T^2 i,j$ and $n_{BE k}^2 = n_{BE i,j}^2$, is denoted by f_k .

At this point, it may be useful to concretize these definitions by means of a simple example. Let's consider a 4×4 MIMO system with BPSK modulation (+1,-1).

For the moment, let us consider a single antenna system focusing on the modulation format. The difference variable is $b_{i,j} = s_i - s_j$ and thus the squared distance at the transmitter is $d_{T i,j}^{2(BPSK)} = b_{i,j}^* b_{i,j}$. For BPSK $d_{T i,j}^{2(BPSK)}$ is either 0 or 4. In case of a single transmit antenna and BPSK the corresponding number of bit errors is either 0 or 1. In Tab. 3.1 the key - parameters of a single antenna system with BPSK modulation are listed. Note, that there are two different symbols (+1,-1) and thus the total number

$ET_k^{(BPSK)}$	$d_{T k}^{2(BPSK)}$	$f_k^{(BPSK)}$	$n_{BE k}^{(BPSK)}$
$ET0^{(BPSK)}$	0	2	0
$ET1^{(BPSK)}$	4	2	1

Table 3.1: ET table for a single antenna system with BPSK modulation.

of crossover events is $2 \cdot 2 = 4$, which can also be identified in Tab. 3.1 as the sum over the column values $f_k^{(BPSK)}$.

Having shown the ETs in a system with one transmit antenna and BPSK modulation³, the ETs of a system with four transmit antennas are analyzed in the following by means of combinatorics. Due to 4 transmit antennas the key-parameters of the ETs can be calculated as:

$$\begin{aligned}
 d_{T k}^2 &= \mathbf{b}_{i,j}^H \mathbf{b}_{i,j} = b_{i,j}(1)^* b_{i,j}(1) + b_{i,j}(2)^* b_{i,j}(2) + b_{i,j}(3)^* b_{i,j}(3) + b_{i,j}(4)^* b_{i,j}(4) \\
 &= d_{T k}^{2(BPSK)}(1) + d_{T k}^{2(BPSK)}(2) + d_{T k}^{2(BPSK)}(3) + d_{T k}^{2(BPSK)}(4) \\
 f_k &= p_k \cdot \left(f_k^{(BPSK)}(1) \cdot f_k^{(BPSK)}(2) \cdot f_k^{(BPSK)}(3) \cdot f_k^{(BPSK)}(4) \right) \\
 n_{BE k} &= n_{BE k}^{(BPSK)}(1) + n_{BE k}^{(BPSK)}(2) + n_{BE k}^{(BPSK)}(3) + n_{BE k}^{(BPSK)}(4). \tag{3.27}
 \end{aligned}$$

p_k is defined further ahead. $d_{T k}^{2(BPSK)}(l) = b_{i,j}(l)^* b_{i,j}(l)$ is the distance corresponding to the l -th transmit antenna. $n_{BE k}^{(BPSK)}(l)$ is the number of bit errors and $f_k^{(BPSK)}(l)$ the frequency of the k -th BPSK-ET corresponding to the l -th transmit antenna and thus to the l -th position in $\mathbf{b}_{i,j}$. The equations above show the calculation of the key-parameters for a system with four transmit antennas (Tab. 3.2) based on the key-parameters of the system with one transmit antenna (Tab. 3.1). In Eqn. (3.27), there are five possible values for $d_{T k}^2$ namely 0, 4, 8, 12 and 16, which are caused by crossover events having no symbol error, one symbol error, two symbol errors, three symbol errors and four symbol errors. Note that the ‘‘positions’’ of the non-zero entries (erroneous symbols) in vector $\mathbf{b}_{i,j}$ are not relevant in the i.i.d. case, i.e., for example $\mathbf{b}_{i,j} = (0020)$ and $\mathbf{b}_{i,j} = (2000)$ are equivalent. One question is still open, namely how often a specific error constellation occurs. This can be answered by the aid of binomial coefficients. Due to the four transmit antennas, there are four transmit symbols, which can be correctly detected ($b_{i,j}(l) = 0$, $ET0^{(BPSK)}$) or wrongly detected ($b_{i,j}(l) = \pm 2$, $ET1^{(BPSK)}$). Hence, from the combinatorics point of view, there are four possible positions in vector $\mathbf{b}_{i,j}$ to ‘‘place’’ $b_{i,j}(l) = 0$ (corresponding to $ET0^{(BPSK)}$) or $b_{i,j}(l) = \pm 2$ (corresponding to $ET1^{(BPSK)}$) (Tab. 3.1). How often $b_{i,j}(l) = 0$ ($ET0^{(BPSK)}$) occurs on these four possible positions in vector $\mathbf{b}_{i,j}$ is denoted by n_k and thus the number of possible constellations p_k having n_k times $b_{i,j}(l) = 0$ ($ET0^{(BPSK)}$) arranged over the four possible positions of $\mathbf{b}_{i,j}$ is denoted by p_k and can be calculated with:

$$p_k = \binom{4}{n_k} = \frac{4!}{n_k! (4 - n_k)!} \tag{3.28}$$

³In the following called BPSK-ETs.

For $d_{T,k}^2$ equal to 0 all symbols must be correctly detected and therefore each position in vector $\mathbf{b}_{i,j}$ is $b_{i,j}(l) = 0$ corresponding $\text{ET0}^{(BPSK)}$. Thus, there is only one possibility to arrange four times $b_{i,j}(l) = 0$ ($\text{ET0}^{(BPSK)}$) on four possible positions ($n_0 = 4$):

$$p_0 = \binom{4}{4} = 1. \quad (3.29)$$

For $d_{T,1}^2$ equal to 4, one symbol is detected erroneously $b_{i,j}(l) = \pm 2$ ($\text{ET1}^{(BPSK)}$) and the other symbols must be correct $b_{i,j}(l) = 0$ ($\text{ET0}^{(BPSK)}$). Thus, $n_1 = 3$ and the possible number of constellations to arrange three times $b_{i,j}(l) = 0$ ($\text{ET0}^{(BPSK)}$) on four possible positions is:

$$p_1 = \binom{4}{3} = 4. \quad (3.30)$$

For the remaining distances $d_{T,k}^2$ equal to 8, 12 and 16 the number of possible constellations are:

$$p_3 = \binom{4}{2} = 6 \quad p_4 = \binom{4}{1} = 4 \quad p_5 = \binom{4}{0} = 1 \quad (3.31)$$

Note that each of the two BPSK-ETs have frequency $f_k^{(BPSK)}=2$ and therefore the total frequency of having a specific constellation of $b_{i,j}(l)$ (BPSK-ETs) in vector $\mathbf{b}_{i,j}$, i.e., for example the first position of the difference vector $\mathbf{b}_{i,j}$ is $b_{i,j}(1) = 0$ corresponds to $\text{ET0}^{(BPSK)}$, the second is $b_{i,j}(2) = \pm 2$ ($\text{ET1}^{(BPSK)}$), the third is $b_{i,j}(3) = \pm 2$ ($\text{ET1}^{(BPSK)}$) and the fourth is $b_{i,j}(4) = 0$ ($\text{ET0}^{(BPSK)}$), is $2 \cdot 2 \cdot 2 \cdot 2 = 16$. This resulting frequency has to be multiplied with the number of possible constellations p_k (according to Eqn. (3.27)) of the BPSK-ETs leading to the same overall distance $d_{T,k}^2$ and to the same number of bit errors n_{BEk} . Thus, for example the resulting entire frequency f_2 of ET2 is $6 \cdot 16 = 96$. The total list of key-parameters for the four antenna systems is:

ET k	$d_{T,k}^2$	f_k	n_{BEk}
ET0	0	16	0
ET1	4	64	1
ET2	8	96	2
ET3	12	64	3
ET4	16	16	4

Table 3.2: ET table for a uncoded MIMO system. uncorrelated fading; BPSK; $n_T = 4$.

The above explained way of finding Tab. 3.2 seems to be rather complicated but it is actually very simple. To substantiate the general explanations, I will now show the detailed calculations for ET2 given in Tab. 3.2. To get a distance $d_{T,2}^2$ equal to 8, two symbols in the transmit symbol vectors \mathbf{s}_i and \mathbf{s}_j have to be different. Therefore, the corresponding difference vector $\mathbf{b}_{i,j}$ consists of two zeros and two non-zero terms of value two. The positions of these values in the vector $\mathbf{b}_{i,j}$ are irrelevant.

First, let's calculate the number n_{BE} of bit errors in case of ET2. Due to Gray coding of the symbols, two erroneous symbols lead to two erroneous bit and thus $n_{BE2} = 2$ (see Tab. 3.2).

Secondly, the frequency f_2 of crossover events, which have the same distance $d_{T,2}^2 = 8$ and the same number of bit errors n_{BE2} is calculated. Due to the BPSK modulation, we know that each of the two BPSK-ETs of Tab. 3.1 has the frequency $f_2^{(BPSK)} = 2$. Thus, a specific constellation of $b_{i,j}(l)$, i.e., for example the first position of the difference vector $\mathbf{b}_{i,j}$ is $b_{i,j}(1) = 0$ corresponding to $\text{ET0}^{(BPSK)}$, the second is $b_{i,j}(2) = \pm 2$ ($\text{ET1}^{(BPSK)}$), the third is $b_{i,j}(3) = \pm 2$ ($\text{ET1}^{(BPSK)}$) and the fourth is $b_{i,j}(4) = 0$ ($\text{ET0}^{(BPSK)}$), has the frequency $2 \cdot 2 \cdot 2 \cdot 2 = 16$. (According to the expression in the brackets of the

second equation in Eqn. (3.27). The number of possible arrangements p_2 of $b_{i,j}(l)$ (BPSK-ETs) in the difference vector $\mathbf{b}_{i,j}$, which leads to $d_{T,2}^2 = 8$ and $n_{BE2} = 2$, results in:

$$p_2 = \binom{4}{2} = 6. \quad (3.32)$$

The number of possible arrangements p_2 of $b_{i,j}(l)$ (BPSK-ETs) multiplied by the frequency of one $b_{i,j}(l)$ (BPSK-ETs) arrangement results in the entire frequency for ET2: $f_2 = 16 \cdot 6 = 96$ (according to Eqn. (3.27)).

The sum over all frequency values f_k in Tab. 3.2 is 256, which is equal to the total number of crossover events, because with BPSK modulation and $n_T = 4$ the number of different transmit vectors is $2^4 = 16$ and thus the number of crossover events is $16^2 = 256$.

Note that matters become more difficult if a higher modulation format is applied. In such a case the combinatorial problem to find the ETs and the corresponding key-parameters can be solved by means of multinomial coefficients [42].

An alternative way to find the table of ETs is an exhaustive computer search. This search should also be subdivided in the two parts discussed above. First focusing on the investigation of the ETs for a system with one transmit antenna and afterwards applying this knowledge to the case with more transmit antennas. In this way a lot of computation time is saved, due to the symmetries of the signal constellation maps. Nevertheless, the effort of the search can be very high, if higher modulation schemes are involved. Think of an $n_T = 4$ system with 256QAM modulation, where $256^4 \cdot 256^4 = 256^8 \approx 1.8447 \cdot 10^{19}$ crossover events exist. For such cases the first step (investigation of the ETs for a system with one transmit antenna) can be very helpful.

Summing up the PEPs for all crossover events results in the double sum in Eqn. (3.18). Due to the introduction of the ETs, the summation over all crossover events can be reduced to the sum over all ETs and thus Eqn. (3.18) reduces to:

$$\text{BER} \leq \sum_{k=1}^{n_{ET}} w_k \text{PEP}_k^{\text{i.i.d.}} \quad \text{with} \quad w_k = \frac{f_k}{|\mathcal{A}|^{n_T} \text{ld}(|\mathcal{A}|) n_T}. \quad (3.33)$$

where PEP_k denotes the PEP for the k -th ET and n_{ET} is the number of distinct ETs. In the special case shown above, n_{ET} is 4. ET0 is not counted as an error type since it corresponds to a correct detection.

By applying Eqn. (3.33), the union bound for the BER for the specific example summarized in Tab. 3.2 can be written as:

$$\begin{aligned} \text{BER} &\leq \sum_{k=1}^{n_{ET}} w_k \text{PEP}_k^{\text{i.i.d.}} \\ &= \frac{64}{2^4 \text{ld}(2)} \frac{1}{4} \text{PEP}_1^{\text{i.i.d.}} + \frac{96}{2^4 \text{ld}(2)} \frac{2}{4} \text{PEP}_2^{\text{i.i.d.}} + \frac{64}{2^4 \text{ld}(2)} \frac{3}{4} \text{PEP}_3^{\text{i.i.d.}} + \frac{16}{2^4 \text{ld}(2)} \frac{4}{4} \text{PEP}_4^{\text{i.i.d.}} \\ &= \text{PEP}_1^{\text{i.i.d.}} + 3 \text{PEP}_2^{\text{i.i.d.}} + 3 \text{PEP}_3^{\text{i.i.d.}} + \text{PEP}_4^{\text{i.i.d.}}. \end{aligned} \quad (3.34)$$

The union bound derived in this section, is compared to simulation results for several MIMO systems and modulation formats in Sec. 3.4.

3.3.2 Spatially Correlated Channels

For spatially correlated channels (correlation characterized by the W-channel model) the correlation matrix $\mathbf{R}_{\mathbf{u}_{i,j}}$ defined in Eqn. (3.20) can be written as:

$$\mathbf{R}_{\mathbf{u}_{i,j}} = E_{\mathbf{H}} \left\{ \mathbf{H} \mathbf{b}_{i,j} \mathbf{b}_{i,j}^H \mathbf{H}^H \right\} = \mathbf{U}_R E_{\mathbf{H}} \left\{ (\tilde{\mathbf{\Omega}} \odot \mathbf{G}) \mathbf{U}_T^T \mathbf{b}_{i,j} \mathbf{b}_{i,j}^H \mathbf{U}_T^* (\tilde{\mathbf{\Omega}} \odot \mathbf{G})^H \right\} \mathbf{U}_R^H$$

$$= \mathbf{U}_R \text{diag}(\lambda_1^{(i,j)}, \lambda_2^{(i,j)}, \dots, \lambda_{n_R}^{(i,j)}) \mathbf{U}_R^H, \quad (3.35)$$

and the eigenvalues can be calculated as:

$$\lambda_m^{(i,j)} = \left((\mathbf{b}_{i,j}^T \mathbf{U}_T) \odot \mathbf{\Omega}_m \right) \mathbf{U}_T^H \mathbf{b}_{i,j}^*, \quad (3.36)$$

where $\mathbf{\Omega}_m$ denotes the m -th row of the power coupling matrix $\mathbf{\Omega}$. The number of non zero eigenvalues of $\mathbf{R}_{\mathbf{u}_{i,j}}$ is denoted by n_{NZ} . Hence, in the correlated case Eqn. (3.22) changes to:

$$d_{R,i,j}^2 = |g_1|^2 \lambda_1^{(i,j)} + |g_2|^2 \lambda_2^{(i,j)} + \dots + |g_{n_{NZ}}|^2 \lambda_{n_{NZ}}^{(i,j)}. \quad (3.37)$$

The sum over independent random variables corresponds to the product of the characteristic functions [27]. Since the random variables $|g_i|^2$ follow a χ^2 -distribution with two degrees of freedom, the characteristic function of $d_{R,i,j}^2$ is

$$\Psi_{d_{R,i,j}^2}(j\omega) = \prod_{m=1}^{n_{NZ}} \frac{1}{1 - j\omega \lambda_m^{(i,j)}}. \quad (3.38)$$

Applying a partial fraction expansion of Eqn. (3.38), the PDF of $d_{R,i,j}^2$ is easily obtained by the inverse Fourier transform of $\Psi_{d_{R,i,j}^2}(-j\omega)$, resulting in:

$$p_{d_{R,i,j}^2}(\xi) = \sum_{m=1}^{n_{NZ}} \frac{(\lambda_m^{(i,j)})^{n_{NZ}-2}}{\prod_{\substack{n=1 \\ n \neq m}}^{n_{NZ}} (\lambda_m^{(i,j)} - \lambda_n^{(i,j)})} e^{-\frac{\xi}{\lambda_m^{(i,j)}}}. \quad (3.39)$$

Note that for the partial fraction expansion it is assumed that all eigenvalues are different, which is indeed the case for ‘‘measured’’ power coupling matrices $\mathbf{\Omega}$, but can eventually be a problem for synthetic $\mathbf{\Omega}$ matrices. Then, with Eqn. (3.7) the mean PEP results in:

$$\begin{aligned} \text{PEP}_{i,j}^W &= \mathbf{E}_{\mathbf{H}} \left\{ Q \left(\sqrt{\frac{d_{R,i,j}^2}{2\sigma_n^2}} \right) \right\} = \sum_{m=1}^{n_{NZ}} \frac{(\lambda_m^{(i,j)})^{n_{NZ}-2}}{\prod_{\substack{n=1 \\ n \neq m}}^{n_{NZ}} (\lambda_m^{(i,j)} - \lambda_n^{(i,j)})} \int_0^\infty Q \left(\sqrt{\frac{\xi}{2\sigma_n^2}} \right) e^{-\frac{\xi}{\lambda_m^{(i,j)}}} d\xi \\ &= \frac{1}{2} \sum_{m=1}^{n_{NZ}} \frac{(\lambda_m^{(i,j)})^{n_{NZ}-1}}{\prod_{\substack{n=1 \\ n \neq m}}^{n_{NZ}} (\lambda_m^{(i,j)} - \lambda_n^{(i,j)})} \left(1 - \sqrt{\frac{\lambda_m^{(i,j)}}{4\sigma_n^2 + \lambda_m^{(i,j)}}} \right). \end{aligned} \quad (3.40)$$

The integral has the same structure as the integral in Eqn. (3.26). As it can be seen in Eqn. (3.40) the relevant parameters, which influence the PEP are the eigenvalues $\lambda_m^{(i,j)}$ ($m=1, 2, \dots, n_{NZ}$). Therefore, in principle we continue in the same way as in the case of an uncorrelated channel: Again, we list all ETs with their key-parameters in a new table quite similar to Tab. 3.2. The only difference is that there are now n_{NZ} parameters $\lambda_m^{(i,j)}$ ($m=1, 2, \dots, n_{NZ}$) instead of the single parameter $d_{T,k}^2$. In the correlated case of the 4×4 MIMO system with BPSK modulation, there are 40 ETs ($n_{ET} = 40$) and therefore the table is postponed to the Appendix E. Due to the dependency of the eigenvalues $\lambda_m^{(i,j)}$ on the power coupling matrix $\mathbf{\Omega}$ (Eqn. (3.36)), the tables listing the ETs and their corresponding key-parameters are different for distinct spatially correlated channels. Note that this table shown in Appendix E has been found by an exhaustive computer search.

The union bound for the BER, taking into account all 256 crossover events, again can be written as the weighted sum over all ETs:

$$\text{BER} \leq \sum_k^{n_{ET}} w_k \text{PEP}_k^W \quad w_k = \frac{f_k}{|\mathcal{A}|^{n_T}} \frac{n_{BEk}}{\text{Id}(|\mathcal{A}|) n_T}. \quad (3.41)$$

The union bound derived in this section, is compared to simulation results for several MIMO systems and modulation formats in Sec. 3.4.

3.3.3 High SNR Approximation of the BER

In order to get more insight into the BER performance and to compare the results for uncorrelated and correlated channels, it is helpful to derive a high SNR approximation for the PEPs. With these approximations for the PEPs, a high SNR approximation for the union bound for the BER can be calculated. This approximation highlights the importance of the diversity degree and quantifies the power loss due to channel correlation.

First, we focus on the PEP. The principle of calculating a high SNR (low σ_n^2) approximation is quite simple. Essentially, a Taylor series expansion of the PEP formula is performed. The first term of the series, which dominates at high SNR is taken as an approximation of the true PEP.

Remember the Taylor series of a function $f(x)$ around the point x_0 is defined as:

$$f(x) = \sum_{n=0}^{\infty} \frac{(x - x_0)^n f^{(n)}(x_0)}{n!}, \quad (3.42)$$

where the superscript (n) denotes the n -th derivative of $f(x)$. The PEP for the i.i.d. model and for the W-model are functions of σ_n^2 and therefore at high SNR the PEPs are approximated around $\sigma_n^2 = 0$. For small σ_n^2 , the first non-zero term of the Taylor series, i.e., the term with the lowest exponent, is the most important one. In the following we consider uncorrelated and correlated channels separately.

3.3.3.1 Spatially Uncorrelated Channels at high SNR

Investigating the PEP for uncorrelated channels it turns out that the first non-zero term of the Taylor series has the exponent n_R and thus the high SNR approximation of the PEP can be calculated as:

$$\text{PEP}_{i,j}^{i.i.d.-high} = \frac{(\sigma_n^2)^{n_R}}{n_R!} \left(\frac{\partial^{n_R} \text{PEP}_{i,j}^{i.i.d.}}{\partial (\sigma_n^2)^{n_R}} \right) \Big|_{\sigma_n^2=0} = \left(\frac{\sigma_n^2}{d_{T,i,j}^2} \right)^{n_R} \underbrace{\sum_{k=0}^{n_R-1} \binom{n_R-1+k}{k}}_{(1/c_{n_R})^{n_R}} = \left(\frac{\sigma_n^2}{d_{T,i,j}^2 c_{n_R}} \right)^{n_R} \quad (3.43)$$

with

$$c_{n_R} = \left[\sum_{k=0}^{n_R-1} \binom{n_R-1+k}{k} \right]^{-1/n_R} \quad (3.44)$$

Due to Eqn. 3.43 the PEP mainly depends on n_R and $d_{T,i,j}^2$. n_R determines the slope and $d_{T,i,j}^2 c_{n_R}$ determines the horizontal shift of the PEP vs. SNR curve. Thus, it is easy to specify the diversity D of such an uncoded MIMO system. Diversity D is defined as the negative slope of the PEP vs. SNR curve (in double logarithmic scale) according to [27]:

$$D = - \lim_{\text{SNR} \rightarrow \infty} \frac{\partial(\log_{10} \text{PEP})}{\partial(\log_{10} \text{SNR})}, \quad (3.45)$$

where the SNR is inversely proportional to the noise variance σ_n^2 (see Eqn. (2.17)). Therefore, the slope for the PEP vs. SNR is the negative slope of the PEP vs. σ_n^2 and we get:

$$D_{i.i.d.} = \lim_{\sigma_n^2 \rightarrow 0} \frac{\partial(\log_{10} \text{PEP}_{i,j}^{i.i.d.-high})}{\partial(\log_{10} \sigma_n^2)} = n_R. \quad (3.46)$$

Note that in the derivation of Eqn. (3.46) the high SNR approximation for the PEP is used.

A high SNR approximation for the union bound for the BER is easily obtained by inserting the high SNR approximation of the PEP into Eqn. (3.33):

$$\text{BER}^{i.i.d.-high} \leq \sum_{k=1}^{n_{ET}} w_k \left(\frac{\sigma_n^2}{d_{T,k}^2 c_{n_R}} \right)^{n_R} = (\sigma_n^2)^{n_R} \sum_{k=1}^{n_{ET}} \frac{w_k}{(d_{T,k}^2 c_{n_R})^{n_R}}. \quad (3.47)$$

By defining a new distance:

$$d_{i.i.d.}^2 = \frac{1}{n_R \sqrt[n_{ET}]{\sum_{k=1}^{n_{ET}} \frac{w_k}{(d_{T,k}^2 c_{n_R})^{n_R}}}}, \quad (3.48)$$

the high SNR approximation for the union bound for the BER can be written as:

$$\text{BER}^{i.i.d.-high} = \left(\frac{\sigma_n^2}{d_{i.i.d.}^2} \right)^{n_R}, \quad (3.49)$$

For the high SNR approximation of the union bound for the BER the same properties as for the high SNR approximation for the PEP are valid, i.e., the slope of the BER vs. SNR curve and thus the diversity is n_R and the horizontal position of the curve is determined by $d_{i.i.d.}^2$.

3.3.3.2 Spatially Correlated Channels at high SNR

In this section essentially the same derivation as for the uncorrelated case is done for correlated channels. Investigating the PEP, it turns out that the first non-zero term of the Taylor series has the exponent n_{NZ} and thus the high SNR approximation of the PEP results in:

$$\text{PEP}_{i,j}^{W-high} = \frac{(\sigma_n^2)^{n_{NZ}}}{n_{NZ}!} \left(\frac{\partial^{n_{NZ}} \text{PEP}_{i,j}^W}{\partial (\sigma_n^2)^{n_{NZ}}} \right) \Big|_{\sigma_n^2=0} = \left(\frac{\sigma_n^2}{d_{W,i,j}^2} \right)^{n_{NZ}} \underbrace{\sum_{k=0}^{n_{NZ}-1} \binom{n_{NZ}-1+k}{k}}_{(1/c_{n_{NZ}})^{n_{NZ}}} = \left(\frac{\sigma_n^2}{d_{W,i,j}^2 c_{n_{NZ}}} \right)^{n_{NZ}}, \quad (3.50)$$

with

$$c_{n_{NZ}} = \left[\sum_{k=0}^{n_{NZ}-1} \binom{n_{NZ}-1+k}{k} \right]^{-1/n_{NZ}} \quad (3.51)$$

and a new effective distance $d_{W,i,j}^2$:

$$d_{W,i,j}^2 = n_{NZ} \sqrt[n_{NZ}]{\prod_{m=1}^{n_{NZ}} \lambda_m^{(i,j)}} = n_{NZ} \sqrt{\det(\mathbf{R}_{\mathbf{u}_{i,j}})}, \quad (3.52)$$

The PEP mainly depends on n_{NZ} and the geometrical mean of the eigenvalues $\lambda_m^{(i,j)}$ ($l=1,2, \dots, n_{NZ}$). The last part of Eqn. (3.52) only holds if $\mathbf{R}_{\mathbf{u}_{i,j}}$ is regular, otherwise the determinant is zero. n_{NZ} determines the slope and $d_{W,i,j}^2$ and the $\lambda_m^{(i,j)}$ determine the horizontal position of the PEP curves. Thus, according to [27] the diversity D_W of such an uncoded MIMO system in correlated fading is:

$$D_W = \lim_{\sigma_n^2 \rightarrow 0} \frac{\partial(\log_{10} \text{PEP}_{i,j}^{W-high})}{\partial(\log_{10} \sigma_n^2)} = n_{NZ}. \quad (3.53)$$

A high SNR approximation of the BER union bound is easily obtained by inserting the high SNR approximation of the PEP (Eqn. (3.50)) into Eqn. (3.41). By defining a new distance $d_{W,i,j}^2$ the high SNR

approximation of the union bound for the BER results in:

$$\text{BER}^{W\text{-high}} = \left(\frac{\sigma_n^2}{d_W^2} \right)^{n_{NZ}} \quad \text{with} \quad d_W^2 = \frac{1}{n_{NZ} \sqrt{\sum_{k=1}^{n_{ET}} \frac{w_k}{(d_{Wk}^{c_{NZ}})^{n_{NZ}}}}} . \quad (3.54)$$

The high SNR approximation of the BER - union bound has the same properties as the high SNR approximation for the PEP, i.e., the slope of the BER vs. SNR curve and thus the diversity is n_{NZ} and the horizontal position of the BER vs. SNR curve is determined by d_W^2 .

3.3.4 Discussion

At this point, I want to emphasize the differences and similarities of the performance of uncoded wireless transmission systems in uncorrelated and in correlated MIMO channels. One very interesting observation is the fact that the diversity order, that is the slope of the BER vs. SNR curve at high SNR according to the definition in [27], is the same for correlated and uncorrelated channels in case of $n_{NZ} = n_R$. This holds, if at least one element in each row of $\mathbf{\Omega}$ is non-zero. If one row is completely filled with zeros, then a diversity loss of order one is observed, two zero-rows in $\mathbf{\Omega}$ cause a diversity loss of two and so on. Hence, a diversity loss L_D due to correlation is defined as

$$L_D = n_R - n_{NZ} . \quad (3.55)$$

Note that the diversity definition in [27] is tailored to high SNR and therefore does not say much about the observed diversity or slope of the BER vs. SNR curve at moderate values of SNR. Actually, the slope of the BER vs. SNR curve at reasonable SNR values (or BER values) is of more practical interest than the slope at $\text{SNR}=\infty$. Nevertheless, with the definition according to [27], correlated and uncorrelated MIMO channels have the same diversity order (if $n_{NZ} = n_R$).

For correlated channels with $n_{NZ} = n_R$ no diversity loss occurs. However, the detrimental influence of spatial channel correlation shows up in a so-called power loss L_P . Due to the same diversity, the BER vs. SNR curves of correlated and uncorrelated channels are in parallel, but horizontally shifted. This shift of the BER curve towards higher SNR due to channel correlation is called power loss L_P and can easily be calculated as:

$$L_P = 10 \log_{10} \left(\frac{d_{i.i.d.}^2}{d_W^2} \right) . \quad (3.56)$$

A simple explanation how the spatial channel correlation and thus the matrix $\mathbf{\Omega}$ influences the **diversity loss** is given above. The influence of the matrix $\mathbf{\Omega}$ on the **power loss** is not that simple to explain. In the following I will show what properties the matrix $\mathbf{\Omega}$ should have, to achieve a power loss as small as possible. Due to Eqn. (3.54) the distance d_{Wk}^2 for each ET should be as large as possible. To get large distances, it is important to have well balanced and large eigenvalues $\lambda_m^{(i,j)}$. This is achieved, if the matrix $\mathbf{\Omega}$ is well balanced. This corresponds to large signal distances and thus to small power losses. The best balanced matrix $\mathbf{\Omega}$ is a matrix, where all entries are identical. With such an ideally balanced matrix $\mathbf{\Omega}$, the W-model degenerates to the i.i.d. model. In this case, there is no spatial correlation and thus the best possible system performance (no power loss) is achieved.

3.4 Examples and further Discussion

In this section the simulated BER performance, the union bound for the BER performance and the high SNR approximation of the BER performance is shown for several MIMO systems, for various modulation formats and for some correlation types.

3.4.1 Uncoded 4×4 MIMO system with BPSK modulation

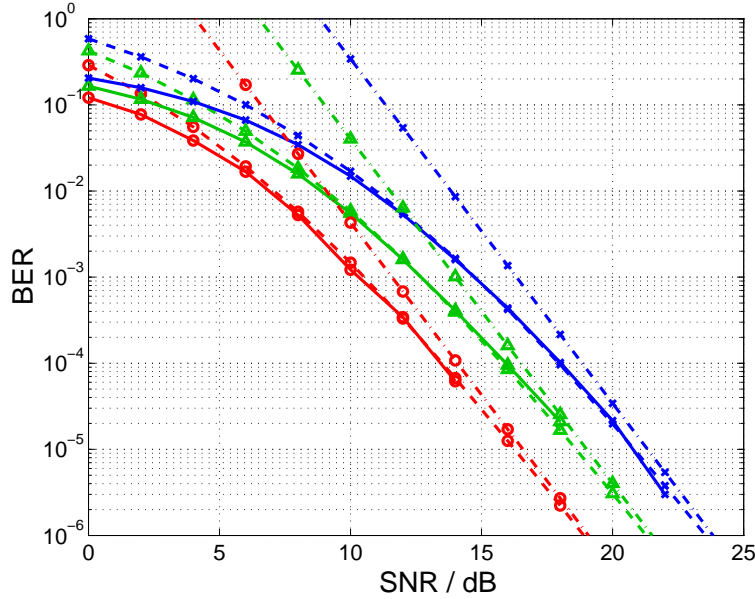


Figure 3.4: BER vs. SNR performance of an uncoded 4×4 MIMO system with BPSK modulation.

Starting with the 4×4 MIMO system with BPSK modulation, the simulated BER vs. SNR curve is compared with the union bound and the high SNR approximation for different correlation types (uncorrelated, 1D3, 14D3) in Fig. 3.4.

In Fig. 3.4 the simulated BER vs. SNR curves are the solid lines, the union bounds are the dashed lines and the dashed-dotted lines are the high SNR approximations. The red curves (labeled by \circ -marker) correspond to uncorrelated channels, the green curves (labeled by \triangle -marker) correspond to the moderate correlation scenario 1D3 and the blue curves (labeled by \times -marker) correspond to the high correlation scenario 14D3.

A comparison of the simulation results with the union bounds shows that the bounds are tight for BER values of approximately 10^{-2} and below. On the other hand, the high SNR approximations are tight only at BERs below approximately 10^{-6} .

3.4.1.1 Performance degradation due to spatial correlation

The high SNR approximations according to Eqn. (3.49) and (3.54), shown in Fig. 3.4 are far away from the true performance at moderate SNR values, but at very high SNR even these approximations become tight and thus they are good indicators for the slope and the horizontal shift of the BER vs. SNR curves and thus for the diversity order and the coding gain (or power loss) of specific transmission schemes. Even in the case of high spatial correlation the matrices Ω have no rows filled with zeros only and thus

the slope of the BER vs. SNR curves are always equal to n_R . The only detrimental influence of spatial correlation is a power loss, which can be calculated with Eqn. (3.56). The power loss for the BER vs. SNR curve corresponding to correlation scenario 1D3 is 2.43dB and for 14D3 it is 4.75dB at high SNR. These values also show up in Fig. 3.4.

3.4.1.2 Tightness of the union bound

In the following I will explain, why the union bound is strictly above the true BER performance at low SNR and why it is so tight at high SNR. Let's focus on the simple example first discussed in Sec. 3.2.2. To simplify matters further, an ideal channel matrix is assumed that does not change the signal constellation map and thus the error performance only depends on the noise: $\mathbf{y} = \mathbf{s} + \mathbf{n}$. The ML-receiver decides in

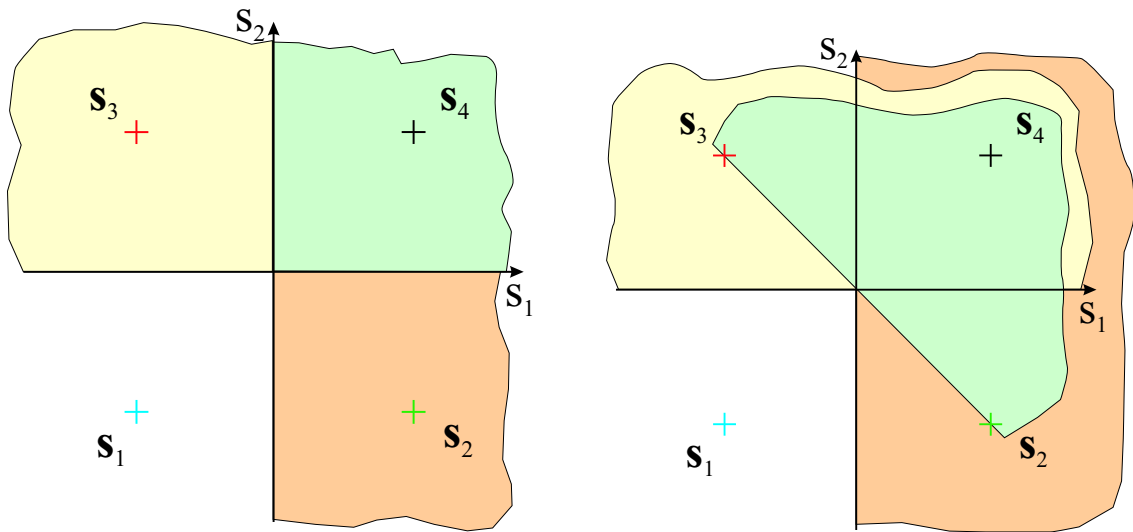


Figure 3.5: Exact decision regions (left plot) and the overlapping integration areas (right plot). BPSK modulation, $n_T = 2$, $\mathbf{H} = \mathbf{I}$.

favor of s_1, s_2, s_3 or s_4 , if the receive vector \mathbf{y} lies in the white, orange, yellow or green decision region shown in the left plot of Fig. 3.5. Therefore, an error occurs, if s_1 is transmitted and the receive vector \mathbf{y} lies outside of the white decision area. The exact probability of having such an error can be calculated by integrating the shifted PDF of the noise (the two dimensional Gaussian PDF of the complex noise variable \mathbf{n} is shifted to the point s_1) over these three areas (yellow, green, orange):

$$P_\varepsilon(\mathbf{s}_1) = P_\varepsilon(\mathbf{s}_2|\mathbf{s}_1) + P_\varepsilon(\mathbf{s}_3|\mathbf{s}_1) + P_\varepsilon(\mathbf{s}_4|\mathbf{s}_1) , \quad (3.57)$$

where the error probabilities $P_\varepsilon(\mathbf{s}_i|\mathbf{s}_1)$ are the integrals over the corresponding areas. This exact probability is upper bounded by the sum over the PEPs:

$$P_\varepsilon(\mathbf{s}_1) \leq \text{PEP}(\mathbf{s}_1 \rightarrow \mathbf{s}_2) + \text{PEP}(\mathbf{s}_1 \rightarrow \mathbf{s}_3) + \text{PEP}(\mathbf{s}_1 \rightarrow \mathbf{s}_4) . \quad (3.58)$$

In the left plot of Fig. 3.5 the so-called integration areas can be seen. Under integration area I denote the area over that the shifted noise PDF is integrated to get the PEPs. For example, calculating the $\text{PEP}(\mathbf{s}_1 \rightarrow \mathbf{s}_4)$ the integration extends over the green area (right plot). As shown in the right hand plot of Fig. 3.5 applying **union bound techniques**, the so-called integration areas are overlapping and thus some parts of the areas are considered twice or even more often. In principle this overlapping of integration areas is the reason why the union bound overestimates the error probability.

Note that even the PEPs themselves are union bounds for the exact error probabilities at low SNR:

$$P_\varepsilon(\mathbf{s}_i|\mathbf{s}_1) < \text{PEP}(\mathbf{s}_1 \rightarrow \mathbf{s}_i) \quad \text{at low SNR} . \quad (3.59)$$

For high SNR, where the overlapping does not essentially contribute to the integration result, these PEPs almost exactly approximate the true values:

$$P_\varepsilon(\mathbf{s}_i|\mathbf{s}_1) \approx \text{PEP}(\mathbf{s}_1 \rightarrow \mathbf{s}_i) \quad \text{at high SNR} . \quad (3.60)$$

In the following, I will show graphically, by means of an example, the influence of these multiple integrations in the union bound approximation. In the left plot of Fig. 3.6 it is shown that for low SNR $P_\varepsilon(\mathbf{s}_3|\mathbf{s}_1)$ is strictly smaller than the $\text{PEP}(\mathbf{s}_1 \rightarrow \mathbf{s}_3)$. Due to the high noise variance the area of the first quadrant substantially contributes to the $\text{PEP}(\mathbf{s}_1 \rightarrow \mathbf{s}_3)$ but not to the exact error probability $P_\varepsilon(\mathbf{s}_3|\mathbf{s}_1)$. I.e. the integral over the first and the second quadrant ($\text{PEP}(\mathbf{s}_1 \rightarrow \mathbf{s}_3)$) is considerably larger than the integral over the second quadrant ($P_\varepsilon(\mathbf{s}_3|\mathbf{s}_1)$) only. Thus the PEP overestimates the exact error probability. The lower noise variance (high SNR; $\text{SNR}_{high} = 4 \cdot \text{SNR}_{low}$) in the right plot of Fig. 3.6 shows that integrating over the first and the second quadrant (as it is done for the PEP) delivers approximately the same error probability as integrating over only the second quadrant (as it should be done for the exact error probability). Therefore, the PEP and the exact error probability are almost equal. Note that $[\mathbf{n}]_i$ denotes the i -th entry of the noise vector \mathbf{n} . Also for the mathematical point of view, the PEP and the

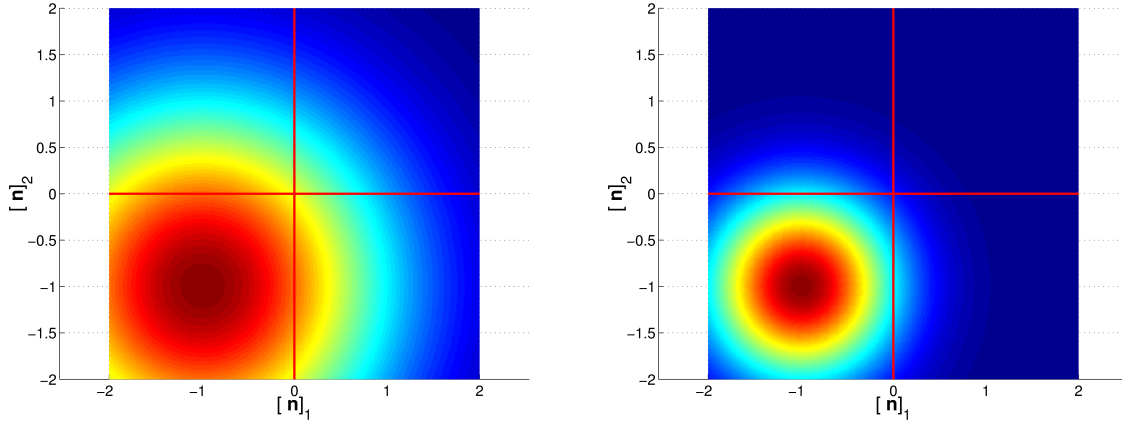


Figure 3.6: 2-D shifted noise PDF for low SNR (left plot) and high SNR (right plot) for 4QAM modulation.

exact error probability are approximately equal for high SNR (low σ_n^2):

$$\text{PEP}(\mathbf{s}_1 \rightarrow \mathbf{s}_3) = Q\left(\frac{1}{\sigma_n^2}\right) \quad (3.61)$$

$$P_\varepsilon(\mathbf{s}_3|\mathbf{s}_1) = Q\left(\frac{1}{\sigma_n^2}\right) - \left[Q\left(\frac{1}{\sigma_n^2}\right)\right]^2 \quad (3.62)$$

3.4.2 Uncoded 2×2 MIMO system with 16QAM modulation

The results for a second example, namely a 2×2 MIMO system with 16QAM modulation, are shown in Fig. 3.7. Note that in Fig. 3.7 the simulated BER vs. SNR curves are the solid lines, the union bounds are

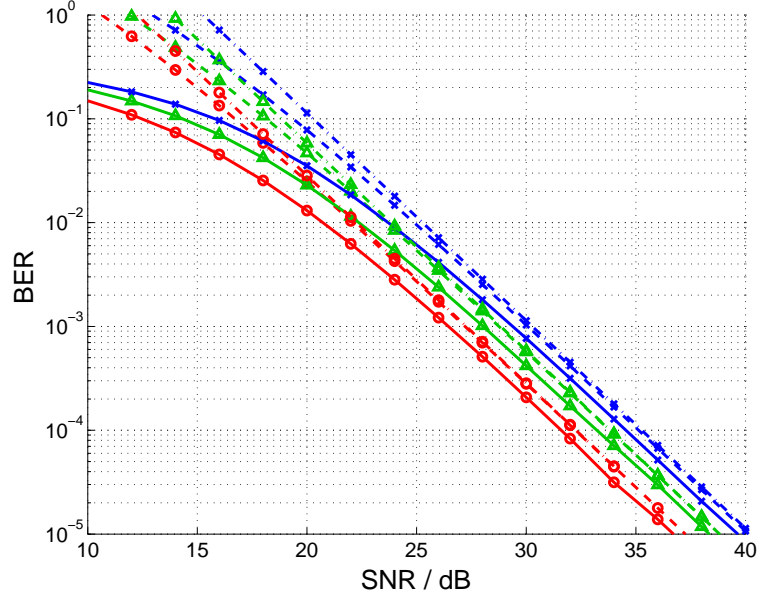


Figure 3.7: BER vs. SNR performance of a uncoded 2×2 MIMO system with 16QAM modulation.

the dashed lines and the dashed-dotted lines are the high SNR approximations. The red curves (labeled by \circ -marker) correspond to uncorrelated channels, the green curves (labeled by \triangle -marker) correspond to the moderate correlation scenario 1D3 and the blue curves (labeled by \times -marker) correspond to the high correlation scenario 14D3. As can be seen in Fig. 3.7 the achieved slope of the BER vs. SNR curve is n_R (maximum slope), due to the well behaved matrices $\mathbf{\Omega}$. The calculated power losses for the scenario 1D3 and 14D3 are 1.57dB and 2.89dB at high SNR. In this case the union bounds are not so tight as in the previous example. The reason for this effect is the strong overlapping of the integration areas due to the large number of ETs ($n_{ET}=574$) and the small number of receive antennas n_R . Additionally, the influence of the overlapping of the integration areas decreases very slowly with increasing SNR and thus a perfect tightness of the union bound as in the previous example does not show up in Fig. 3.7.

3.5 Optimal Precoding

In Fig. 3.4 and in Fig. 3.7 it can be seen that the BER performance degrades if the MIMO channel is spatially correlated. This loss can be measured by the diversity loss L_D and the power loss L_P defined in Sec. 3.3.3. In order to mitigate the detrimental effect of spatial correlation, a linear precoding filter \mathbf{F} can be introduced at the transmitter. The main goal of this approach is to show what kind of improvement could be obtained if such a rather involved signal processing of the transmit signal is applied.

With this precoding matrix, the resulting system model results in:

$$\mathbf{y} = \mathbf{H}\mathbf{F}\mathbf{s} + \mathbf{n} \quad (3.63)$$

With this modification of the transmit signal, the correlation matrix $\mathbf{R}_{\mathbf{u}_{i,j}}$ defined in Eqn. (3.20) results in:

$$\begin{aligned} \mathbf{R}_{\mathbf{u}_{i,j}}(\mathbf{F}) &= \mathbf{U}_R \text{diag}(\lambda_1^{(i,j)}(\mathbf{F}), \lambda_2^{(i,j)}(\mathbf{F}), \dots, \lambda_{n_R}^{(i,j)}(\mathbf{F})) \mathbf{U}_R^H, \\ \lambda_m^{(i,j)}(\mathbf{F}) &= \left((\mathbf{b}_{i,j}^T \mathbf{F}^T \mathbf{U}_T) \odot \Omega_m \right) \mathbf{U}_T^H \mathbf{F}^* \mathbf{b}_{i,j}^* \end{aligned} \quad (3.64)$$

Now, the distance $d_{W,i,j}^2$, the total effective distance d_W^2 and the power loss L_P depend on the prefilter \mathbf{F} and thus they are denoted by $d_{W,i,j}^2(\mathbf{F})$, $d_W^2(\mathbf{F})$ and $L_P(\mathbf{F})$.

The optimal prefilter \mathbf{F}_{opt} minimizes the power loss⁴:

$$\mathbf{F}_{opt} = \arg \min_{\mathbf{F}} \{L_P(\mathbf{F})\} = \arg \max_{\mathbf{F}} \{d_W^2(\mathbf{F})\} = \arg \min_{\mathbf{F}} \left\{ \sum_{k=1}^{n_{ET}} \frac{w_k}{\det(\mathbf{R}_{\mathbf{u}_k}(\mathbf{F}))} \right\} \quad (3.65)$$

with the side constraint (power constraint):

$$\text{tr}(\mathbf{F}_{opt}^H \mathbf{F}_{opt}) = n_T. \quad (3.66)$$

This constraint assures that no power amplification due to the precoding matrix occurs. This minimization problem has to be solved for each type of uncoded MIMO system separately, due to the specific entities w_k , n_{ET} . Therefore, in the following I will focus on the simplest uncoded MIMO system, namely a 2×2 system with BPSK modulation. For this system and for the spatial correlation scenario 14D3, the ETs and their corresponding key-parameters are listed in the Tab. 3.3. In the last column of

ET	$\lambda_1^{(k)}$	$\lambda_2^{(k)}$	n_{BEk}	f_k	d_{Wk}^2	d_{Tk}^2
0	0	0	0	4	0	0
1	6.8640	1.1565	1	4	2.8175	4
2	6.7277	1.1390	1	4	2.7682	4
3	3.4735	0.9960	2	2	1.8600	8
4	23.7098	3.5951	2	2	9.2325	8

Table 3.3: ET table for a uncoded MIMO system. Correlation scenario 14D3; BPSK; $n_T = 2$.

Tab. 3.3 the distances for the i.i.d. case are shown. The power loss for this correlation scenario is 2.8dB and no diversity loss is observed. With the knowledge of the ETs and the corresponding key-parameters, the minimization problem can be written as:

$$\mathbf{F}_{opt} = \arg \min_{\mathbf{F}} \left\{ \sum_{k=1}^4 \frac{1}{\lambda_1^{(k)}(\mathbf{F}) \cdot \lambda_2^{(k)}(\mathbf{F})} \right\} = \arg \min_{\mathbf{F}} \{M(\mathbf{F})\} \quad (3.67)$$

⁴Using Eqn. (3.56), Eqn. (3.54) and Eqn. (3.52)

and the side constraint is

$$\text{tr}(\mathbf{F}^H \mathbf{F}) = 2. \quad (3.68)$$

Such an optimization problem can be solved by the Lagrange multiplier technique [43] by solving the following equations:

$$\begin{aligned} G(\mathbf{F}, \lambda) &= M(\mathbf{F}) + \lambda \cdot \text{tr}(\mathbf{F}^H \mathbf{F}) \\ \frac{\partial G(\mathbf{F}, \lambda)}{\partial \mathbf{F}} &= 0 \\ \frac{\partial G(\mathbf{F}, \lambda)}{\partial \lambda} &= 0 \end{aligned} \quad (3.69)$$

But even in this simplest possible case (2×2 , BPSK) the optimization problem is still too complex to be analytically solved.

Therefore, I have solved the optimization problem numerically by using a gradient algorithm, which is explained in the following: In the first step a prefilter matrix \mathbf{F} is chosen randomly. Then the gradient is approximately calculated by:

$$\frac{\partial M(\mathbf{F})}{\partial \mathbf{F}} \approx \frac{\Delta M(\mathbf{F})}{\Delta \mathbf{F}}, \quad (3.70)$$

where $M(\mathbf{F})$ is defined in Eqn. (3.67). In order to approach the minimum, iterations with small steps Δ_S are performed as:

$$\mathbf{F}_{i+1} = \mathbf{F}_i - \Delta_S \frac{\Delta M(\mathbf{F})}{\Delta \mathbf{F}} \quad (3.71)$$

At each step the matrix \mathbf{F}_{i+1} is normalized such that the side constraint is fulfilled. Then the next iteration starts and the gradient of M with the updated matrix \mathbf{F}_{i+1} is calculated and so on. Performing enough iterations, the Algorithm approaches to a local minimum. Actually, we want to find the global minimum and therefore the iteration algorithm is repeated 10000 times, i.e., 10000 random start values are considered. Thus, I guess that the probability of finding the global minimum is quite high. The result of this search for the optimum precoder matrix \mathbf{F}_{opt} with 10000 random start values is shown in the histogram in Fig. 3.8. There are three cluster points, i.e., three local minima. The local minimum leading

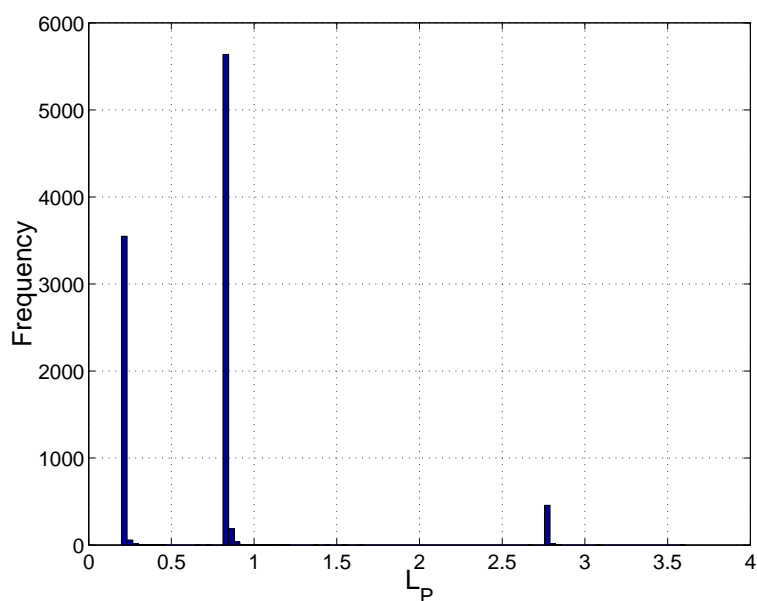


Figure 3.8: Histogram of the power loss after optimization.

to the smallest power loss is supposed to be the global minimum. The global minimum corresponds to a power loss of 0.2dB. The modified key-parameters of the ETs are listed in Tab. 3.4. As it can be seen

ET	$\lambda_1^{(k)}$	$\lambda_2^{(k)}$	n_{BEk}	f_k	d_{Wk}^2	d_{Tk}^2
0	0	0	0	4.0000	0	0
1	10.1606	1.5809	1.0000	4.0000	4.0079	4
2	10.1106	1.5725	1.0000	4.0000	3.9873	4
3	13.1983	2.0010	2.0000	2.0000	5.1390	8
4	27.3440	4.3058	2.0000	2.0000	10.8507	8

Table 3.4: ET table for a precoded MIMO system. Correlation scenario 14D3; BPSK; $n_T = 2$.

from the table, the distances are much better than without precoding and approximately as good as the distances for the i.i.d. case (last column). This result also shows up in the BER vs. SNR curves shown in the Fig. 3.9. In Fig. 3.9 the black curve is for spatially uncorrelated fading, the blue curve for the

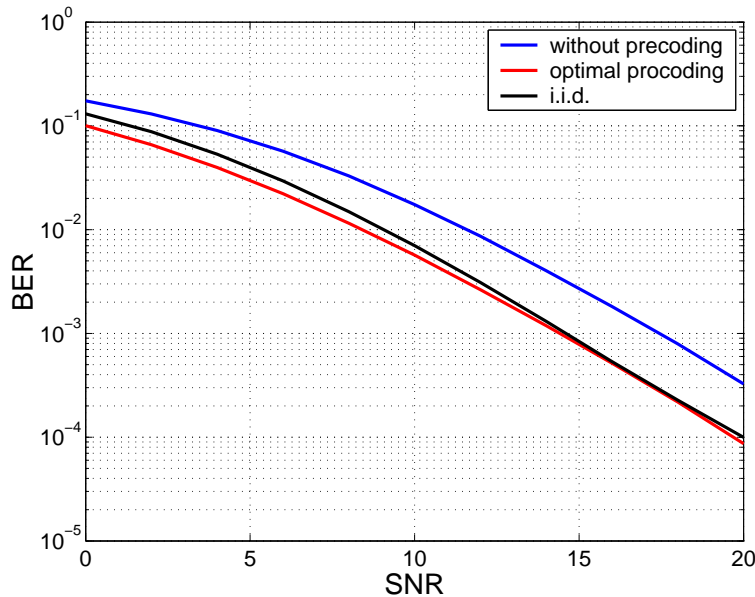


Figure 3.9: BER vs. SNR curves for a precoded 2×2 MIMO system using BPSK modulation.

correlation scenario 14D3 without precoding and the red curve is for the correlation scenario 14D3 with optimal precoding. The interesting result is that the precoded MIMO system performs even better in spatially correlated channels in the low SNR regime than the uncoded system performs in uncorrelated channels. In the high SNR domain both curves are almost identical. The calculated power loss predicts a performance difference of 0.2dB that will only show up at very high SNR. This gain at low SNR was also observed in [44], although the authors do not use the optimal criteria in their paper.

Chapter 4

Space-Time Block Coded Data Transmission

In this section we focus on the analytic calculation of the BER-performance of standard Space-Time Block Codes (STBCs) in quasi static, frequency flat Rayleigh fading. Spatially uncorrelated and spatially correlated MIMO channels will be considered. At the beginning I will summarize the fundamentals of space-time block coding. Then a tight **union bound** for the BER is derived. Sec. 4.3 covers the derivation of a very tight **lower bound** for the BER. In the last section results of several STBCs using various modulation formats are presented and discussed.

4.1 Fundamentals of Space-Time Block Codes

As mentioned above, the scope of this thesis are standard STBCs. In this context the term “standard” means that I do not take into account codes designed especially for fast fading, frequency selective fading or other advanced coding techniques, which do not fit into the system model introduced in Sec. 2.1. The current thesis also does not cover the performance calculation of space time trellis codes [5], concatenated codes [47] and space time turbo codes [48]. In the following we are only concerned with STBCs.

First let’s repeat some basic definitions: The code word difference matrix $\mathbf{B}_{i,j}$ and the corresponding distance matrix $\mathbf{A}_{i,j}$ are defined as:

$$\mathbf{B}_{i,j} = \mathbf{S}_i - \mathbf{S}_j, \quad \mathbf{A}_{i,j} = \mathbf{B}_{i,j}^H \mathbf{B}_{i,j}, \quad (4.1)$$

where \mathbf{S}_i and \mathbf{S}_j are two valid STBC matrices. The symbol rate R_s is defined as the number of independent symbols n_{IS} transmitted in one code block divided by the number of occupied times slots n_{OTS} :

$$R_s = \frac{n_{IS}}{n_{OTS}}. \quad (4.2)$$

Additionally, it is pointed out what we understand under single, double, ... and multiple symbol errors: STBC words defined further ahead are functions of the transmitted information symbols: $\mathbf{S}(s_1, s_2, \dots, s_{n_{IS}})$. A single symbol error occurs if the code matrix $\mathbf{S}(s_1, s_2, \dots, s_{n_{IS}})$ is transmitted and the receiver decides in favor of the code matrix $\mathbf{S}'(s'_1, s_2, \dots, s_{n_{IS}})$ with $s'_1 \neq s_1$. In general, single symbol errors between two valid code matrices are errors where only one information symbol (out of n_{IS} symbols) is erroneous. If two symbols (out of n_{IS} symbols) in two valid code words are different, then we speak of double symbol errors. An example for a double symbol error is: $\mathbf{S}(s_1, s_2, \dots, s_{n_{IS}})$ is transmitted and $\mathbf{S}(s'_1, s'_2, \dots, s_{n_{IS}})$ is decoded. Multiple symbol errors are all errors except for the single symbol errors. Note that, according

to the above definition, we speak of single symbol errors, even if more than one entry of the difference matrix is non-zero, since in general each information symbol s_i shows up in more than one position in an STBC matrix! The number of non-zero entries in the difference matrix corresponds to the number of entries in which this symbol shows up in the STBC matrix.

4.1.1 Space-Time Block Coding Techniques

In the following two special subsets of STBCs are distinguished, namely orthogonal and non-orthogonal STBCs. Additionally, their corresponding properties are explained.

4.1.1.1 Orthogonal Space-Time Block Codes

O-STBCs are defined as:

Definition 4.1 A STBC (defined by the entire set of code words \mathcal{S}) is called orthogonal if and only if the distance matrix is a scaled identity matrix: $\mathbf{A}_{i,j} = \left(|s_1 - s'_1|^2 + |s_2 - s'_2|^2 + \dots + |s_{n_{IS}} - s'_{n_{IS}}|^2 \right) \mathbf{I}^1$ for all possible code word indices i, j .

The most prominent representative of an O-STBCs is the Alamouti code [49]. The Alamouti STBC is defined by the following code word matrix:

$$\mathbf{S} = \begin{pmatrix} s_1 & -s_2^* \\ s_2 & s_1^* \end{pmatrix}, \quad (4.3)$$

i.e., the symbols s_1 and s_2 are transmitted from antenna 1 and 2 in the first time slot and $-s_2^*$ and s_1^* are transmitted from antenna 1 and 2 in the second time slot. Considering only one receive antenna ($n_R = 1$), the received signal vector corresponding to two successive time slots can be written as:

$$\begin{aligned} \mathbf{y}^T &= \mathbf{h}^T \mathbf{S} + \mathbf{n}^T \\ (y_1 \ y_2) &= (h_{11} \ h_{12}) \begin{pmatrix} s_1 & -s_2^* \\ s_2 & s_1^* \end{pmatrix} + (n_1 \ n_2) \end{aligned} \quad (4.4)$$

An equivalent notation is

$$\underbrace{\begin{pmatrix} y_1 \\ y_2^* \end{pmatrix}}_{\tilde{\mathbf{y}}} = \underbrace{\begin{pmatrix} h_{11} & h_{12} \\ h_{12}^* & -h_{11}^* \end{pmatrix}}_{\mathbf{H}_v} \underbrace{\begin{pmatrix} s_1 \\ s_2 \end{pmatrix}}_{\mathbf{s}} + \underbrace{\begin{pmatrix} n_1 \\ n_2^* \end{pmatrix}}_{\tilde{\mathbf{n}}}. \quad (4.5)$$

In this notation the transmission system behaves as a (2×2) uncoded MIMO system with a strongly structured virtual channel matrix:

$$\mathbf{H}_v = \begin{pmatrix} h_{11} & h_{12} \\ h_{12}^* & -h_{11}^* \end{pmatrix}. \quad (4.6)$$

Applying a matched filter \mathbf{H}_v^H at the receiver, we get:

$$\mathbf{H}_v^H \tilde{\mathbf{y}} = \mathbf{H}_v^H \mathbf{H}_v \mathbf{s} + \mathbf{H}_v^H \tilde{\mathbf{n}} = (|h_{11}|^2 + |h_{12}|^2) \mathbf{s} + \mathbf{H}_v^H \tilde{\mathbf{n}} \quad (4.7)$$

¹A similar definition holds for ‘‘STBCs from the generalized orthogonal design’’. For these codes the distance matrix is always diagonal: $\mathbf{A}_{i,j} = \mathbf{D}_{i,j}$ but not necessarily a scaled identity matrix.

As it can be seen, after matched filtering the signal vector $\mathbf{H}_v^H \tilde{\mathbf{y}}$ results in the noisy transmit vector \mathbf{s} multiplied by a channel dependent gain factor $(|h_{11}|^2 + |h_{12}|^2)$, i.e., the receiver can detect (quantize) the symbols s_1 and s_2 independently. In this way, the ML performance is achieved with strongly reduced receiver complexity. Additionally, it is easy to recognize that a diversity order of two is achieved, since the factor in front of the symbol vector \mathbf{s} consists of twice the squared magnitude of independent random variables representing two independent paths. These two properties (full diversity and ML detection by a linear matched filter) are generally valid for O-STBCs. The disadvantage of O-STBCs is a loss in symbol rate, since O-STBCs with symbol rate $R_S = 1$ (full rate) only exist for $n_T = 2$. For higher values of n_T , O-STBCs only exist with symbol rates $R_S < 1$. Summarizing the properties of O-STBCs, we get:

-) Very simple ML decoding algorithm
-) O-STBCs always achieve full diversity order of $D = n_R n_T$
-) The achievable symbol rate is one for $n_T = 2$ only. For higher n_T the symbol rate is smaller than 1.

As an illustrative example I show an O-STBC for $n_T = 4$ and $R_S = 3/4$ that is investigated further ahead [52]:

$$\mathbf{S}_{orth} = \begin{pmatrix} s_1 & -s_2^* & -s_3^* & 0 \\ s_2 & s_1^* & 0 & -s_3^* \\ s_3 & 0 & s_1^* & s_2^* \\ 0 & s_3 & -s_2 & s_1 \end{pmatrix}. \quad (4.8)$$

4.1.1.2 Non-Orthogonal Space-Time Block Codes

Non-Orthogonal Space-Time Block Codes (NO-STBCs) are all other STBCs that do not obey the constraints given in Def. 4.1. The important properties of such codes are that they can achieve higher symbol rates than O-STBCs, however they do not achieve the full diversity advantage and ML decoding is more involved than for O-STBCs. Some NO-STBCs that are of special interest in the rest of this chapter are listed below. The first and here most often used NO-STBC is the cyclic STBC [34]:

$$\mathbf{S}_{cyclic} = \begin{pmatrix} s_1 & s_4 & s_3 & s_2 \\ s_2 & s_1 & s_4 & s_3 \\ s_3 & s_2 & s_1 & s_4 \\ s_4 & s_3 & s_2 & s_1 \end{pmatrix}, \quad (4.9)$$

which offers $R_S = 1$ information symbol per time slot. The name cyclic comes from the cyclically shifted columns and rows in the code matrix \mathbf{S}_{cyclic} . Another NO-STBC is the so-called Extended Alamouti (EA) code [46], which is also of interest in this thesis:

$$\mathbf{S}_{EA} = \left(\begin{array}{cc|cc} s_1 & s_2^* & s_3^* & s_4 \\ s_2 & -s_1^* & s_4^* & -s_3 \\ \hline s_3 & s_4^* & -s_1^* & -s_2 \\ s_4 & -s_3^* & -s_2^* & s_1 \end{array} \right). \quad (4.10)$$

This code has also full rate $R_S = 1$. It essentially consists of two independent pairs of the simple (2×2) Alamouti code. The first Alamouti pair consists of the symbols s_1 and s_2 and the second of s_3 and s_4 .

The last code discussed in detail in the current thesis is the so-called Double-Space Time Transmit Diversity (D-STTD) code proposed in [45], which consists of two independent Alamouti code blocks

$$\mathbf{S}_{D-STTD} = \begin{pmatrix} s_1 & s_2^* \\ s_2 & -s_1^* \\ \hline s_3 & s_4^* \\ s_4 & -s_3^* \end{pmatrix}, \quad (4.11)$$

achieving a rate R_S of 2 information symbols per time slot.

4.1.2 Code Design Criteria

Code Design Criteria are on one hand very important in order to design good codes and on the other hand to get more insight into the behavior of existing STBCs. In order to find meaningful design criteria, the overall BER has to be calculated and afterwards conditions have to be found to minimize the BER. As it is already known from the derivations in Sec. 3, the overall BER can be upper bounded by the sum over all possible PEPs. Therefore, minimizing the total BER results in optimizing all individual PEPs. For this reason, we start with calculating the PEP by following the same strategy as in Sec. 3.1 resulting in:

$$P(\mathbf{S}_i \rightarrow \mathbf{S}_j) = P(\|\mathbf{Y} - \mathbf{H}\mathbf{S}_i\|_F^2 > \|\mathbf{Y} - \mathbf{H}\mathbf{S}_j\|_F^2) = P(\|\mathbf{N}\|_F^2 > \underbrace{\|\mathbf{H}(\mathbf{S}_i - \mathbf{S}_j) + \mathbf{N}\|_F^2}_{\mathbf{B}_{i,j}}), \quad (4.12)$$

This inequality can be further simplified to:

$$\begin{aligned} \|\mathbf{N}\|_F^2 &> \|\mathbf{H}\mathbf{B}_{i,j} + \mathbf{N}\|_F^2 \\ \sum_{k=1}^{n_R} \mathbf{n}_k^T \mathbf{n}_k &> \sum_{k=1}^{n_R} (\mathbf{h}_k^T \mathbf{B}_{i,j} + \mathbf{n}_k^T) (\mathbf{h}_k^T \mathbf{B}_{i,j} + \mathbf{n}_k^T)^H \\ \sum_{k=1}^{n_R} \mathbf{n}_k^T \mathbf{n}_k &> \sum_{k=1}^{n_R} (\mathbf{h}_k^T \mathbf{B}_{i,j} \mathbf{n}_k^* + \mathbf{n}_k^T \mathbf{n}_k^* + \mathbf{h}_k^T \mathbf{B}_{i,j} \mathbf{B}_{i,j}^H \mathbf{h}_k^* + \mathbf{n}_k^T \mathbf{B}_{i,j}^H \mathbf{h}_k^*) \\ - \sum_{k=1}^{n_R} \mathbf{h}_k^T \mathbf{B}_{i,j} \mathbf{B}_{i,j}^H \mathbf{h}_k^* &> \underbrace{\sum_{k=1}^{n_R} 2 \operatorname{Re} \{ \mathbf{h}_k^T \mathbf{B}_{i,j} \mathbf{n}_k^* \}}_{z_{i,j}} \end{aligned} \quad (4.13)$$

\mathbf{n}_k^T is the k -th row of \mathbf{N} and \mathbf{h}_k^T is the k -th row of \mathbf{H} . Let's assume for the moment \mathbf{h}_k and $\mathbf{B}_{i,j}$ to be fixed and let's focus on the statistics of $z_{i,j}$ with respect to the channel noise \mathbf{n}_k . Linear manipulations do not change the Gaussian statistic and therefore $z_{i,j}$ is a real Gaussian random variable with mean:

$$\mu_{z_{i,j}} = E_{\mathbf{n}} \left\{ \sum_{k=1}^{n_R} 2 \operatorname{Re} \{ \mathbf{h}_k^T \mathbf{B}_{i,j} \mathbf{n}_k^* \} \right\} = 0 \quad (4.14)$$

and variance

$$\sigma_{z_{i,j}}^2 = E_{\mathbf{n}} \left\{ \sum_{k=1}^{n_R} 2 \operatorname{Re} \{ \mathbf{h}_k^T \mathbf{B}_{i,j} \mathbf{n}_k^* \} 2 \operatorname{Re} \{ \mathbf{n}_k^T \mathbf{B}_{i,j}^H \mathbf{h}_k^* \} \right\} = \dots = 2\sigma_n^2 \sum_{k=1}^{n_R} \mathbf{h}_k^T \mathbf{B}_{i,j} \mathbf{B}_{i,j}^H \mathbf{h}_k^*, \quad (4.15)$$

resulting in the following PEP ($P(\mathbf{S}_i \rightarrow \mathbf{S}_j) = \text{PEP}_{i,j}$):

$$\text{PEP}_{i,j} = P(z_{i,j} < - \sum_{k=1}^{n_R} \mathbf{h}_k^T \mathbf{B}_{i,j} \mathbf{B}_{i,j}^H \mathbf{h}_k^*) = Q \left(\sqrt{\frac{\sum_{k=1}^{n_R} \mathbf{h}_k^T \mathbf{B}_{i,j} \mathbf{B}_{i,j}^H \mathbf{h}_k^*}{2\sigma_n^2}} \right) = Q \left(\sqrt{\frac{d_{R,i,j}^2}{2\sigma_n^2}} \right) \quad (4.16)$$

The squared distance at the receiver $d_{R,i,j}^2$ is now defined by

$$d_{R,i,j}^2 = \sum_{k=1}^{n_R} \mathbf{h}_k^T \mathbf{B}_{i,j} \mathbf{B}_{i,j}^H \mathbf{h}_k^* = \|\mathbf{H}\mathbf{B}_{i,j}\|_F^2 = \operatorname{tr}(\mathbf{H}\mathbf{B}_{i,j} \mathbf{B}_{i,j}^H \mathbf{H}^H) = \operatorname{tr}(\mathbf{H}\mathbf{A}_{i,j} \mathbf{H}^H). \quad (4.17)$$

The distance between the code matrices \mathbf{S}_i and \mathbf{S}_j at the **transmitter** is defined as:

$$d_{T,i,j}^2 = \|\mathbf{B}_{i,j}\|_F^2 = \operatorname{tr}(\mathbf{B}_{i,j} \mathbf{B}_{i,j}^H) = \operatorname{tr}(\mathbf{A}_{i,j}). \quad (4.18)$$

Obviously, the distance $d_{R,i,j}^2$ at the receiver governs the error performance in Eqn. (4.16). In the following the PEP is averaged with respect to the distance as a function of the channel parameters, in order to get a mean PEP. For this reason, the statistics of the squared distance has to be known. For this purpose, we focus on uncorrelated quasi static Rayleigh fading channels. The distance at the **receiver** can be further simplified to:

$$\begin{aligned} d_{R,i,j}^2 &= \sum_{k=1}^{n_R} \mathbf{h}_k^T \underbrace{\mathbf{B}_{i,j} \mathbf{B}_{i,j}^H}_{\mathbf{A}_{i,j}} \mathbf{h}_k^* = \sum_{k=1}^{n_R} \mathbf{h}_k^T \underbrace{\mathbf{A}_{i,j}}_{\mathbf{U}_{i,j} \mathbf{D}_{i,j} \mathbf{U}_{i,j}^H} \mathbf{h}_k^* = \sum_{k=1}^{n_R} \underbrace{\mathbf{h}_k^T \mathbf{U}_{i,j}}_{\mathbf{h}_k^{(i,j)T}} \mathbf{D}_{i,j} \underbrace{\mathbf{U}_{i,j}^H \mathbf{h}_k^*}_{\mathbf{h}_k^{(i,j)*}} \\ &= \sum_{k=1}^{n_R} \mathbf{h}_k^{(i,j)T} \mathbf{D}_{i,j} \mathbf{h}_k^{(i,j)*} = \sum_{l=1}^{r_{i,j}} \underbrace{\sum_{k=1}^{n_R} |h_{k,l}^{(i,j)}|^2}_{\alpha_l^{(i,j)}} \lambda_l^{(i,j)} = \sum_{l=1}^{r_{i,j}} \alpha_l^{(i,j)} \lambda_l^{(i,j)}, \end{aligned} \quad (4.19)$$

where $\mathbf{D}_{i,j} = \text{diag}(\lambda_1^{(i,j)}, \lambda_2^{(i,j)}, \dots, \lambda_{r_{i,j}}^{(i,j)})$, the $\lambda_l^{(i,j)}$ are the eigenvalues of the so-called distance matrix $\mathbf{A}_{i,j}$, $r_{i,j}$ denotes the rank of $\mathbf{A}_{i,j}$ and the row vector $\mathbf{h}_k^{(i,j)T} = (h_{k,1}^{(i,j)} \ h_{k,2}^{(i,j)} \ \dots \ h_{k,n_T}^{(i,j)})$. Note that the multiplication $\mathbf{h}_k^T \mathbf{U}_{i,j}$ does not change the Gaussian statistic of \mathbf{h}_k^T and therefore the random variables $\alpha_l^{(i,j)}$ are χ^2 distributed with $2n_R$ degrees of freedom with variance 1. Their PDF is thus the same as in Eqn. (3.25). In order to get meaningful but not too complicated design criteria, the well known Chernoff bound [27] is used to approximated the Gaussian Q-function:

$$Q(x) \leq e^{-x^2/2}. \quad (4.20)$$

With this approximation, the union bound for the mean PEP results in²:

$$\begin{aligned} \text{PEP}_{i,j}^{(ub)} &\leq E_{\mathbf{H}} \left\{ e^{-\frac{d_{R,i,j}^2}{4\sigma_n^2}} \right\} = E_{\mathbf{H}} \left\{ e^{-\frac{\sum_{l=1}^{r_{i,j}} \alpha_l^{(i,j)} \lambda_l^{(i,j)}}{4\sigma_n^2}} \right\} = \prod_{l=1}^{r_{i,j}} E_{\mathbf{H}} \left\{ e^{-\frac{\alpha_l^{(i,j)} \lambda_l^{(i,j)}}{4\sigma_n^2}} \right\} = \\ &\prod_{l=1}^{r_{i,j}} \left(1 + \frac{\lambda_l^{(i,j)}}{4\sigma_n^2} \right)^{-n_R} = \prod_{l=1}^{r_{i,j}} \left(1 + \lambda_l^{(i,j)} \frac{\text{SNR}}{4n_T} \right)^{-n_R}. \end{aligned} \quad (4.21)$$

Rewriting the above product we get:

$$\text{PEP}_{i,j}^{(ub)} \leq 1 + \left(\sum_{l=1}^{r_{i,j}} \lambda_l^{(i,j)} \frac{\text{SNR}}{4n_T} \right)^{-n_R} + \dots + \left(\sqrt{\prod_{l=1}^{r_{i,j}} \lambda_l^{(i,j)} \frac{\text{SNR}}{4n_T}} \right)^{-r_{i,j} n_R}. \quad (4.22)$$

With this equation it is possible to formulate two code design criteria, namely on one hand for low SNR and on the other hand for high SNR. The first design rule is suited for the low SNR regime where the first two terms in Eqn. (4.22) are essential.

Design Rule 4.1 For the low SNR regime the trace of the distance matrix $\mathbf{A}_{i,j}$ for all code pairs (i, j) should be as larger as possible (Trace Criterion), since $\sum_{l=1}^{r_{i,j}} \lambda_l^{(i,j)} = \text{tr}(\mathbf{A}_{i,j})$.

The code design criterion described in Theorem 4.1 has been proposed first in [5].

The more widely known design criterion is suited for the high SNR domain, where the last term in Eqn. (4.22) is the most important one leading to:

²Note that the modulation format has mean power $P_S = 1$.

Design Rule 4.2 For the high SNR regime we have two aims: Firstly, the rank $r_{i,j}$ of the distance matrix $\mathbf{A}_{i,j}$ should be as large as possible for all code pairs (i, j) (*Rank criterion*). Having optimal rank, the second aim is to maximize $\prod_{l=1}^{r_{i,j}} \lambda_l^{(i,j)} = \det(\mathbf{A}_{i,j})$ for all code pairs (i, j) (*Determinant Criterion*).

This code design criterion has been introduced by Tarokh [29].

The best one can do with respect to a good code design is to aim at both design criteria. For example, for the code design in the high SNR domain the *Rank* and *Determinant Criteria* should be maximized first. If the code search results in more than one optimal solution with respect to these two criteria, then the final optimum is that code, which maximizes the *Trace Criterion* too.

A further conclusion of the derivation above is that only the eigenvalues $\lambda_l^{(i,j)}$ of the distance matrix $\mathbf{A}^{(i,j)}$ govern the error performance of STBCs.

Additionally, a *loose union bound* for the PEP can be found by neglecting the one-term in the bracket of the last term in Eqn. (4.21) resulting in:

$$\text{PEP}_{i,j}^{(ub)} \leq \prod_{l=1}^{r_{i,j}} \left(\lambda_l^{(i,j)} \frac{\text{SNR}}{4n_T} \right)^{-n_R} = \left(\frac{\sqrt[r_{i,j}]{\prod_{l=1}^{r_{i,j}} \lambda_l^{(i,j)}} \text{SNR}}{4n_T} \right)^{-r_{i,j} n_R}. \quad (4.23)$$

The factor in front of the SNR is called coding advantage³. The exponent in Eqn. (4.23) determines the slope of the mean PEP vs. SNR curve and is called diversity gain.

³Note the slight difference between coding gain and coding advantage. In principle the term coding gain only exists in non fading channels. In fading channels the coding theory only specifies a diversity gain and an coding advantage.

4.1.3 Block Coding: SISO vs. MIMO

In this section I want to point out the main differences between SISO and MIMO block coding, to get a feeling for the error mechanism in both cases.

4.1.3.1 Distance Properties

SISO Block Codes:

Consider first a simple repetition code, where the information symbols s_1 to $s_{n_{IS}}$ are simply repeated once:

$$\mathbf{S} = (s_1 \ s_2 \ \dots \ s_{n_{IS}} \ s_1 \ s_2 \ \dots \ s_{n_{IS}}) . \quad (4.24)$$

The distance between \mathbf{S} and another valid \mathbf{S}' with

$$\mathbf{S}' = (s'_1 \ s'_2 \ \dots \ s'_{n_{IS}} \ s'_1 \ s'_2 \ \dots \ s'_{n_{IS}}) \quad (4.25)$$

(at the transmitter) is:

$$d_T^2 = \left(2|s_1 - s'_1|^2 + 2|s_2 - s'_2|^2 + \dots + 2|s_{n_{IS}} - s'_{n_{IS}}|^2 \right) . \quad (4.26)$$

With channel gain h the distance at the receiver is simply

$$d_R^2 = |h|^2 \left(2|s_1 - s'_1|^2 + 2|s_2 - s'_2|^2 + \dots + 2|s_{n_{IS}} - s'_{n_{IS}}|^2 \right) = |h|^2 d_T^2 . \quad (4.27)$$

The distance at the receiver is simply a scaled version of the code word distance at the transmitter and thus code pairs that have the smallest (largest) distance at the transmitter, have the smallest (largest) distance at the receiver too. In the following, this behavior is called the *Distance Proportion Preservation Property*. The second interesting observation is that the distance at the receiver can become zero ($d_R^2 = 0$) if and only if the channel gain is zero ($|h|^2 = 0$). The third property is that the distance (irrespective whether it is measured at the receiver or at the transmitter) of code word pairs with single symbol errors is always smaller than the distance between code word pairs with double or multiple symbol errors. Therefore, we can conclude that the error performance is governed by single symbol errors. These properties are not new but useful in the following discussion.

O-STBCs:

In the following the distance properties of pairs of valid code words are discussed for O-STBCs. As defined in Def. 4.1, O-STBCs have a scaled identity distance matrix for all code pairs:

$$\mathbf{A} = \left(|s_1 - s'_1|^2 + |s_2 - s'_2|^2 + \dots + |s_{n_{IS}} - s'_{n_{IS}}|^2 \right) \mathbf{I} \quad (4.28)$$

With this knowledge and the aid of Eqn.(4.17) and Eqn.(4.18) the distance at the **transmitter** reads as:

$$d_T^2 = \text{tr}(\mathbf{A}) = \left(|s_1 - s'_1|^2 + |s_2 - s'_2|^2 + \dots + |s_{n_{IS}} - s'_{n_{IS}}|^2 \right) \quad (4.29)$$

and the distance at the **receiver**:

$$\begin{aligned} d_R^2 &= \text{tr}(\mathbf{H}\mathbf{A}\mathbf{H}^H) \\ &= \left(|h_{11}|^2 + |h_{12}|^2 + \dots + |h_{n_R n_T}|^2 \right) \left(|s_1 - s'_1|^2 + |s_2 - s'_2|^2 + \dots + |s_{n_{IS}} - s'_{n_{IS}}|^2 \right) \\ &= \left(|h_{11}|^2 + |h_{12}|^2 + \dots + |h_{n_R n_T}|^2 \right) d_T^2 \end{aligned} \quad (4.30)$$

Comparing these distance equations with the distance equations for the SISO case, it can be seen that O-STBCs have essentially the same properties as the block codes in SISO channels.

Thus, we can summarize the distance properties for block codes in SISO channels and O-STBCs:

-) Distance Proportion Preservation Property
-) Zero distance at the receiver is possible if and only if the channel gain vanishes
-) Single symbol errors lead to the smallest distances at the receiver

Due to property 3 it can be concluded that the BER performance of such codes is governed by single symbol errors.

NO-STBC:

For NO-STBC things are quite different. In fact, these three distance properties cited above are not valid in general. It is not easy to show that these properties are not fulfilled for the entire set of NO-STBCs. Therefore, I will show two difference matrices for a simple NO-STBC as examples to illustrate these different distance properties. Let's discuss the following simple NO-STBC:

$$\mathbf{S} = \begin{pmatrix} s_1 & s_2 \\ s_2 & s_1 \end{pmatrix}, \quad (4.31)$$

which could be used in a 2×1 MIMO system using BPSK modulation for example. Choosing the code matrix \mathbf{S} and \mathbf{S}' in such a way that the difference matrix for a double symbol error results in

$$\mathbf{B}_2 = \mathbf{S} - \mathbf{S}' = \begin{pmatrix} 2 & 2 \\ 2 & 2 \end{pmatrix}, \quad (4.32)$$

the distance at the transmitter for this specific difference matrix is:

$$d_T^2 = \text{tr}(\mathbf{A}_2) = 16. \quad (4.33)$$

Choosing the channel vector $\mathbf{h} = (1 \ -1)$, the distance at the receiver is:

$$d_R^2 = \text{tr}(\mathbf{h}\mathbf{A}_2\mathbf{h}^H) = 0. \quad (4.34)$$

Note that the distance at the receiver vanishes if and only if

$$\mathbf{H}\mathbf{B} = \mathbf{0}. \quad (4.35)$$

A necessary condition for getting an all zero matrix as the result of a matrix multiplication is that both involved matrices have to be singular, i.e., the determinant of each matrix is zero [50]. A vanishing determinant is equivalent to the fact that the corresponding matrix is rank deficient.

Let's consider a second difference matrix from the STBC defined in Eqn. (4.31). For a single symbol error, with s_1 erroneously, the difference matrix is:

$$\mathbf{B}_1 = \mathbf{S} - \mathbf{S}' = \begin{pmatrix} 2 & 0 \\ 0 & 2 \end{pmatrix}. \quad (4.36)$$

The distances at the transmitter and at the receiver are:

$$d_T^2 = \text{tr}(\mathbf{A}_{i,j}^{(2)}) = 8 \quad d_R^2 = \text{tr}(\mathbf{h}\mathbf{A}_{i,j}^{(2)}\mathbf{h}^H) = 8. \quad (4.37)$$

With these two simple examples I have illustrated that the three properties, which are valued for SISO block coding and O-STBCs, are not valid in case of NO-STBCs. The first property, Distance Proportion

Preservation Property, says that if the distance of one code pair is larger than the other at the transmitter, then it must also be larger at the receiver. Consider the two code pairs above, this is not true for the code in Eqn. (4.31) and thus it is not true in general for the entire set of NO-STBCs.

The next property is that the distance at the receiver can become zero if and only if the entire channel gain vanishes. Considering the first example (\mathbf{B}_2), the distance at the receiver is zero, although the channel gain is not zero: $|h|^2 = |h_{11}|^2 + |h_{12}|^2 = 2$. Thus, the second property does not hold in this case.

The third property, the smallest distance corresponds to single symbol errors, is also not valid here, since the distance at the receiver for \mathbf{B}_2 corresponding to a double symbol error is smaller (actually zero) than the distance at the receiver in case of a single symbol error.

Therefore, we formulate a so-called MIMO-paradoxon:

The distance properties valid for block codes in SISO systems and for O-STBCs are in general not valid for NO-STBCs and most important: large distances at the transmitter can be transformed into small distances at the receiver.

Therefore, in case of data transmission over MIMO systems a fundamental question arises: What kind of errors dominate the BER performance in case of NO-STBCs at various levels of SNR. This question will be answered in the following section.

4.1.3.2 Dominating Errors

In this section we want to find out what kind of errors dominate the BER performance of NO-STBCs. Unfortunately, this cannot be solved in general. Therefore, we first focus on the simple example shown in Sec. 4.1.3.1, Eqn. (4.31). As shown in Sec. 4.1.2 the PEPs strongly depend on the eigenvalues of the distance matrix. Thus calculating the eigenvalues of the distance matrix can help to get more insight into the BER performance of NO-STBCs. The eigenvalues corresponding to the single symbol error (difference matrix \mathbf{B}_1 , Eqn. (4.36)) are $\lambda_1^{(1)} = \lambda_2^{(1)} = 2$ in this example, and the eigenvalues corresponding to the double symbol error (difference matrix \mathbf{B}_2 , Eqn. (4.32)) are $\lambda_1^{(2)} = 16$ and $\lambda_2^{(2)} = 0$. As it is already known from Sec. 4.1.2, at low SNR the trace of \mathbf{A} determines the BER performance. Thus, in the low SNR regime the single symbol error is dominating due to the small trace of \mathbf{A}_1 ($\text{tr}(\mathbf{A}_1)=4$), whereas for the double error case we have $\text{tr}(\mathbf{A}_2)=16$. In contrast, in the high SNR domain a high rank of \mathbf{A} is important and thus the double error case dominates the BER. In Fig. 4.1 the PEPs vs. SNR corresponding to the single symbol error and the double symbol error are plotted. For this purpose the PEP approximation of Eqn. (4.21) is used. Fig. 4.1 confirms the expected behavior of the PEPs. The single symbol error (\mathbf{B}_1 , blue line) dominates the BER at low SNR and the double symbol error (\mathbf{B}_2 , black line) dominates the BER at high SNR.

This behavior, namely that single symbol errors dominate the BER at low SNR and multiple symbol errors dominate the BER at high SNR, has been observed for all NO-STBCs we have investigated. This is not a prove in a mathematical sense, but it is an interesting empirical result that strengthens our general claim and philosophy.

Moreover, Fig. 4.1 confirms the code design criteria derived in Sec. 4.1.2. The PEP is minimized in the low SNR domain if the trace of the distance matrix \mathbf{A} is maximized. In the high SNR domain a high rank of \mathbf{A} reduces the PEP.

In the following we show an alternative explanation why multiple errors can dominate the performance in some SNR regions, which is based on the distance distributions of code word pairs at the receiver. Once again, we focus on the simple code example presented in Eqn. (4.31). According to Eqn. (4.19) the distance at the receiver is χ^2 distributed with 4 degrees of freedom and a total variance of 2 ($\lambda_1 = \lambda_2 = 2$)

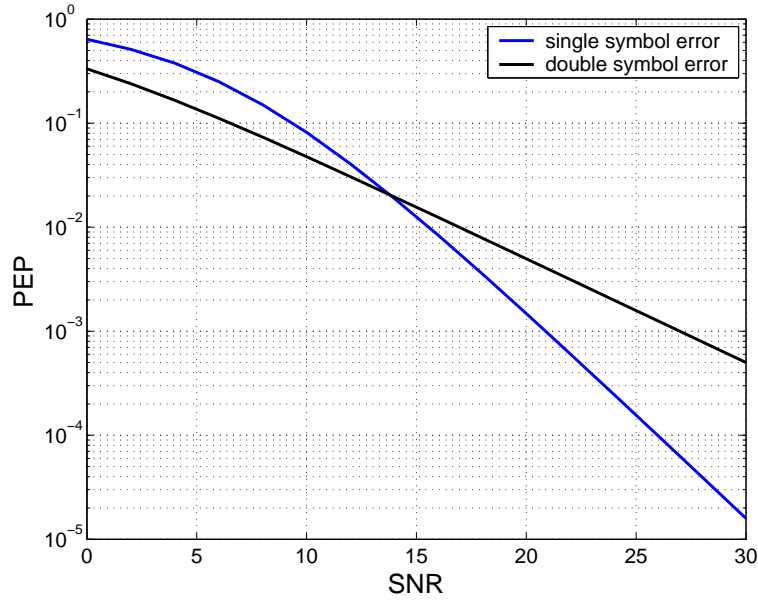


Figure 4.1: PEP vs. SNR performance for the cyclic STBC. BPSK modulation; $n_T = 2$, $n_R = 1$.

for the single symbol error. The code word distance at the receiver for the double symbol error is χ^2 distributed with 2 degrees of freedom and total variance of 16 ($\lambda_1 = 16$). The PEP is the expectation value of the Gaussian Q-function with respect to the distance ξ that means

$$\text{PEP} = \int_0^{\infty} Q\left(\frac{\xi}{2\sigma_n^2}\right) p_{d^2}(\xi) d\xi, \quad (4.38)$$

i.e., the Gaussian Q-function has to be multiplied by the PDF of the distance ξ and the area under the weighted Q-function is the mean PEP. The distribution of the code word distances at the receiver for a single symbol error (\mathbf{B}_1) and a double symbol error (\mathbf{B}_2) is shown in Fig. 4.2. Including the Q-function⁴

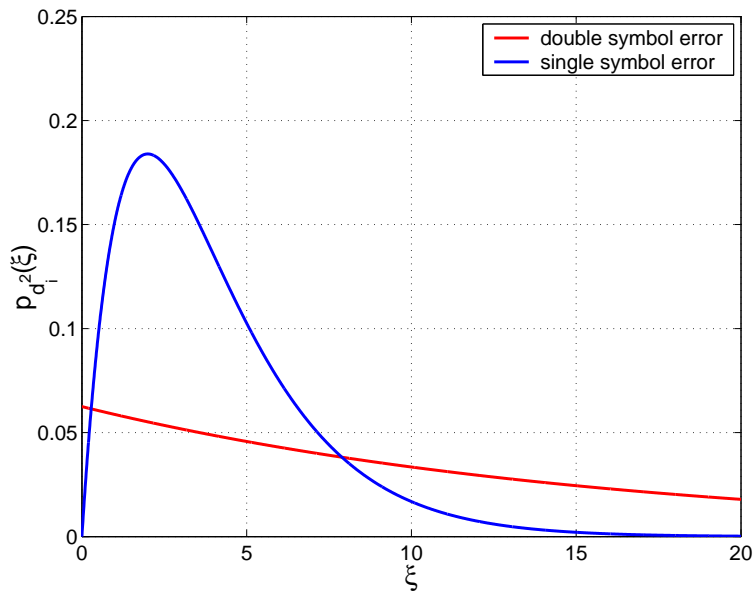


Figure 4.2: PDFs of the code word distances at the receiver for the cyclic code. BPSK modulation; $n_T = 2$, $n_R = 1$.

for different SNR values in a zoomed version of Fig. 4.2 for small values of ξ , leads to the curves in Fig. 4.3. In Fig. 4.3 one can easily estimate the multiplication of the PDF and the Q-function simply by looking at the curves. The resulting product has to be integrated over the entire range of ξ to find the mean PEP. Let's consider the Q-function for SNR=6dB and the two PDFs of the distance corresponding

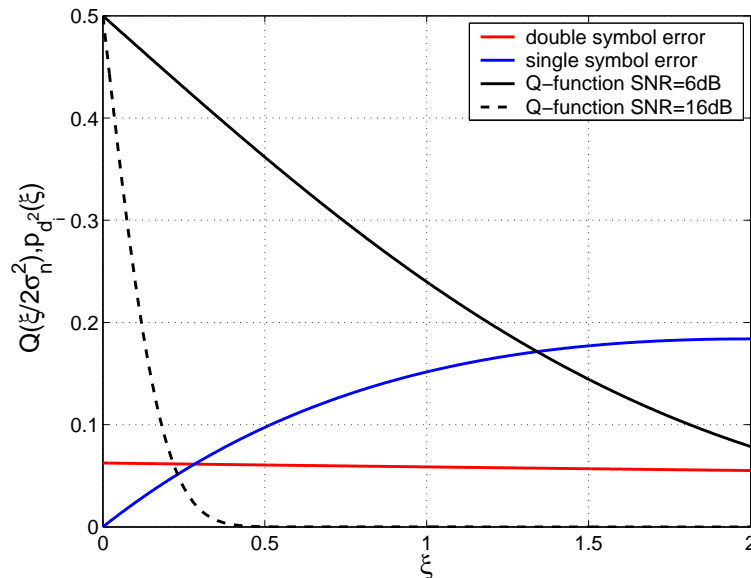


Figure 4.3: PDFs of the code word distances at the receiver for the cyclic code using BPSK modulation and the Gaussian Q-function.

to a single symbol error and a double symbol error. The product of the black solid line and the blue line is much higher than the product of the black solid line and the red line. Thus the integral over the resulting product is also essentially larger for the product with the blue line and thus single symbol errors dominate at low SNR (6dB). At 16dB SNR, where the dashed line is used as a weighting function for the blue and the red line, the contribution of the red curve dominates and therefore double symbol errors dominate the BER at high SNR (16dB).

A further general conclusion can be drawn, namely that essentially the **distance distribution around small distance values** determines the error performance **at high SNR**, which has already been observed in [53].

⁴The unusual shape of the Q-function is due to the linear scaled vertical axis.

4.2 Union Bound of the BER

In this section we derive a tight union bound for the BER performance of STBCs in spatially uncorrelated and correlated MIMO channels. The essential results have already been published in [54]. First, all derivations are performed for the general case and afterwards a simple example illustrates the results.

The union bound of the error probability P_ε is simply calculated by summing up all PEPs as already performed in Sec. 3:

$$P_\varepsilon \leq \frac{1}{|\mathcal{A}|^{n_{IS}}} \sum_{i=1}^{|\mathcal{A}|^{n_{IS}}} \sum_{\substack{j=1 \\ j \neq i}}^{|\mathcal{A}|^{n_{IS}}} \text{PEP}_{i,j}. \quad (4.39)$$

Note that Eqn. (4.39) implicitly assumes that the code words occur equally likely. In order to obtain a union bound for the BER, a further step is necessary. For each crossover event $\mathbf{S}_i \rightarrow \mathbf{S}_j$ a different number of symbols and thus a different number of bits are erroneous. For this reason, a so-called weighting factor $\tilde{w}_{i,j}$ is introduced. This factor turns the code word error probability into the BER, by counting the number of erroneous bits $n_{BE i,j}$ in the numerator and the number of transmitted bits per code word, that is $\text{ld}(|\mathcal{A}|) n_{IS}$, in the denominator:

$$\tilde{w}_{i,j} = \frac{n_{BE i,j}}{\text{ld}(|\mathcal{A}|) n_{IS}}. \quad (4.40)$$

Then, we get:

$$\text{BER} \leq \frac{1}{|\mathcal{A}|^{n_{IS}}} \sum_{i=1}^{|\mathcal{A}|^{n_{IS}}} \sum_{\substack{j=1 \\ j \neq i}}^{|\mathcal{A}|^{n_{IS}}} \tilde{w}_{i,j} \text{PEP}_{i,j}. \quad (4.41)$$

The final essential task to do, is the calculation of the exact $\text{PEP}_{i,j}$. As can be seen in Eqn. (4.16), the PEP is governed by the Euclidean distance $d_{R i,j}^2$ at the receiver. Therefore, the statistics of the distance has to be calculated and afterwards the Gaussian Q-function has to be averaged with respect to the distance distribution. Due to the different methods to calculate the PDFs of the distances at the receiver, the two spatial correlation types are considered separately.

4.2.1 Spatially Uncorrelated Channels

In this section, the union bound for spatially uncorrelated channels is derived. For uncorrelated channels, the code word distance at the receiver is (Eqn. (4.19)):

$$d_{R i,j}^2 = \sum_{l=1}^{r_{i,j}} \lambda_l^{(i,j)} \sum_{k=1}^{n_R} |h_{k,l}^{(i,j)}|^2, \quad (4.42)$$

where $\lambda_l^{(i,j)}$ are the eigenvalues of the distance matrix $\mathbf{A}_{i,j}$. Here, two cases are considered separately: There are code pairs with distance matrices $\mathbf{A}_{i,j}$ that lead to $r_{i,j}$ **equal** eigenvalues and matrices $\mathbf{A}_{i,j}$ that have different eigenvalues, i.e., the eigenvalues of the distance matrix can be different from each other or there can be two eigenvalues that are equal and additionally two different eigenvalues, and all other combinations of eigenvalues.

In the case where all non-zero eigenvalues are equal, the distance $d_{R i,j}^2$ is χ^2 -distributed with $2r_{i,j}n_R$ degrees of freedom ⁵:

$$p_{d_{R i,j}^2}(\xi) = \frac{\xi^{r_{i,j}n_R-1}}{(\lambda^{(i,j)})^{r_{i,j}n_R} \Gamma(r_{i,j}n_R)} e^{-\frac{\xi}{\lambda^{(i,j)}}} \quad (4.43)$$

⁵The index l at $\lambda_l^{(i,j)}$ is omitted, because all eigenvalues are equal.

Averaging over distances ξ in the Gaussian Q-function results in the mean PEP:

$$\begin{aligned} \text{PEP}_e^{\text{i.i.d.}}(\lambda^{(i,j)}, r_{i,j}) &= \int_0^\infty Q\left(\sqrt{\frac{\xi}{2\sigma_n^2}}\right) \frac{\xi^{r_{i,j} n_R - 1}}{(\lambda^{(i,j)})^{r_{i,j} n_R} \Gamma(r_{i,j} n_R)} e^{-\frac{\xi}{\lambda^{(i,j)}}} d\xi \\ &= \left(\frac{1 - \mu_{i,j}}{2}\right)^{r_{i,j} n_R} \sum_{l=0}^{r_{i,j} n_R - 1} \binom{r_{i,j} n_R - 1 + l}{l} \left(\frac{1 + \mu_{i,j}}{2}\right)^l, \\ &\quad \text{with } \mu_{i,j} = \sqrt{\frac{\lambda^{(i,j)}}{4\sigma_n^2 + \lambda^{(i,j)}}}. \end{aligned} \quad (4.44)$$

The solution of the integral is taken from [36].

For other code pairs with a general set of eigenvalues of $\mathbf{A}_{i,j}$, we start with an example. Consider the case where $\lambda_1^{(i,j)} = \lambda_3^{(i,j)}$, then this eigenvalue is denoted by $\lambda_1'^{(i,j)}$, and if $\lambda_2^{(i,j)} = \lambda_4^{(i,j)}$, then this eigenvalue by $\lambda_2'^{(i,j)}$ (assuming $r_{i,j} = 4$). Then, the distance at the receiver (Eqn. (4.42)) reads as:

$$\begin{aligned} d_{Ri,j}^2 &= \lambda_1^{(i,j)} \sum_{k=1}^{n_R} |h_{k,1}^{(i,j)}|^2 + \lambda_2^{(i,j)} \sum_{k=1}^{n_R} |h_{k,2}^{(i,j)}|^2 + \lambda_3^{(i,j)} \sum_{k=1}^{n_R} |h_{k,3}^{(i,j)}|^2 + \lambda_4^{(i,j)} \sum_{k=1}^{n_R} |h_{k,4}^{(i,j)}|^2 \\ &= \lambda_1'^{(i,j)} \left(\sum_{k=1}^{n_R} |h_{k,1}^{(i,j)}|^2 + \sum_{k=1}^{n_R} |h_{k,3}^{(i,j)}|^2 \right) + \lambda_2'^{(i,j)} \left(\sum_{k=1}^{n_R} |h_{k,2}^{(i,j)}|^2 + \sum_{k=1}^{n_R} |h_{k,4}^{(i,j)}|^2 \right) \\ &= \sum_{q=1}^2 \lambda_q'^{(i,j)} \sum_{n=1}^{2n_R} |h_n^{(q)}|^2, \end{aligned} \quad (4.45)$$

where $h_n^{(1)}$ summarizes the elements $h_{k,1}^{(i,j)}$ and $h_{k,3}^{(i,j)}$ for all k ($k = 1, 2, \dots, n_R$) and $h_n^{(2)}$ summarizes the elements $h_{k,2}^{(i,j)}$ and $h_{k,4}^{(i,j)}$ for all k ($k = 1, 2, \dots, n_R$).

For general considerations we denote the number of different eigenvalues by $e^{(i,j)}$ and the frequency of the q -th eigenvalue is denoted by $f_q^{(i,j)}$. Then, the distance at the receiver (Eqn. (4.45)) can be rewritten as:

$$d_{Ri,j}^2 = \sum_{q=1}^{e^{(i,j)}} \lambda_q'^{(i,j)} \sum_{n=1}^{f_q^{(i,j)} n_R} |h_n^{(q)}|^2, \quad (4.46)$$

where the elements $h_n^{(q)}$ are a subset of the set of all elements $h_{k,l}^{(i,j)}$ as explained in the example above.

Thus, the Characteristic Function (CF) of the squared distance $d_{Ri,j}^2$ results in:

$$\Psi_{d_{Ri,j}^2}(\omega) = \frac{1}{\prod_{q=1}^{e^{(i,j)}} \left(1 - j\omega \lambda_q'^{(i,j)}\right)^{f_q^{(i,j)} n_R}}.$$

After a partial fraction expansion the CF can be written in the form::

$$\Psi_{d_{Ri,j}^2}(\omega) = \sum_{q=1}^{e^{(i,j)}} \sum_{p=1}^{f_q^{(i,j)} n_R} \frac{K_{pq}^{(i,j)}}{\left(1 - j\omega \lambda_q'^{(i,j)}\right)^p}.$$

Knowing the CF we can calculate the PDF of the squared distance by applying the inverse Fourier transform on $\Psi_{d_{Ri,j}^2}(-\omega)$ resulting in:

$$p_{d_{Ri,j}^2}(\xi) = \sum_{q=1}^{e^{(i,j)}} \sum_{p=1}^{f_q^{(i,j)} n_R} \frac{K_{pq}^{(i,j)} \xi^{p-1}}{(\lambda_q'^{(i,j)})^p (p-1)!} e^{-\frac{\xi}{\lambda_q'^{(i,j)}}}$$

with

$$K_{pq}^{(i,j)} = \frac{\left\{ \frac{d^{f_q^{(i,j)} n_R - p}}{dx^{f_q^{(i,j)} n_R - p}} \left(1 + x \lambda_q'^{(i,j)} \right)^{f_q^{(i,j)} n_R} e^{(i,j)} \prod_{q=1}^{f_q^{(i,j)} n_R} \left(\frac{1}{1 + x \lambda_q'^{(i,j)}} \right)^{f_q^{(i,j)} n_R} \right\} \Big|_{x = -\frac{1}{\lambda_q'^{(i,j)}}}}{(f_q^{(i,j)} n_R - p)! (\lambda_q'^{(i,j)})^{f_q^{(i,j)} n_R - p}}$$

Averaging over the distances in the Gaussian Q-function results in the mean PEP:

$$\begin{aligned} \text{PEP}_{ue}^{\text{i.i.d.}}(\lambda_q'^{(i,j)}, f_q^{(i,j)}) &= \int_0^\infty Q\left(\sqrt{\frac{\xi}{2\sigma_n^2}}\right) p_{d_{R,i,j}^2}(\xi) d\xi \\ &= \sum_{q=1}^{e^{(i,j)}} \sum_{p=1}^{f_q^{(i,j)} n_R} K_{pq}^{(i,j)} \left(\frac{1 - \mu_q^{(i,j)}}{2}\right)^p \sum_{l=0}^{p-1} \binom{p-1+l}{l} \left(\frac{1 + \mu_q^{(i,j)}}{2}\right)^l \\ &\text{with } \mu_q^{(i,j)} = \sqrt{\frac{\lambda_q'^{(i,j)}}{4\sigma_n^2 + \lambda_q'^{(i,j)}}} \end{aligned} \quad (4.47)$$

Investigating the eigenvalues of $\mathbf{A}_{i,j}$ for all crossover events can help to simplify the summation in Eqn. (4.41). According to Def. 3.1 the key-parameters determining the BER-performance are the eigenvalues of $\mathbf{A}_{i,j}$.

In order to show the entire calculation of the union bound for the BER in all details, I will concretize my investigations by focusing on one specific example. In this example, the cyclic code ($n_T = 4$) defined in Eqn. (4.9) is used. BPSK is used as the modulation format. For most codes the Error Types (ETs) and their corresponding parameters can only be found by an exhaustive search. Exceptions are for example orthogonal codes, the cyclic code and the EA code, because their eigenvectors are the same for all crossover events and therefore we can easily find analytic expressions for the eigenvalues. With these expressions it is possible to list all ETs and the corresponding key-parameters in a similar manner as it has been shown in Sec. (3.3.1). If an exhaustive search is used to find the key-parameters of the various ETs, it is advantageous to utilize the symmetries of the underlying modulation format, in order to save computation time. The ETs and their corresponding key-parameters of the cyclic code defined in Eqn. (4.9) are shown in Table. 4.1. Here, the key-parameter of the ETs are: the sets of eigenvalues,

ET k	$\lambda_1^{(k)}$	$\lambda_2^{(k)}$	$\lambda_3^{(k)}$	$\lambda_4^{(k)}$	f_k	n_{BEk}
k	0	0	0	0	16	0
1	4	4	4	4	64	1
2	16	8	8	0	64	2
3	16	16	0	0	32	2
4	36	4	4	4	32	3
5	20	20	4	4	32	3
6	16	16	16	16	8	4
7	32	32	0	0	4	4
8	64	0	0	0	4	4

Table 4.1: ET table for the cyclic STBC. BPSK modulation; $n_T = 4$.

the number f_k of crossover events leading to a certain ET and the corresponding number n_{BEk} of different information bits. In this example it can be seen that the ETs with number $k=1,3,6,7,8$ have equal eigenvalues and therefore the $\text{PEP}_e^{\text{i.i.d.}}(\lambda^{(i,j)}, r_{i,j})$ given in Eqn. (4.44) is used to calculate the

corresponding PEP. For the remaining ETs with number $k=2,4,5$ the $\text{PEP}_{ue}^{\text{i.i.d.}}(\lambda_q^{(i,j)}, f_q^{(i,j)})$ given in Eqn. (4.47) is used. Due to only two different eigenvalues the PEP is governed by only four parameters and therefore it is denoted by $\text{PEP}_{ue}^{\text{i.i.d.}}(\lambda_1^{(i,j)}, f_1^{(i,j)}, \lambda_2^{(i,j)}, f_2^{(i,j)})$ instead of $\text{PEP}_{ue}^{\text{i.i.d.}}(\lambda_q^{(i,j)}, f_q^{(i,j)})$.

Summing up the PEPs for all crossover events results in the double sum given in Eqn. (4.41). Due to the introduction of the ETs, the summation over all crossover events can be reduced to a single sum over all ETs and thus Eqn. (4.41) reduces to:

$$\text{BER} \leq \sum_{k=1}^{n_{ET}} w_k \text{PEP}_k^{\text{i.i.d.}}, \quad \text{with} \quad w_k = \frac{f_k}{|\mathcal{A}|^{n_{IS}}} \frac{n_{BEk}}{\text{ld}(|\mathcal{A}|) n_{IS}}, \quad (4.48)$$

where $\text{PEP}_k^{\text{i.i.d.}}$ denotes the PEP for the k -th ET and n_{ET} is the number of distinct ETs. In the special case of the cyclic STBC ($n_T = 4$) discussed here, n_{ET} is 8 (ET0 is of no relevance, since it corresponds to a correct code word detection).

Inserting the parameters given in Table. 4.1 the union bound for the BER of this cyclic code ($n_T = 4$) can be written as:

$$\begin{aligned} \text{BER} \leq & 1 \cdot \text{PEP}_e^{\text{i.i.d.}}(4, 4) + 2 \cdot \text{PEP}_{ue}^{\text{i.i.d.}}(16, 1, 8, 2) + 1 \cdot \text{PEP}_e^{\text{i.i.d.}}(16, 2) + \frac{3}{2} \cdot \text{PEP}_{ue}^{\text{i.i.d.}}(36, 1, 4, 3) + \\ & \frac{3}{2} \cdot \text{PEP}_{ue}^{\text{i.i.d.}}(20, 2, 4, 2) + \frac{1}{2} \cdot \text{PEP}_e^{\text{i.i.d.}}(16, 4) + \frac{1}{4} \cdot \text{PEP}_e^{\text{i.i.d.}}(32, 2) + \frac{1}{4} \cdot \text{PEP}_e^{\text{i.i.d.}}(64, 1). \end{aligned} \quad (4.49)$$

The union bound derived in this section is compared to the well known and commonly used, but rather loose Tarokh union bound and to simulation results for this specific code using BPSK modulation in Sec. 4.2.5.

4.2.2 Spatially Correlated Channels

Here, I will show a summary of the essential calculations to obtain the union bound of the BER performance in spatially correlated channels. The channel correlation is modelled according to the W-model, introduced in Sec. 2.2. Again, the code word distances at the receiver are the essential parameters determining the BER and therefore I will start with calculating $d_{Ri,j}^2$ in the case of spatial correlation (Eqn. (4.17)):

$$d_{Ri,j}^2 = \text{tr}(\mathbf{H}\mathbf{A}_{i,j}\mathbf{H}^H) = \mathbf{h}^T \tilde{\mathbf{A}}_{i,j} \mathbf{h}^*, \quad (4.50)$$

where $\mathbf{h}^T = (\mathbf{h}_1^T \ \mathbf{h}_2^T \ \dots \ \mathbf{h}_{n_R}^T)$ and \mathbf{h}_i^T is the i -th row vector of \mathbf{H} . The matrix $\tilde{\mathbf{A}}_{i,j}$ is a block-diagonal matrix including n_R -times the matrix $\mathbf{A}_{i,j}$: $\tilde{\mathbf{A}}_{i,j} = \text{diag}(\mathbf{A}_{i,j}, \mathbf{A}_{i,j}, \dots, \mathbf{A}_{i,j})$. The next step is to model the statistical behavior of the vector \mathbf{h} , which is done as follows:

$$\mathbf{h}^T = \mathbf{g}^T \tilde{\mathbf{R}}_H^{1/2}, \quad (4.51)$$

where $\tilde{\mathbf{R}}_H$ can be calculated as:

$$\tilde{\mathbf{R}}_H = E_H \left\{ \mathbf{h}^* \mathbf{h}^T \right\} = \mathbf{U}_{\tilde{\mathbf{R}}_H}^* \mathbf{D}_{\tilde{\mathbf{R}}_H} \mathbf{U}_{\tilde{\mathbf{R}}_H}^T, \quad (4.52)$$

where

$$\mathbf{U}_{\tilde{\mathbf{R}}_H} = (\mathbf{u}_{\tilde{\mathbf{R}}_H 1,1} \ \mathbf{u}_{\tilde{\mathbf{R}}_H 2,1} \ \dots \ \mathbf{u}_{\tilde{\mathbf{R}}_H n_R,1} \ \dots \ \mathbf{u}_{\tilde{\mathbf{R}}_H 1,n_T} \ \dots \ \mathbf{u}_{\tilde{\mathbf{R}}_H n_R,n_T}), \quad (4.53)$$

and $\mathbf{u}_{\tilde{\mathbf{R}}_H k,l} = \mathbf{u}_{R,k} \otimes \mathbf{u}_{T,l}$. \otimes denotes the Kronecker product (in fact stacking weighted versions of $\mathbf{u}_{T,l}$). The vector $\mathbf{u}_{R,k}$ is the k -th column vector of \mathbf{U}_R and the vector $\mathbf{u}_{T,l}$ is the l -th column vector

of \mathbf{U}_T . Both matrices are defined in Sec. 2.2. The diagonal matrix $\mathbf{D}_{\tilde{\mathbf{R}}_H}$ consists of power coupling parameters $\omega_{i,j}$:

$$\mathbf{D}_{\tilde{\mathbf{R}}_H} = \text{diag}(\omega_{1,1}, \omega_{1,2}, \dots, \omega_{1,n_R}, \dots, \omega_{n_T,1}, \dots, \omega_{n_T,n_R}). \quad (4.54)$$

With these parameters the distance $d_{Ri,j}^2$ can be written as:

$$d_{Ri,j}^2 = \mathbf{g}^T \tilde{\mathbf{R}}_H^{1/2} \tilde{\mathbf{A}}_{i,j} \tilde{\mathbf{R}}_H^{1/2} \mathbf{g}^* = \mathbf{g}^T \mathbf{U}_{\tilde{\mathbf{R}}_H}^* \underbrace{\mathbf{D}_{\tilde{\mathbf{R}}_H}^{1/2} \mathbf{U}_{\tilde{\mathbf{R}}_H}^T \tilde{\mathbf{A}}_{i,j} \mathbf{U}_{\tilde{\mathbf{R}}_H}^* \mathbf{D}_{\tilde{\mathbf{R}}_H}^{1/2}}_{\mathbf{Z}_{i,j}} \mathbf{U}_{\tilde{\mathbf{R}}_H}^T \mathbf{g}^*. \quad (4.55)$$

Remember that the statistics of an i.i.d. complex Gaussian random vector does not change by a multiplication with a unitary matrix. Eqn. (4.55) can be further simplified to:

$$d_{Ri,j}^2 = \sum_{m=1}^{n_{NZ}^{(i,j)}} |g_m|^2 \lambda_{\mathbf{Z}_{i,j}}^{(m)}, \quad (4.56)$$

where $\lambda_{\mathbf{Z}_{i,j}}^{(m)}$ are the eigenvalues of $\mathbf{Z}_{i,j}$, the variables g_m are the elements of \mathbf{g}^T and $n_{NZ}^{(i,j)}$ is the number of non-zero eigenvalues of the matrix $\mathbf{Z}_{i,j}$. The matrix $\mathbf{Z}_{i,j}$ can be written as:

$$\mathbf{Z}_{i,j} = \begin{pmatrix} \mathbf{D}_{11} & \mathbf{D}_{12} & \dots & \mathbf{D}_{1n_T} \\ \mathbf{D}_{21} & \mathbf{D}_{22} & \dots & \mathbf{D}_{2n_T} \\ \vdots & \vdots & \ddots & \vdots \\ \mathbf{D}_{n_T1} & \mathbf{D}_{n_T2} & \dots & \mathbf{D}_{n_T n_T} \end{pmatrix} \quad (4.57)$$

and

$$\mathbf{D}_{kl} = \begin{pmatrix} \sqrt{\omega_{k1}} \mathbf{u}_{T k}^T \mathbf{A}_{i,j} \mathbf{u}_{T l}^* \sqrt{\omega_{l1}} & 0 & \dots & 0 \\ 0 & \sqrt{\omega_{k2}} \mathbf{u}_{T k}^T \mathbf{A}_{i,j} \mathbf{u}_{T l}^* \sqrt{\omega_{l2}} & \dots & 0 \\ \vdots & \vdots & \ddots & \vdots \\ 0 & 0 & \dots & \sqrt{\omega_{kn_R}} \mathbf{u}_{T k}^T \mathbf{A}_{i,j} \mathbf{u}_{T l}^* \sqrt{\omega_{ln_R}} \end{pmatrix} \quad (4.58)$$

Now, it is possible to calculate the PDF $p_{d_{Ri,j}^2}(\xi)$ of the distance at the receiver. According to Eqn. (4.56) $d_{Ri,j}^2$ is the sum over weighted, independent χ^2 distributed random variables. The CF of the sum of independent random variable is the product of the corresponding CF's. Thus, the CF of the distance $d_{Ri,j}^2$ at the receiver results in:

$$\Psi_{d_{Ri,j}^2}(j\omega) = \prod_{m=1}^{n_{NZ}^{(i,j)}} \frac{1}{1 - j\omega \lambda_{\mathbf{Z}_{i,j}}^{(m)}}. \quad (4.59)$$

Note, that $n_{NZ}^{(i,j)} = n_R r_{i,j}$, if the matrix $\tilde{\mathbf{R}}_H$ is non-singular. $r_{i,j}$ is the rank of $\mathbf{A}_{i,j}$. The matrix $\tilde{\mathbf{R}}_H$ is non-singular, if all elements of $\mathbf{\Omega}$ are non zero (Eqn. 4.54). The maximum value of $n_{NZ} = n_R n_T$ is achieved, if and only if both matrices $\mathbf{A}_{i,j}$, $\tilde{\mathbf{R}}_H$ are regular. Applying a partial fraction expansion to Eqn. (4.59), the PDF of $d_{Ri,j}^2$ is easily obtained by the inverse Fourier transform of $\Psi_{d_{Ri,j}^2}(-j\omega)$, resulting in:

$$p_{d_{Ri,j}^2}(\xi) = \sum_{m=1}^{n_{NZ}^{(i,j)}} \frac{\left(\lambda_{\mathbf{Z}_{i,j}}^{(m)}\right)^{n_{NZ}^{(i,j)} - 2}}{\prod_{\substack{n=1 \\ n \neq m}}^{n_{NZ}^{(i,j)}} \left(\lambda_{\mathbf{Z}_{i,j}}^{(m)} - \lambda_{\mathbf{Z}_{i,j}}^{(n)}\right)} e^{-\frac{\xi}{\lambda_{\mathbf{Z}_{i,j}}^{(m)}}}. \quad (4.60)$$

Note, that for the partial fraction expansion it is assumed that all eigenvalues are different, which is the case for “measured” power coupling matrices $\mathbf{\Omega}$, but can eventually be a problem for synthetic $\mathbf{\Omega}$ matrices.

The mean PEP results in:

$$\begin{aligned} \text{PEP}_{i,j}^{\text{W}} &= \mathbf{E}_{\mathbf{H}} \left\{ Q \left(\sqrt{\frac{d_{Ri,j}^2}{2\sigma_n^2}} \right) \right\} = \sum_{m=1}^{n_{NZ}^{(i,j)}} \frac{\left(\lambda_{\mathbf{Z}_{i,j}^{(m)}} \right)^{n_{NZ}^{(i,j)}-2}}{\prod_{\substack{n=1 \\ n \neq m}}^{n_{NZ}^{(i,j)}} \left(\lambda_{\mathbf{Z}_{i,j}^{(m)}} - \lambda_{\mathbf{Z}_{i,j}^{(n)}} \right)} \int_0^\infty Q \left(\sqrt{\frac{\xi}{2\sigma_n^2}} \right) e^{-\frac{\xi}{\lambda_{\mathbf{Z}_{i,j}^{(m)}}}} d\xi \\ &= \frac{1}{2} \sum_{m=1}^{n_{NZ}^{(i,j)}} \frac{\left(\lambda_{\mathbf{Z}_{i,j}^{(m)}} \right)^{n_{NZ}^{(i,j)}-1}}{\prod_{\substack{n=1 \\ n \neq m}}^{n_{NZ}^{(i,j)}} \left(\lambda_{\mathbf{Z}_{i,j}^{(m)}} - \lambda_{\mathbf{Z}_{i,j}^{(n)}} \right)} \left(1 - \sqrt{\frac{\lambda_{\mathbf{Z}_{i,j}^{(m)}}}{4\sigma_n^2 + \lambda_{\mathbf{Z}_{i,j}^{(m)}}}} \right). \end{aligned} \quad (4.61)$$

The integral has the same structure as the integral in Eqn. (3.26). The superscript W in $\text{PEP}_{i,j}^{\text{W}}$ indicates that this PEP corresponds to the W channel model.

With the results for the exact PEP the general derivations are now finished and again the cyclic code is considered as an example, in order to show all details necessary to calculate this union bound. For spatially correlated channels, the key-parameters governing the BER are the eigenvalues of $\mathbf{Z}_{i,j}$. The eigenvalues of $\mathbf{Z}_{i,j}$ depend on the channel correlation type, e.g. 1D3,14D3, and therefore the ET-table has to be constructed for each correlation type separately. Due to the large number of key-parameters, the ET-tables for the correlation types 1D3 and 14D3 are shown in Appendix F.

Instead of summing up the contributions of all crossover events, only the weighted PEPs of the smaller number of ETs are summed up:

$$\text{BER} \leq \sum_{k=1}^{n_{ET}} w_k \text{PEP}_k^{\text{W}} \quad \text{with} \quad w_k = \frac{f_k}{|\mathcal{A}|^{n_{IS}}} \frac{n_{BEk}}{\text{ld}(|\mathcal{A}|) n_{IS}}. \quad (4.62)$$

where PEP_k^{W} denotes the PEP for the k-th ET and n_{ET} is the number of distinct ETs.

The union bound derived in this section is discussed and compared to simulation results for this specific code with BPSK modulation for several correlation types in Sec. 4.2.5.

4.2.3 High SNR Approximation

In order to get a better insight into the BER performance and to compare the results for uncorrelated and correlated channels, it is helpful to calculate a high SNR approximation for the PEPs. With these approximations for the PEPs, a high SNR approximation for the union bound for the BER can be calculated. This approximation highlights the diversity degree and a so-called power loss due to channel correlation.

First, let us consider the PEP. The principle of calculating a high SNR (low σ_n^2) approximation is fairly simple. A Taylor series expansion of the PEP formula is performed. The first term of the series, which dominates the BER at high SNR is taken as an approximation of the true PEP.

Let's remember the Taylor series for a function $f(x)$ around the point x_0 :

$$f(x) = \sum_{n=0}^{\infty} \frac{(x - x_0)^n f^{(n)}(x_0)}{n!}, \quad (4.63)$$

where the superscript (n) denotes the n -th derivative of $f(x)$. The PEP for the i.i.d. channel model and for the W channel model are functions of σ_n^2 and therefore the PEPs have to be approximated around $\sigma_n^2 = 0$, in order to get a high SNR approximation. For small values σ_n^2 , the first non-zero term of the Taylor series, i.e., the term with the lowest exponent, is the most important one. In the following uncorrelated and correlated channels are treated separately.

4.2.3.1 Spatially Uncorrelated Channels

There are two different PEP formulas (Eqn. (4.44) and Eqn. (4.47)) for the spatially uncorrelated channel. The high SNR approximation of the PEP formula for equal eigenvalues (Eqn. (4.44)) reads as:

$$\begin{aligned} \text{PEP}_{i,j}^{i.i.d.-high} &= \frac{(\sigma_n^2)^{r_{i,j}n_R}}{(r_{i,j}n_R)!} \left(\frac{\partial^{r_{i,j}n_R} \text{PEP}_{i,j}^{i.i.d.}}{\partial (\sigma_n^2)^{r_{i,j}n_R}} \right) \Big|_{\sigma_n^2=0} \\ &= \left(\frac{\sigma_n^2}{\lambda^{(i,j)}} \right)^{r_{i,j}n_R} \underbrace{\sum_{k=0}^{r_{i,j}n_R-1} \binom{r_{i,j}n_R-1+k}{k}}_{(1/c^{(i,j)})^{r_{i,j}n_R}} = \left(\frac{\sigma_n^2}{\lambda^{(i,j)} c^{(i,j)}} \right)^{r_{i,j}n_R} \end{aligned} \quad (4.64)$$

with

$$c^{(i,j)} = \left[\sum_{k=0}^{r_{i,j}n_R-1} \binom{r_{i,j}n_R-1+k}{k} \right]^{-1/(r_{i,j}n_R)} \quad (4.65)$$

Due to Eqn. (4.64) the PEP mainly depends on $r_{i,j}$, n_R and $\lambda^{(i,j)}$. $r_{i,j}n_R$ determines the slope and $\lambda^{(i,j)} c^{(i,j)}$ determines the horizontal position of the PEP vs. SNR curve. Therefore, the diversity that is defined as the negative slope of the PEP vs. SNR curve or the slope of the PEP vs. σ_n^2 curve according to [27] is:

$$D_{i.i.d.} = \lim_{\sigma_n^2 \rightarrow 0} \frac{\partial(\log_{10} \text{PEP}_{i,j}^{i.i.d.-high})}{\partial(\log_{10} \sigma_n^2)} = r_{i,j}n_R. \quad (4.66)$$

Note that in the derivation in Eqn. (4.66) the high SNR approximation for the PEP is used.

The derivation for the PEP formula for different eigenvalues (Eqn. (4.47)) could be done in the same way as in the previous case. But due to the complicate form of this PEP formula, I describe another way, in order to simplify the necessary calculation. By expressing the Gaussian Q-function according to [53] by:

$$Q(x) = \frac{1}{\pi} \int_0^{\pi/2} e^{-\frac{x^2}{2 \sin^2(\phi)}} d\phi, \quad (4.67)$$

I get the following result for the exact PEP:

$$\text{PEP} = \frac{1}{\pi} \int_0^{\pi/2} \Psi_{d_{Ri,j}^2} \left(-\frac{1}{j4 \sin^2(\phi) \sigma_n^2} \right) d\phi, \quad (4.68)$$

where $\Psi_{d_{Ri,j}^2}$ is the Characteristic Function (CF) of the distance $d_{Ri,j}^2$. The CF can be expanded in a power series and the integral could be calculated for all terms of the series. For a high SNR approximation of the PEP only the term with the lowest exponent for σ_n^2 is of interest and therefore a high SNR approximation of the CF is used and the integration in Eqn. (4.68) considers only the dominating term, to come up with an high SNR approximation for the PEP:

$$\text{PEP}_{i,j}^{i.i.d.-high} = \left(\frac{\sigma_n^2}{r_{i,j} \sqrt{\prod_{m=1}^{r_{i,j}} \lambda_m^{(i,j)} c^{(i,j)}}} \right)^{r_{i,j} n_R} \quad (4.69)$$

Comparing the two high SNR approximations for the PEP (Eqn. (4.64) and Eqn. (4.69)), it is easy to see that they are almost identical. The only difference is that the eigenvalue $\lambda^{(i,j)}$ in Eqn. (4.64) is replaced by the geometric mean of the eigenvalues. The effective distance, irrespective of which type of PEP is considered, can be defined as:

$$d_{i.i.d.-i,j}^2 = r_{i,j} \sqrt{\prod_{m=1}^{r_{i,j}} \lambda_m^{(i,j)}} \quad (4.70)$$

A high SNR approximation for the union bound for the BER is easily obtained by taking only those ETs into account, which have minimum diversity. Minimum diversity is achieved by ETs with minimum rank r_{min} . In the following the number of ETs, which have minimum rank is denoted by n_{min} . Then, the high SNR approximation for the BER results in⁶:

$$\text{BER}^{i.i.d.-high} \leq \sum_{k=1}^{n_{min}} w_k \left(\frac{\sigma_n^2}{r_{min} \sqrt{\prod_{m=1}^{r_{min}} \lambda_m^{(k)} c^{(k)}}} \right)^{r_{min} n_R}. \quad (4.71)$$

It is rather convenient to define a new distance parameter $d_{i.i.d.}^2$:

$$d_{i.i.d.}^2 = \frac{1}{r_{min} n_R \sqrt{\sum_{k=1}^{n_{min}} \frac{w_k}{\left(r_{min} \sqrt{\prod_{m=1}^{r_{min}} \lambda_m^{(k)} c^{(k)}} \right)^{r_{min} n_R}}}}. \quad (4.72)$$

With this new parameter, the high SNR approximation of the union bound for the BER can be written as:

$$\text{BER}^{i.i.d.-high} = \left(\frac{\sigma_n^2}{d_{i.i.d.}^2} \right)^{r_{min} n_R}, \quad (4.73)$$

For the high SNR approximation of the union bound for the BER the same properties hold as for the high SNR approximation of the exact PEP, i.e., the slope of the BER vs. SNR curve and thus the diversity is $r_{min} n_R$ and the horizontal position of the curve is determined by $d_{i.i.d.}^2$.

⁶Note that we now focus on ETs instead of crossover events and thus the index i, j is replaced by k .

4.2.3.2 Spatially Correlated Channels

In this section essentially the same derivation as for the uncorrelated case is done for correlated channels. Investigating the PEP, it turns out that the first non-zero term of the Taylor series has the exponent $n_{NZ}^{(i,j)}$ (number of non-zero eigenvalues) and thus the high SNR approximation of the PEP results in:

$$\begin{aligned} \text{PEP}_{i,j}^{W-high} &= \frac{(\sigma_n^2)^{n_{NZ}^{(i,j)}}}{n_{NZ}^{(i,j)}!} \left(\frac{\partial^{n_{NZ}^{(i,j)}} \text{PEP}_{i,j}^W}{\partial (\sigma_n^2)^{n_{NZ}^{(i,j)}}} \right) \Big|_{\sigma_n^2=0} \\ &= \left(\frac{\sigma_n^2}{d_{W,i,j}^2} \right)^{n_{NZ}^{(i,j)}} \underbrace{\sum_{k=0}^{n_{NZ}^{(i,j)}-1} \binom{n_{NZ}^{(i,j)}-1+k}{k}}_{(1/c_{n_{NZ}^{(i,j)}})^{n_{NZ}^{(i,j)}}} = \left(\frac{\sigma_n^2}{d_{W,i,j}^2 c_{n_{NZ}^{(i,j)}}} \right)^{n_{NZ}^{(i,j)}}, \end{aligned} \quad (4.74)$$

with

$$c_{n_{NZ}^{(i,j)}} = \left[\sum_{k=0}^{n_{NZ}^{(i,j)}-1} \binom{n_{NZ}^{(i,j)}-1+k}{k} \right]^{-1/n_{NZ}^{(i,j)}} \quad (4.75)$$

where a new effective distance $d_{W,i,j}^2$ has been introduced:

$$d_{W,i,j}^2 = n_{NZ}^{(i,j)} \sqrt{\prod_{n=1}^{n_{NZ}^{(i,j)}} \lambda_{\mathbf{Z}_{i,j}}^{(n)}} \quad (4.76)$$

The PEP mainly depends on $n_{NZ}^{(i,j)}$ and $\lambda_{\mathbf{Z}_{i,j}}^{(n)}$ ($n=1,2, \dots, n_{NZ}^{(i,j)}$). $n_{NZ}^{(i,j)}$ determines the slope and $d_{W,i,j}^2$, and thus the eigenvalues $\lambda_{\mathbf{Z}_{i,j}}^{(n)}$, determine the horizontal position of the PEP curve. Thus, according to [27] the diversity D_W of such a coded MIMO system in correlated fading is:

$$D_W = \lim_{\sigma_n^2 \rightarrow 0} \frac{\partial(\log_{10} \text{PEP}_{i,j}^{W-high})}{\partial(\log_{10} \sigma_n^2)} = n_{NZ}^{(i,j)}. \quad (4.77)$$

By defining a new distance d_W^2 the high SNR approximation of the union bound for the BER results in⁷:

$$\text{BER}^{W-high} = \left(\frac{\sigma_n^2}{d_W^2} \right)^{n_{NZmin}} \quad \text{with} \quad d_W^2 = \frac{1}{n_{NZmin} \sqrt{\sum_{k=1}^{n_{ETmin}} \frac{w_k}{(d_{W,k}^2 c_{n_{NZ}^{(k)}})^{n_{NZmin}}}}}. \quad (4.78)$$

Here, n_{NZmin} denotes the minimum number of non-zero eigenvalues and n_{ETmin} is the number of ETs, which have this minimum number of eigenvalues. For the high SNR approximation of the union bound for the BER the same properties as for the high SNR approximation for the PEP are valid, i.e., the slope of the BER vs. SNR curve and thus the Diversity is n_{NZmin} and the horizontal position of the curve is determined by d_W^2 .

⁷Note that we now focus on ETs instead of crossover events and thus the index i, j is replaced by k .

4.2.4 Diversity Loss and Loss of Coding Advantage due to Channel Correlation

At this point, I want to emphasize the differences and similarities of the BER performance of coded wireless transmission systems in uncorrelated and in correlated MIMO channels. One very interesting observation is that the diversity order and thus the slope of the BER vs. SNR curve at high SNR (according to the definition in [27]), for correlated and uncorrelated channels is the same, if $n_{NZ_{min}} = r_{min}n_R$. This is at least the case for power coupling matrices $\mathbf{\Omega}$ of the W-channel model with non-zero entries only⁸. All matrices $\mathbf{\Omega}$ extracted from measurement data have only non-zero entries (see Appendix D). Hence, a diversity loss L_D due to correlation can be defined as

$$L_D = r_{min}n_R - n_{NZ_{min}} . \quad (4.79)$$

Note that the diversity definition in [27] does not say much about the really observed diversity or really observed slope of the BER vs. SNR curve at **moderate** values of SNR. Actually, the slope of the BER vs. SNR curve at medium SNR values (or BER values) is of more practical interest than the slope at $SNR=\infty$. However, with the definition according to [27], correlated and uncorrelated MIMO channels have the same diversity order (if $n_{NZ_{min}} = r_{min}n_R$).

For correlated channels with $n_{NZ_{min}} = r_{min}n_R$ no diversity loss occurs. However the detrimental influence of spatial channel correlation shows up in a so-called power loss L_P . Due to the same diversity, the BER vs. SNR curves of correlated and uncorrelated channels are in parallel, but horizontally shifted. This shift towards higher SNR due to channel correlation is called power loss L_P and can easily be calculated as:

$$L_P = 10 \log_{10} \left(\frac{d_{i.i.d.}^2}{d_W^2} \right) . \quad (4.80)$$

A simple explanation how the spatial channel correlation and thus the matrix $\mathbf{\Omega}$ influences the **diversity loss** is given above. The influence of the matrix $\mathbf{\Omega}$ on the **power loss** is not that simple to explain. In the following I will explain what properties the matrix $\mathbf{\Omega}$ should have, to achieve a power loss as small as possible: Due to Eqn. (4.78) the distance $d_{W_k}^2$ for each ET should be as large as possible. To get large distances, it is important to have well balanced and large eigenvalues $\lambda_{\mathbf{Z}_{i,j}^{(n)}}$. This is achieved, if the matrix $\mathbf{\Omega}$ is well balanced. Then the largest distances occur and thus the smallest power loss is observed. The best balanced matrix $\mathbf{\Omega}$ is a matrix, where all entries are identical. With such an ideally balanced matrix $\mathbf{\Omega}$, the W-model degenerates to the i.i.d. model. Then, there is no spatial correlation and thus the best possible performance (no power loss) is achieved.

⁸Note that there are other matrices $\mathbf{\Omega}$ that lead to the property $n_{NZ_{min}} = r_{min}n_R$, but these matrices $\mathbf{\Omega}$ are different for different codes.

4.2.5 Examples

In this section, I want to discuss our results regarding the BER vs. SNR performance of four different codes specified in Sec. 4.1. The tight union bounds are compared to simulation results and to high SNR approximations.

4.2.5.1 Cyclic Code

In Fig. 4.4 the BER vs. SNR performance of the cyclic code defined in Eqn. (4.9) for BPSK signaling in a uncorrelated 4×4 MIMO system is shown. In this figure, the Tarokh union bound is the dashed-dotted

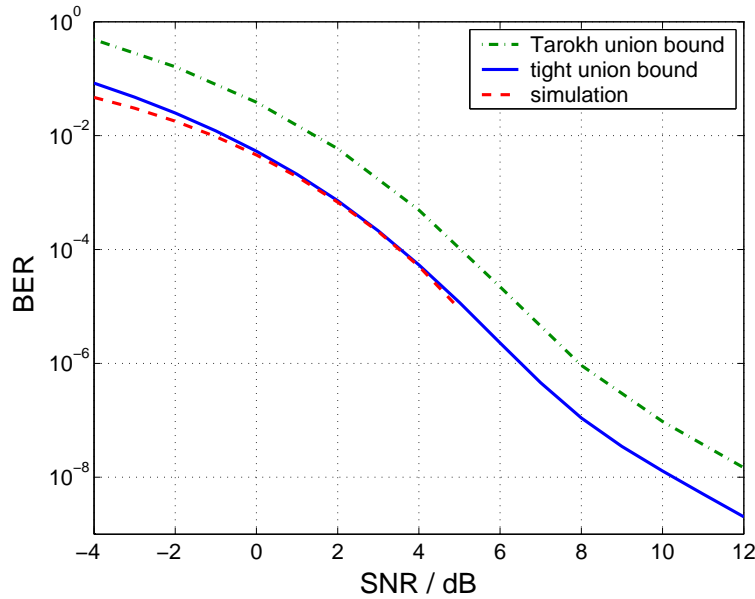


Figure 4.4: BER vs. SNR performance of the cyclic STBC. BPSK modulation; $n_T = n_R = 4$; uncorrelated MIMO channels.

green curve, the tight union bound according to Eqn. (4.49) is the solid blue curve and the simulated performance is the dashed red curve. As it can be seen the Tarokh union bound⁹ is quite far from the simulation results. This bound only reflects the behavior of the BER performance as a function of the SNR. Our tight union bound is tight for BER values below 10^{-3} . The interesting s-shape of the tight union bound comes from several contributions of different PEPs with different slopes. In order to illustrate this fact, the dominating PEPs at low and at high SNR values corresponding to ET1 and ET8 listed in Table. 4.1 are shown in Fig. 4.5. As it can be seen, the flat slope of the BER curve at high SNR results from ET8, which is a rank-one ET and corresponds to multiple symbol errors. At medium SNR the performance is dominated by ET1, which is a full rank ET and corresponds to single symbol errors. This flat slope of the BER curve is only visible for BER values lower than 10^{-6} and thus it is of no practical relevance.

Now, let's focus on the BER performance in correlated fading. The tight union bound (solid blue curves), the high SNR approximation (dashed-dotted black curves) and the simulated BER vs. SNR performance (dashed red curves) in correlated fading are shown in Fig. 4.6. The curves corresponding to uncorrelated channels are labeled with a \triangle -marker, the curves corresponding to correlation scenario 1D3 are labeled

⁹The Tarokh union bound is in principle the same approximation as the tight union bound Eqn. (4.49). The difference is that in the Tarokh bound the exact PEPs are replaced by the Chernoff bound approximation derived in Eqn. (4.21).

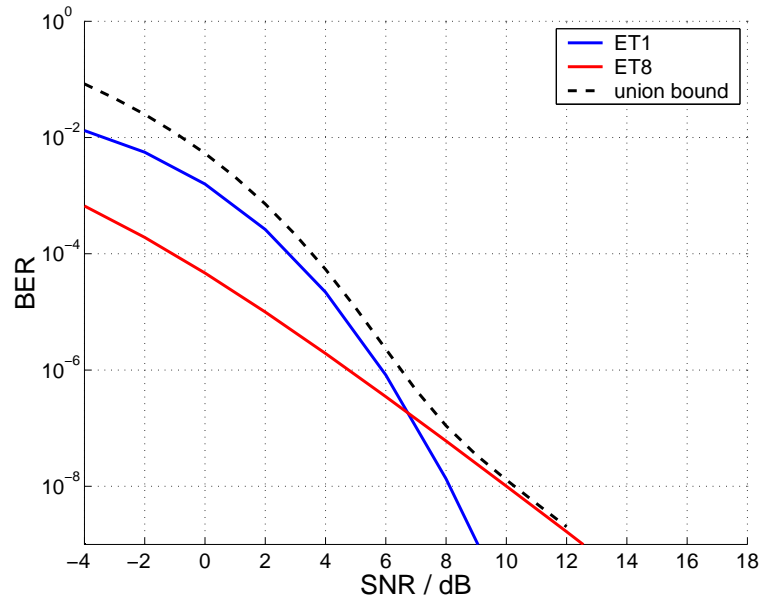


Figure 4.5: Influence of the dominating ETs on the BER vs. SNR performance of the cyclic STBC. BPSK modulation; $n_T = n_R = 4$; uncorrelated MIMO channels.

with a \circ -marker and the curves corresponding to correlation scenario 14D3 are labeled with a $+$ -marker. The tight union bounds approximate the simulated performance very well. The high SNR approximations are obviously only valid for high SNR and they are only tight in this SNR domain. From the high SNR approximations it is possible to draw the following conclusions: The slope of the BER curves at high SNR is equal to the diversity order $D = n_R = 4$ for all correlation scenarios, due to the rank one ETs. Therefore, there is no diversity loss due to channel correlation. However, the calculated power loss is $L_P = 6.89dB$ and $7.33dB$ for the spatially correlated scenarios 1D3 and 14D3. It is interesting to note

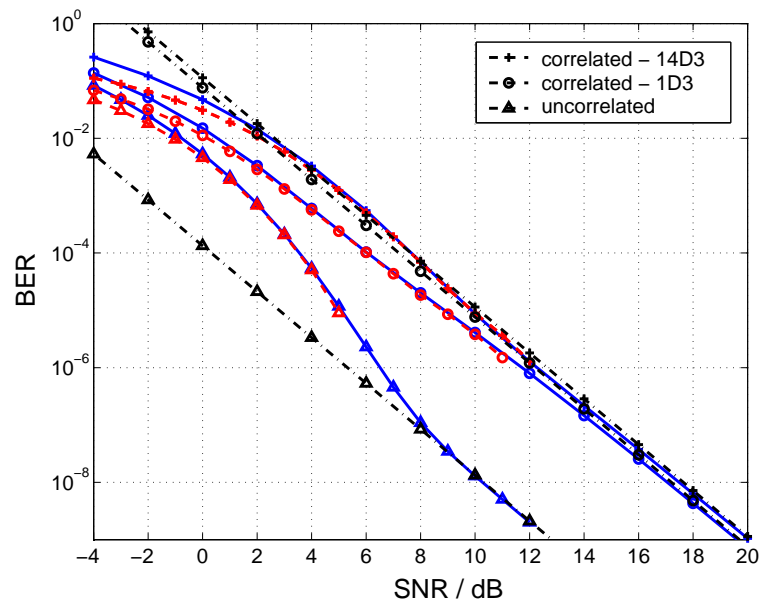


Figure 4.6: BER vs. SNR performance of the cyclic STBC. BPSK modulation; $n_T = n_R = 4$; several correlation types.

that both correlation scenarios achieve almost the same performance at high SNR, but quite different results for medium SNR. For the correlated case the flat slope of the rank one ETs is already visible at high BER values (low SNR - values).

In the following I will explain why the BER performance for the cyclic code for both correlation types is very similar. The dominating ETs and the union bound for the BER are shown in Fig. 4.7 for the scenario 1D3 and 14D3. In principal, the PEPs have the same shape as in the uncorrelated case, i.e., for

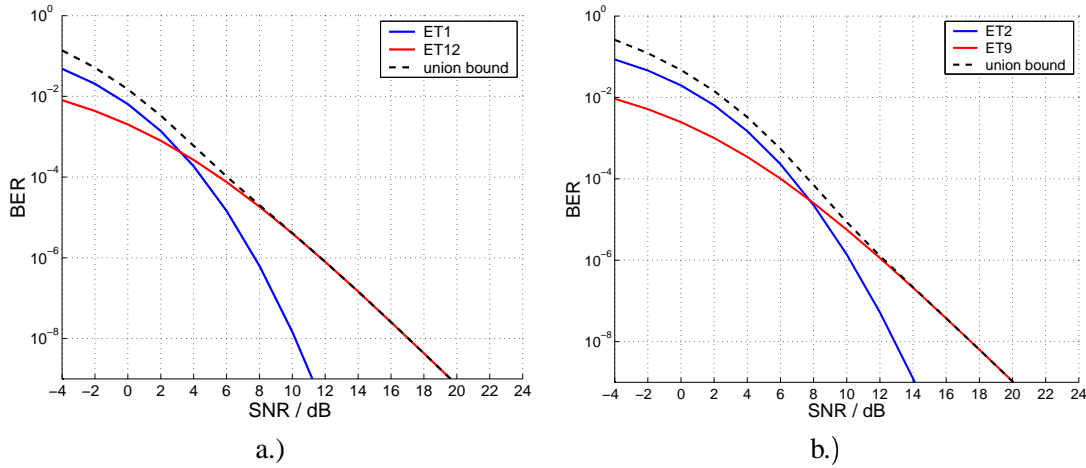


Figure 4.7: Influence of the dominating ETs on the BER vs. SNR performance of the cyclic STBC in correlated fading. BPSK modulation; $n_T = n_R = 4$; a.) correlation type 1D3. b.) correlation type 14D3.

all correlation types the BER vs. SNR curves are flattening out at high SNR - values. In order to show the influence of correlation it is better to display all dominating PEP curves in one figure (Fig. 4.8). In

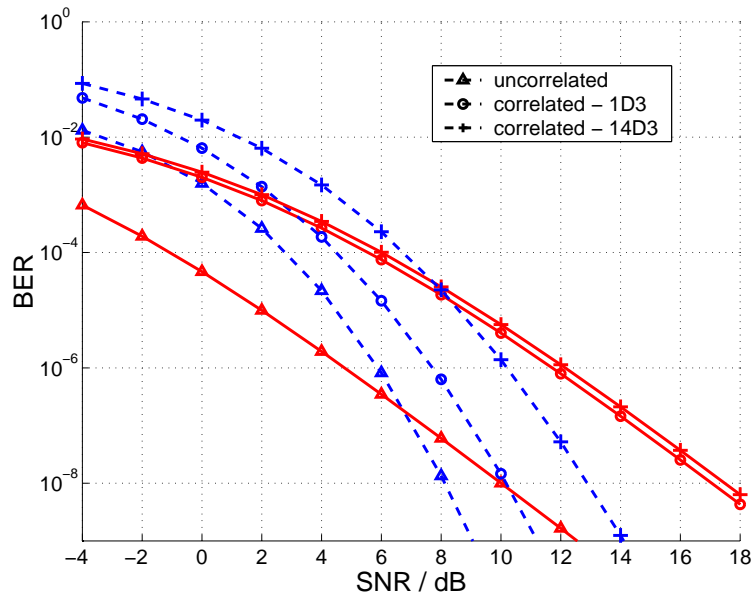


Figure 4.8: Comparison of the dominating ETs of the cyclic STBC in correlated fading. BPSK modulation; $n_T = n_R = 4$;

Fig. 4.8 the red solid lines are the PEP vs. SNR for ETs that dominate at high SNR (ET8 for uncorrelated, ET12 for 1D3, ET9 for 14D3). The blue dashed curves are the PEP vs. SNR for ETs that dominate at medium SNR (ET1 for uncorrelated, ET1 for 1D3, ET2 for 14D3). This curves are plotted for several

correlation types: uncorrelated (Δ -marker), 1D3 (\circ -marker) and 14D3 ($+$ -marker). Interestingly, the effect of correlation is different for different ETs. For the correlation type 1D3 the shift towards higher SNR for the ET that dominates at high SNR is larger than for the ET that dominates at medium SNR. The ET dominating at medium SNR is shifted by approximately 2dB SNR but the high SNR dominating ET is shifted by almost 7dB. Thus, the flattening of the BER vs. SNR curve occurs already at high BER values. For the correlation type 14D3 both ETs are shifted approximately by the same amount: 5dB for the ET dominating at medium SNR, and 7.5dB for the ET dominating at high SNR. Therefore, the flattening out of the BER curve occurs at lower BER values than for correlation type 1D3.

Note, that the performance of the ETs dominating at medium SNR deteriorates proportionally to the amount of correlation, whereas the performance loss of the ETs dominating at high SNR is almost equal.

4.2.5.2 Extended Alamouti Code

In this section, I will discuss the performance of the EA code defined in Eqn. (4.10) with $n_R = 4$ and $n_T = 4$ using QPSK modulation. As already explained in the previous example (cyclic code) the performance of the code (the shape of the BER vs. SNR curve) can be explained by means of the ET table. For this reason, I have analyzed the $4^8 = 65536$ possible distance matrices \mathbf{A}_{ij} and the corresponding sets of eigenvalues. Due to the structure of the code and the higher modulation format, there are all together only 20 different sets of eigenvalues (ETs) listed in Table 4.2, where f_k is the number of crossover events leading to a certain ET and n_{BEk} is the corresponding number of different information bits. Note that the minimum rank is 2 (only 2 non-zero eigenvalues), but this rank deficiencies (full rank is 4) are very seldom (only 2080 crossover events corresponding to ET5, ET9, ET17 and ET20 out of all possible 65536 crossover events have rank 2).

ET k	$\lambda_1^{(k)}$	$\lambda_2^{(k)}$	$\lambda_3^{(k)}$	$\lambda_4^{(k)}$	f_k	n_{BEk}
k	0	0	0	0	256	0
1	2	2	2	2	2048	1
2	4	4	4	4	6144	2
3	6	6	6	6	8192	3
4	8	8	8	8	4864	4
5	8	8	0	0	1024	2
6	10	10	2	2	6144	3
7	12	12	4	4	12288	4
8	14	14	6	6	8192	5
9	16	16	0	0	768	4
10	18	18	2	2	3072	5
11	20	20	4	4	3072	6
12	10	10	10	10	3072	5
13	12	12	12	12	3072	6
14	16	16	8	8	768	6
15	18	18	10	10	1536	7
16	16	16	16	16	96	8
17	24	24	0	0	256	6
18	26	26	2	2	512	7
19	24	24	8	8	128	8
20	32	32	0	0	32	8

Table 4.2: ET table for the Extended Alamouti STBC. QPSK modulation; $n_T = 4$; uncorrelated fading.

According to Sec. 4.2, we can calculate a tight union bound, with the aid of the ET table. In Fig. 4.9 the simulated BER vs. SNR performance (dashed red curve) is compared with this union bound (solid blue curve). Here we can see, that the bound is tight for BER values below 10^{-3} . A diversity order of almost 8 shows up at high SNR.

Focusing on the ET table, we can see that there are two dominating ETs. As we already know, the product of the non-zero eigenvalues determines the horizontal position of the BER vs. SNR curve (remember design rule of Eqn. (4.22); high SNR approximation Eqn. (4.64) and Eqn. (4.69)). Considering first the ETs with full rank, ET1 has the smallest product of eigenvalues and thus will strongly contribute to the total BER performance. For the rank 2 ETs, ET5 has the smallest eigenvalues and therefore has the strongest influence on the BER. Focusing on these two dominating ETs (ET1 and ET5), we can see how

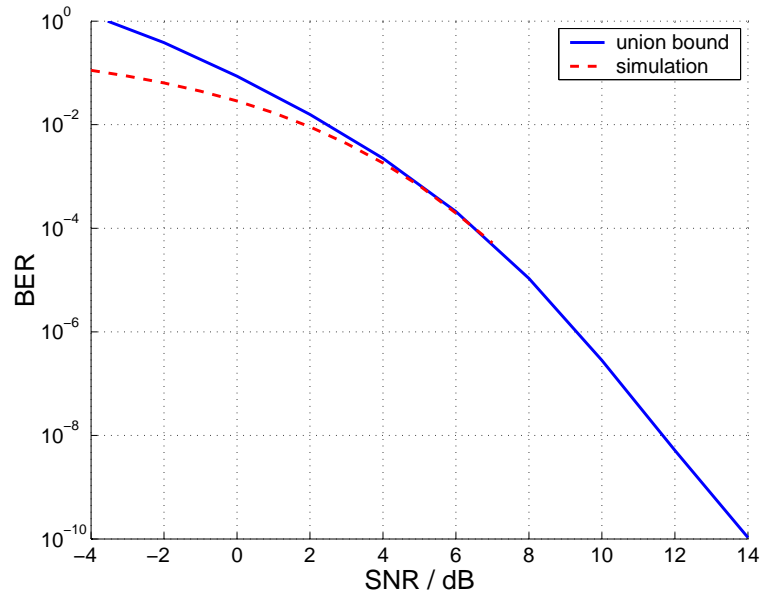


Figure 4.9: BER vs. SNR performance for the Extended Alamouti STBC. QPSK modulation; $n_T = n_R = 4$; uncorrelated MIMO channels.

this BER performance in Fig. 4.9 evolves. The BER contributions due to the 2 dominating ETs and the resulting union bound are shown in Fig. 4.10. ET1 dominates at medium SNR whereas ET5 dominates

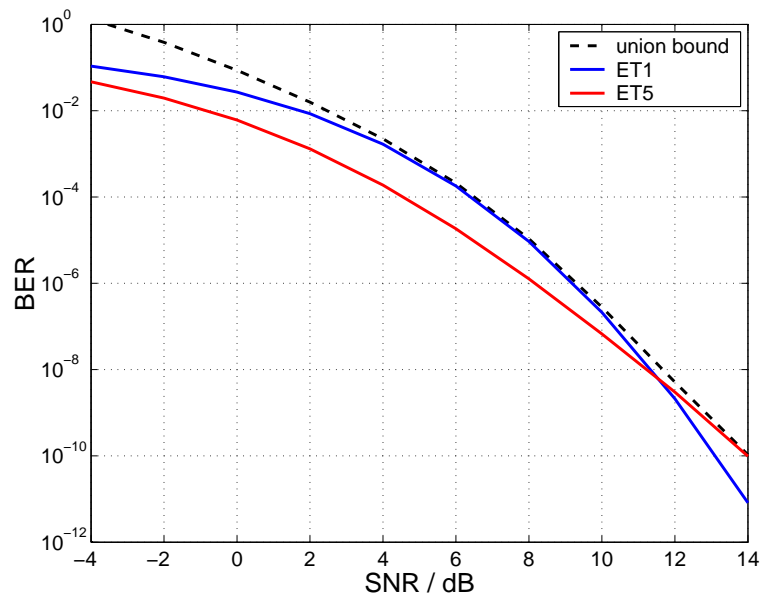


Figure 4.10: Influence of the dominating ETs on the BER vs. SNR performance of the Extended Alamouti STBC. QPSK modulation; $n_T = n_R = 4$; uncorrelated MIMO channels.

the BER performance at high SNR. The resulting slope of the BER curve stems from the superposition of the BER contributions of ET1 and ET5. The ultimate slope corresponding to diversity $n_R r_{min} = 8$ only is achieved in the limit of $\text{SNR} \rightarrow \infty$. In fact, this slope would only be visible at BER values of 10^{-12} and below.

In Fig. 4.11 the simulation results (dashed red curves), the union bounds (solid blue curves) and the high

SNR approximation (dashed-dotted black curves) according to Sec. 4.2.3 for several correlation types are shown. The spatial correlation types are: uncorrelated (Δ -marker), 1D3 (\circ -marker) and 14D3 ($+$ -marker). For these correlation types too, the union bounds are quite tight for BER values below 10^{-3} .

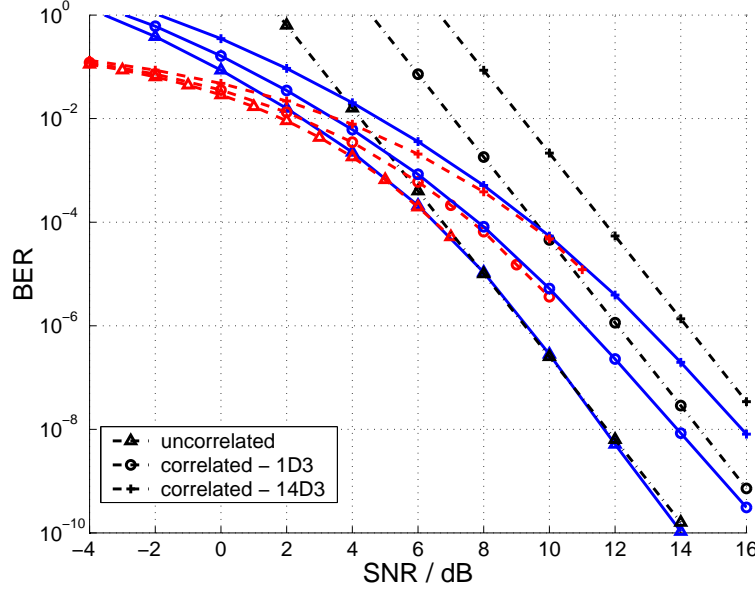


Figure 4.11: BER vs. SNR performance of the Extended Alamouti STBC. QPSK modulation; $n_T = n_R = 4$; several correlation types.

The slopes of the BER vs. SNR curves in the practical SNR range are different for different correlation types, but for really high SNR (high SNR approximations) we can see that the slope of the curves are equal. Therefore, we can conclude that the diversity order is $n_R r_{min} = 8$ irrespective of the correlation type. Additionally we can determine a so-called power loss according to Eqn. (4.80). For correlation type 1D3 we observe an SNR loss of 2.81dB and for 14D3 we observe a 4.91dB loss.

Fig. 4.12 shows how the union bounds are assembled by the dominating ETs (a.) for 1D3 and b.) for 14D3). Note, that for correlated MIMO channels the ET tables are different. The main point is that in case of correlated channels the eigenvalues of the matrix \mathbf{Z} (Eqn. (4.57)) are essential, instead of the eigenvalues of the code word distance matrix \mathbf{A} . For each correlation type we get a different ET table. Due to the hugeness of these tables they are not listed here. It is not really relevant, which ET-number k is used, but to show a correspondence to the uncorrelated case we use the same ET-numbers. For correlated channels we again number the ET dominating at high SNR also by ET5 (although ET5 is nowhere specified). In Fig. 4.12 we show how the dominating ETs are influenced by spatial correlation. It can be seen why the slope is between $n_R n_T = 16$ (ET1) and $r_{min} n_R = 8$ (ET5). ET5 becomes dominant at very low BER values and therefore for practical systems ET5 is not relevant. It is interesting to note that the high SNR dominating ET (ET5) for the EA code (in contrast to the cyclic code) has not much influence on the data transmission in the range of practically relevant SNR values (in spatially correlated and uncorrelated channels).

In Fig. 4.13 the red solid lines show the PEP vs. SNR for ETs that dominate at high SNR (ET5) and the blue dashed curves show the PEP vs. SNR for ETs that dominate at medium SNR (ET1). These curves are plotted for several correlation types: uncorrelated (Δ -marker), 1D3 (\circ -marker) and 14D3 ($+$ -marker). Note that the power loss for different ETs is different, i.e., focusing on Fig. 4.13 it can be seen that the curves for ET1 are almost equidistant. In contrast, the curves corresponding to ET5 do not show this property. Comparing the correlation type 1D3 with the uncorrelated case, it can be seen that the power loss regarding ET5 is essentially higher than the power loss regarding ET1. Comparing the

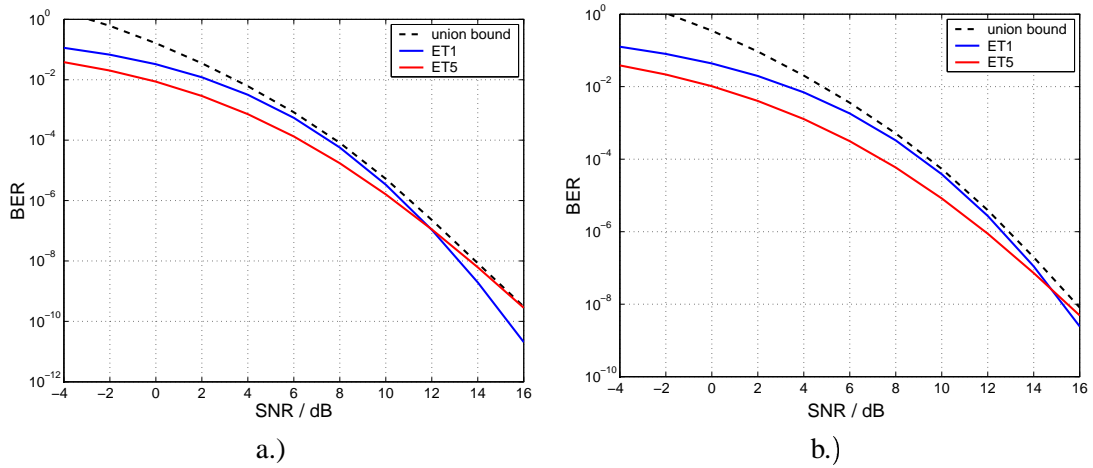


Figure 4.12: Influence of the dominating ETs on the BER vs. SNR performance of the Extended Alamouti STBC in correlated fading. QPSK modulation; $n_T = n_R = 4$; a.) correlation type 1D3. b.) correlation type 14D3.

correlation type 14D3 with 1D3, it can be seen that the loss regarding ET5 is essentially smaller than the loss regarding ET1.

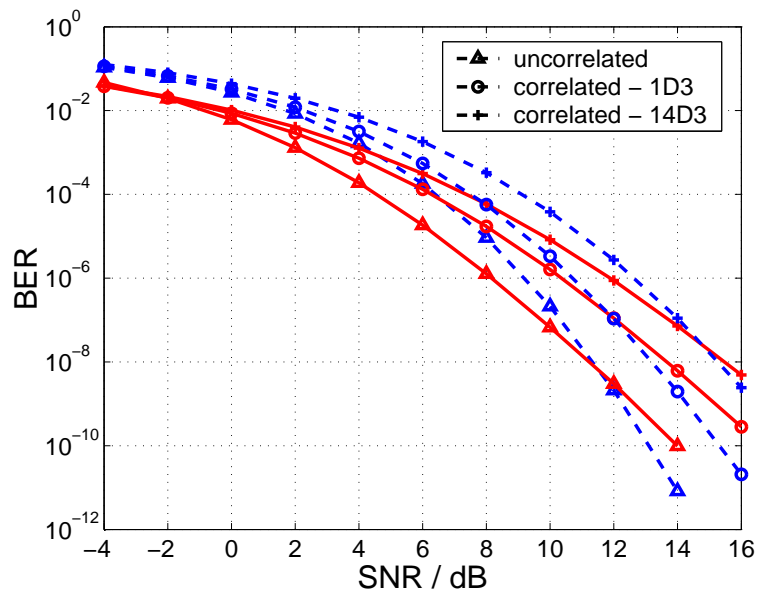


Figure 4.13: Comparison of the dominating ETs of the Extended Alamouti STBC in correlated fading. QPSK modulation; $n_T = n_R = 4$;

4.2.5.3 Specific Orthogonal Code

In the following I will discuss the performance of a specific orthogonal STBC defined in Eqn. (4.8) using 4 transmit antennas. First we focus on all possible crossover events in order to find the ET table. The result is listed in Table 4.3, where we can see that there are only ETs with full rank and equal eigenvalues, as it is typical for all orthogonal codes defined in Def. 4.1. f_k is the number of crossover events leading to

ET $_k$	$\lambda_1^{(k)}$	$\lambda_2^{(k)}$	$\lambda_3^{(k)}$	$\lambda_4^{(k)}$	f_k	n_{BEk}
k	0	0	0	0	64	0
1	2	2	2	2	384	1
2	4	4	4	4	960	2
3	6	6	6	6	1280	3
4	8	8	8	8	960	4
5	10	10	10	10	384	5
6	12	12	12	12	64	6

Table 4.3: ET-table for the specific orthogonal STBC. QPSK modulation; $n_T = 4$; uncorrelated fading.

a certain ET and n_{BEk} is the corresponding number of different information bits. As it can be seen from the ET table, there is only one dominating ET, namely ET1 with the smallest eigenvalues $\lambda_i^{(1)} = 2$. This is one specialty of orthogonal codes, that it can be characterized fully by only one ET. This is contrary to the previously discussed STBCs.

In Fig. 4.14 simulation results (dashed red curve), the union bound (solid blue curve), the high SNR approximation (green solid curve) and the performance of the dominating ET (black dashed-dotted curve) are compared. The union bound is tight for low BER values, like for all code examples considered up

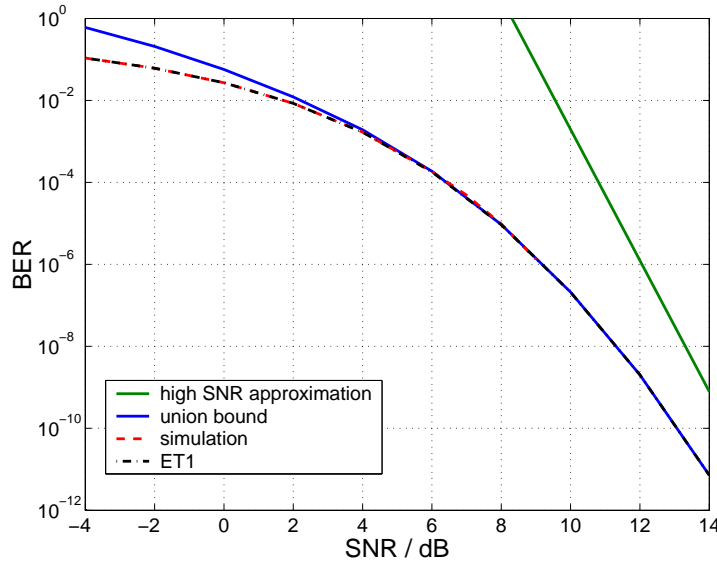


Figure 4.14: BER vs. SNR performance of a specific orthogonal STBC. QPSK modulation; $n_T = n_R = 4$; uncorrelated MIMO channels.

to now. The performance of the dominating ET coincides with the exact performance. Due to the high diversity degree, the slope of the high SNR approximation is very steep and the exact performance or the union bound only shows this slope at very low BER values, which is not visible here.

The influence of spatial correlation is shown in Fig. 4.15. The dashed red curves show the simulated performance, the solid blue curves are the union bounds and the dashed dotted black curves are the high SNR approximations. The spatial correlation types are: uncorrelated (Δ -marker), 1D3 (\circ -marker) and 14D3 (+-marker). The union bounds are tight for BER values below 10^{-3} , also for the spatially corre-

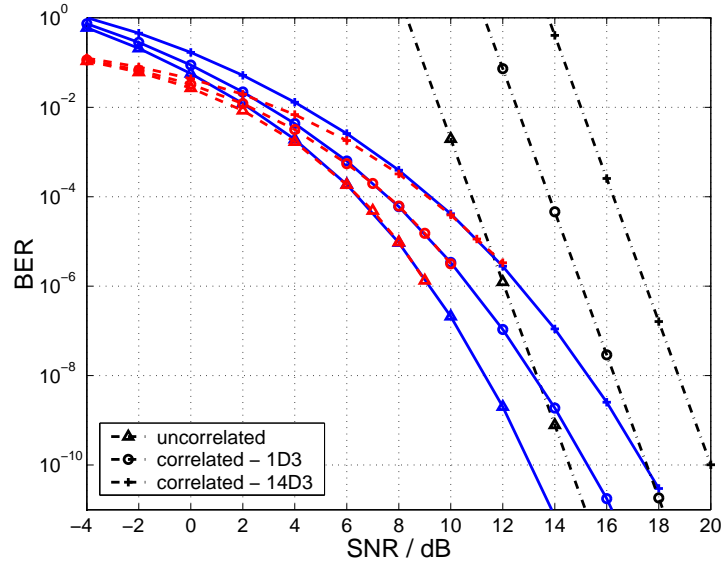


Figure 4.15: BER vs. SNR performance of the Extended Alamouti STBC. QPSK modulation; $n_T = n_R = 4$; several correlation types.

lated case. The high SNR approximations show that there is no diversity loss due to spatial correlation. Correlation only leads to a shift of the BER vs. SNR curves, corresponding to some power loss. The power loss for scenario 1D3 is 2.98dB and 5.45dB for scenario 14D3.

The performance of the dominating ET is compared to the union bound and the simulation result in Fig. 4.16. The performance of the dominating ET coincides with the exact performance, also for spatially correlated channels.

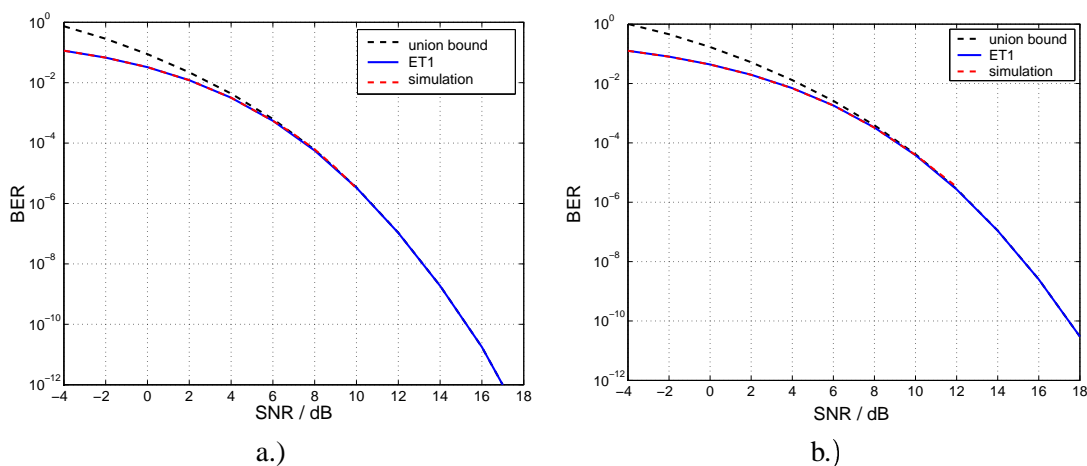


Figure 4.16: Influence of the dominating ETs on the BER vs. SNR performance of a specific orthogonal STBC in correlated fading. QPSK modulation; $n_T = n_R = 4$; a.) correlation type 1D3. b.) correlation type 14D3.

4.2.5.4 D-STTD Code

The last code discussed in this thesis is the D-STTD scheme for 4 transmit antennas with $R_S = 2$ information symbols per time slot defined in Eqn. (4.11). Starting once again with the ET table (Table 4.4), we can see that all ETs have only rank 2. Therefore, there is only one dominating ET, that is ET1, due to its small eigenvalues. Here, f_k is the number of crossover events leading to a certain ET and n_{BEk} is

ET k	$\lambda_1^{(k)}$	$\lambda_2^{(k)}$	$\lambda_3^{(k)}$	$\lambda_4^{(k)}$	f_k	n_{BEk}
k	0	0	0	0	256	0
1	2	2	0	0	2048	1
2	4	4	0	0	7168	2
3	6	6	0	0	14336	3
4	8	8	0	0	17920	4
5	10	10	0	0	14336	5
6	12	12	0	0	7168	6
7	14	14	0	0	2048	7
8	16	16	0	0	256	8

Table 4.4: ET-table for the D-STTD code. QPSK modulation; $n_T = 4$; uncorrelated fading.

the number of different information bits. In Fig. 4.17 the simulation results (dashed red curve), the union bound (solid blue curve), the high SNR approximation (green solid curve) for the BER vs. SNR performance and the performance of the dominating ET (black dashed-dotted curve) are compared. The union bound is tight for BER values of 10^{-3} and below. The dominating ET approximates the performance quite well.

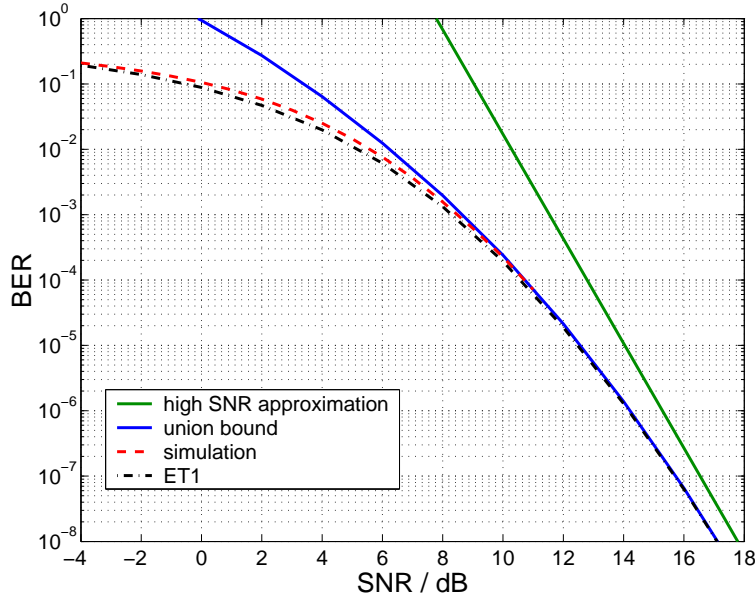


Figure 4.17: BER vs. SNR performance of the D-STTD code. QPSK modulation; $n_T = n_R = 4$; uncorrelated MIMO channels.

In Fig. 4.18 the simulated BER vs. SNR performance (dashed red curves), the tight union bounds for the BER vs. SNR performance (solid blue curves) and the high SNR approximation for the BER vs.

SNR performance (dashed-dotted black curves) for D-STTD code ($n_T = n_R = 4$) utilizing QPSK modulation are shown. Several spatial correlation types are considered: uncorrelated (\triangle -marker), 1D3 (\circ -marker) and 14D3 ($+$ -marker). The union bounds are also very tight for spatially correlated channels. The high SNR approximation indicates identical slopes for all correlation scenarios. The power losses are 2.37dB and 4.59dB for the scenarios 1D3 and 14D3, respectively.

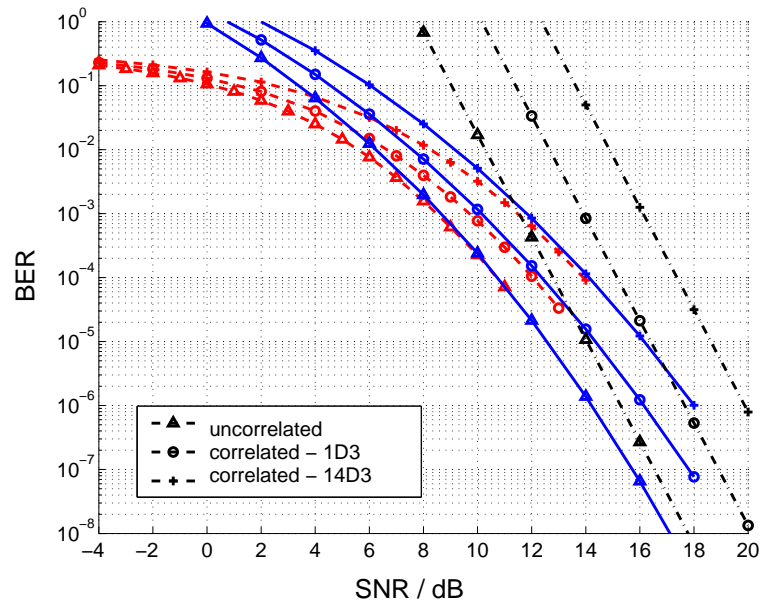


Figure 4.18: BER vs. SNR performance of the D-STTD code. QPSK modulation; $n_T = n_R = 4$; several correlation types.

In Fig. 4.19 the dominating ET for the correlation types 1D3 and 14D3 are shown. One interesting observation is that the dominating ET is not that tight as for the uncorrelated case.

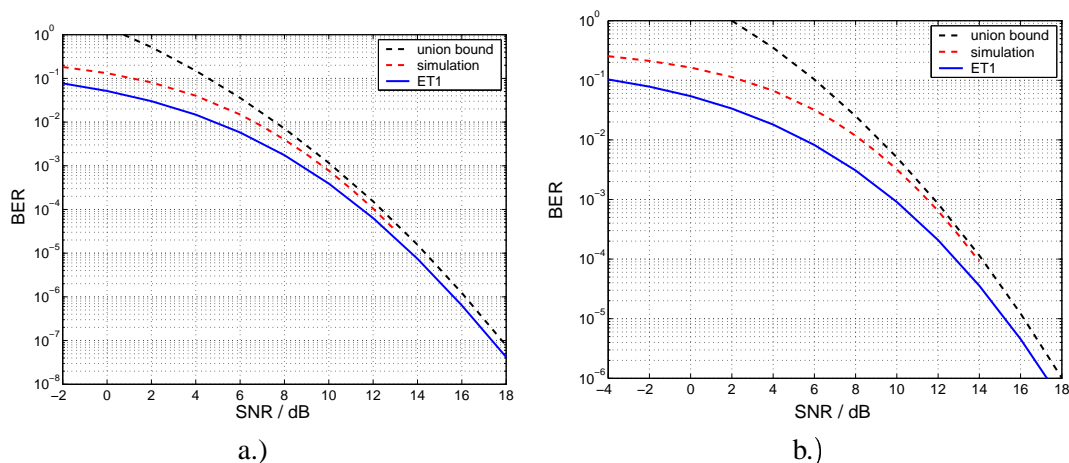


Figure 4.19: Influence of the dominating ETs on the BER vs. SNR performance of the D-STTD in correlated fading. QPSK modulation; $n_T = n_R = 4$; a.) correlation type 1D3. b.) correlation type 14D3.

4.2.6 Optimal Precoding

In the preceding section it has been shown that the BER performance of the system degrades, if the MIMO channel is spatially correlated. This loss can be quantified by the diversity loss L_D and even more appropriate by the power loss L_P defined in Sec. 4.2.3. In order to mitigate the detrimental effect of spatial correlation, a linear precoding matrix \mathbf{F} can be introduced at the transmitter. Then, the resulting system model can be described by

$$\mathbf{y} = \mathbf{H}\mathbf{F}\mathbf{s} + \mathbf{n} \quad (4.81)$$

With this modification of the transmit signal, the matrix $\mathbf{Z}_{i,j}$ defined in Eqn. (4.57) can be redefined as:

$$\mathbf{Z}_{i,j}(\mathbf{F}) = \mathbf{D}_{\tilde{\mathbf{R}}_H}^{1/2} \mathbf{U}_{\tilde{\mathbf{R}}_H}^T \tilde{\mathbf{A}}_{i,j}(\mathbf{F}) \mathbf{U}_{\tilde{\mathbf{R}}_H}^* \mathbf{D}_{\tilde{\mathbf{R}}_H}^{1/2}, \quad (4.82)$$

where $\tilde{\mathbf{A}}_{i,j}(\mathbf{F}) = \text{diag}(\mathbf{F}\mathbf{A}_{i,j}\mathbf{F}^H, \mathbf{F}\mathbf{A}_{i,j}\mathbf{F}^H, \dots, \mathbf{F}\mathbf{A}_{i,j}\mathbf{F}^H)$. Note that $\mathbf{Z}_{i,j}(\mathbf{F})$ not only depends on \mathbf{F} , but also on the distance matrix $\mathbf{A}_{i,j}$. In principle, \mathbf{F} can be optimized for each $\mathbf{A}_{i,j}$ ¹⁰. Obviously, improving the PEP vs. SNR performance for one specific \mathbf{A}_k by a specific precoder \mathbf{F} , can lead to a worse performance of the PEP corresponding to other distance matrices \mathbf{A}_l ($l = 1, 2, \dots, n_{ET}; l \neq k$). Thus, an optimization of \mathbf{F} for one specific ET does not make sense. The optimal solution can only be found by taking into account all distance matrices (all ETs). Thus, we have to find a cost function, which includes all ETs.

In contrast to the approach in this thesis, in [55] the authors concentrate only on the distance matrix that leads to the minimum distance. This is in general not the right way, as explained above. Fortunately, the authors of [55] apply this precoder only to orthogonal codes, where the optimization of the ET corresponding to the minimum distance, does not degrade the performance of the remaining ETs. However, in general this is not true.

In order to find a performance measure, which takes into account the overall performance and can be used to solve the entire optimization problem, I define a generalized power loss parameter according to Eqn. (4.80):

$$L_P^{(n_{NZ_i})} = 10 \log_{10} \left(\frac{d_{i,i.d.r_i}^2}{d_{W,n_{NZ_i}}^2} \right), \quad (4.83)$$

where $r_i = n_{NZ_i}/n_R$ and $d_{i,i.d.r_i}^2$ is the effective distance representing all ETs with rank r_i in the i.i.d. case:

$$d_{i,i.d.r_i}^2 = \frac{1}{r_i n_R \sqrt{\sum_{k=1}^{n_{ET} r_i} \frac{w_k}{(d_{T,k}^2 c^{(k)})^{r_i n_R}}}}. \quad (4.84)$$

$n_{ET r_i}$ is the number of ETs with rank r_i . For example, for the cyclic code and $r_i = 2$, $n_{ET r_i} = 2$ (see Tab. 4.1). $d_{W,n_{NZ_i}}^2$ is the effective distance representing all ETs with n_{NZ_i} non-zero eigenvalues in the correlated case:

$$d_{W,n_{NZ_i}}^2 = \frac{1}{n_{NZ_i} \sqrt{\sum_{k=1}^{n_{ET} n_{NZ_i}} \frac{w_k}{(d_{W,k}^2 c_{NZ}^{(k)})^{n_{NZ_i}}}}}, \quad (4.85)$$

where $n_{ET n_{NZ_i}}$ is the number of ETs, which have n_{NZ_i} non zero eigenvalues. For example, for the cyclic code and $n_{NZ_i} = 8$, $n_{ET n_{NZ_i}} = 3$ (see Tab. C.1 or Tab. C.2).

¹⁰In the following I will focus on ETs instead of crossover events, as it is often done in this thesis, and thus the index k is used instead of i, j .

With these definitions all ETs corresponding to a specific slope (n_{NZ_i}) of the PEP curve can be characterized by a single number, namely the power loss $L_P^{(n_{NZ_i})}$. In order to find a single measure assessing the entire performance, I simply sum up all power losses, which results in the overall power loss $L_{P\ all}$:

$$L_{P\ all}(\mathbf{F}) = \sum_i^{n_{PL}} L_P^{(n_{NZ_i})}(\mathbf{F}), \quad (4.86)$$

where n_{PL} is the number of different power losses or slopes of PEP vs. SNR curves for the code under investigation (e.g. $n_{PL} = 4$ for the cyclic code).

At this point I want to explain what the overall power loss says about the cyclic code in correlated channels. The PEP vs. SNR curves of the ETs of the cyclic code shows only four different slopes, namely 4,8,12 and 16 BER decades / 10dB SNR. Summarizing the PEPs with slope 4 for the i.i.d. and the correlated channel and calculating the SNR difference between these curves leads to the power loss for the ETs with slope 4. This is also done for 8,12 and 16. The overall power loss is thus the sum over all SNR shifts between the i.i.d. and the correlated channel. Therefore, it shows somehow the potential of improvement, if the overall power loss is zero, the i.i.d. performance is achieved.

Note that the total power loss $M(\mathbf{F})$ does not say much about the performance of the entire system, but it is merely used in the following as a cost function for the optimization problem. The ‘‘optimal’’ prefilter can be found by solving the following minimization problem:

$$\mathbf{F}_{opt} = \arg \min_{\mathbf{F}} \left\{ \sum_i^{n_{PL}} L_P^{(n_{NZ_i})}(\mathbf{F}) \right\} = \arg \min_{\mathbf{F}} \{M(\mathbf{F})\} \quad (4.87)$$

with the side constraint:

$$\text{tr}(\mathbf{F}_{opt}^H \mathbf{F}_{opt}) = n_T. \quad (4.88)$$

This constraint ensures that the precoding matrix does not introduce any power gain. With \mathbf{F}_{opt} the individual power losses are jointly optimized. Note, that in Eqn. (4.87) all power losses are considered to be equally important. This is an ad hoc approach and there might be chances for further improvements.

Unfortunately, this minimization problem has to be solved for each type of code separately. Therefore, in the following I will illustrate the main results for the cyclic code utilizing a 4×4 MIMO system with BPSK modulation. For this system and for the spatial correlation scenario 14D3, the ETs and their corresponding key-parameters are listed in the Tab. C.2. With the knowledge of the ETs and the corresponding key-parameters, the minimization problem can be written as:

$$\mathbf{F}_{opt} = \arg \min_{\mathbf{F}} \left\{ L_P^{(4)}(\mathbf{F}) + L_P^{(8)}(\mathbf{F}) + L_P^{(12)}(\mathbf{F}) + L_P^{(16)}(\mathbf{F}) \right\} = \arg \min_{\mathbf{F}} \{M(\mathbf{F})\} \quad (4.89)$$

with the side constraint

$$\text{tr}(\mathbf{F}^H \mathbf{F}) = 4. \quad (4.90)$$

The above stated optimization problem can be solved by the Lagrange multiplier technique [43] by solving the following equations:

$$\begin{aligned} G(\mathbf{F}, \lambda) &= M(\mathbf{F}) + \lambda \cdot \text{tr}(\mathbf{F}^H \mathbf{F}) \\ \frac{\partial G(\mathbf{F}, \lambda)}{\partial \mathbf{F}} &= 0 \\ \frac{\partial G(\mathbf{F}, \lambda)}{\partial \lambda} &= 0 \end{aligned} \quad (4.91)$$

Unfortunately, the problem is too complex to be solved analytically. Therefore, I have solved it numerically by using a gradient algorithm, which is explained in the following: In the first step a prefilter matrix \mathbf{F} is chosen randomly. Then the gradient is approximately calculated by:

$$\frac{\partial M(\mathbf{F})}{\partial \mathbf{F}} \approx \frac{\Delta M(\mathbf{F})}{\Delta \mathbf{F}} \quad (4.92)$$

In order to approach the minimum, a small step Δ_S towards the negative gradient is performed:

$$\mathbf{F}_{i+1} = \mathbf{F}_i - \Delta_S \frac{\Delta M(\mathbf{F})}{\Delta \mathbf{F}} \quad (4.93)$$

Then the matrix \mathbf{F}_{i+1} is normalized such that the side constraint (power normalization) is fulfilled. Then the next iteration starts and the gradient of the updated matrix \mathbf{F}_{i+1} is calculated and so on. Going through enough iteration steps, the algorithm approaches a local minimum. Actually, we want to find the global minimum and therefore the iteration algorithm has been repeated 500 times, i.e., 500 random start values of \mathbf{F} have been chosen arbitrarily. In this way, it can be assumed that the probability of finding the global minimum is quite high. The surprising result of the optimum search with 500 random start values is that always the same minimum is found. Therefore, I conjecture that I have found the global optimum!

Applying the optimum prefilter in data transmission simulations lead to the results shown in Fig. 4.20. Here, the black curve corresponds to spatially uncorrelated fading, the blue curve corresponds to the correlation scenario 14D3 without precoding and the red curve corresponds to the correlation scenario 14D3 with optimal precoding. The interesting result is that in the low SNR regime the precoded MIMO

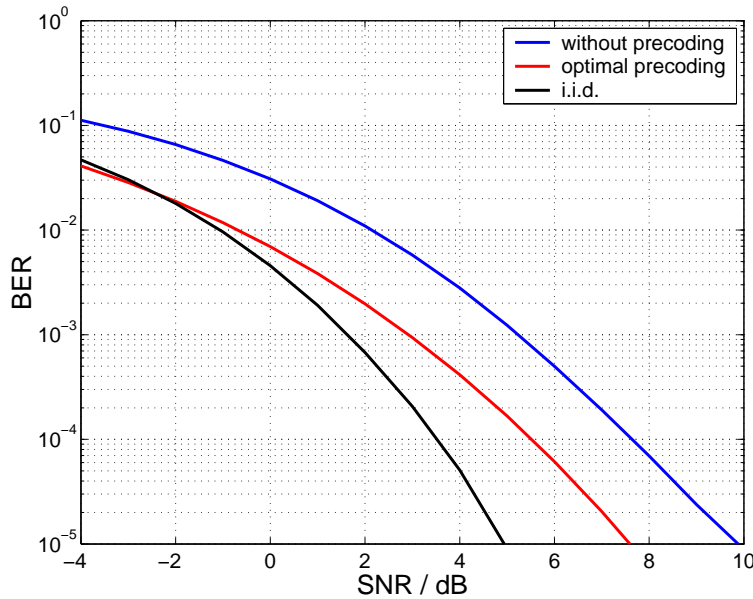


Figure 4.20: BER vs. SNR performance for the precoded cyclic STB coded system. BPSK modulation; $n_T = n_R = 4$; correlation scenario 14D3; medium SNR.

system performs even slightly better in spatially correlated channels than the system works without precoding and operating on uncorrelated channels. In the high SNR domain the i.i.d. performance is better than the performance of the precoded system in correlated channels. Assessing the performance difference by a single number is not really reasonable, due to the peculiar shape of the BER vs. SNR curves. In Fig. 4.20 an SNR improvement of roughly 2 dB due to the optimal precoder can be seen. In Fig. 4.21 the black curve corresponds to spatially uncorrelated fading, the blue curve corresponds to the

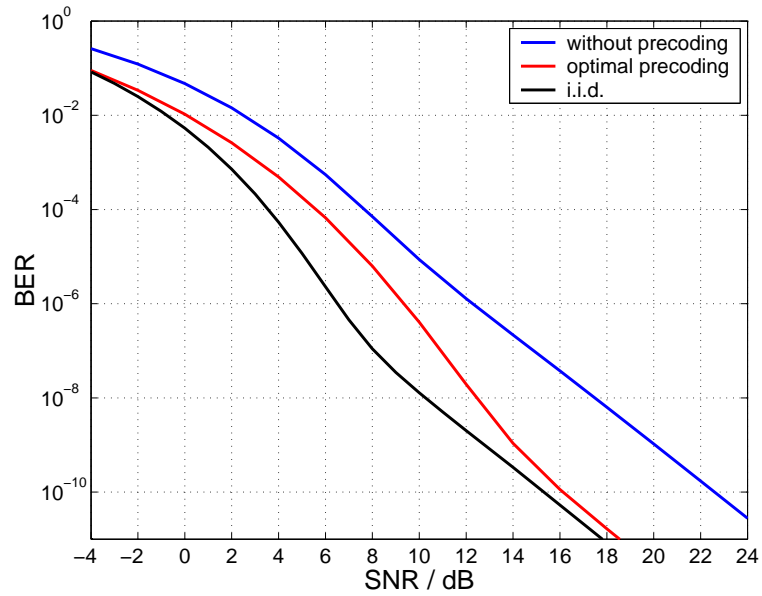


Figure 4.21: BER vs. SNR performance for the precoded cyclic STBC. BPSK modulation; $n_T = n_R = 4$; correlation scenario 14D3; high SNR.

correlation scenario 14D3 without precoding and the red curve corresponds to the correlation scenario 14D3 with optimal precoding. Considering the union bounds (Eqn. (4.62)) shown in Fig. 4.21 at very high SNR, a small power loss of 0.5dB compared to the uncorrelated case is visible, which results from the power loss for the ETs with slope four $L_P^{(4)}(\mathbf{F}_{opt})$, which is 0.9dB. Note, that a different weighting of the different power losses in Eqn. (4.89), can help to improve the optimization in different SNR regions. For example, if the goal is to improve the BER at low SNR, the power loss for the slope 16 ETs $L_P^{(16)}(\mathbf{F}_{opt})$ should be weighted more. The curves shown in Fig. 4.22 have the following meaning: The

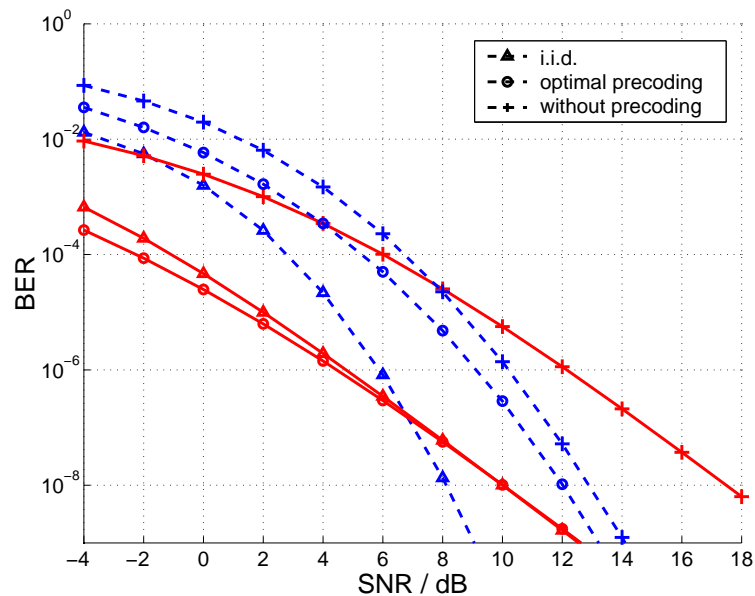


Figure 4.22: Dominating ETs for the precoded cyclic STBC. BPSK modulation; $n_T = n_R = 4$; correlation scenario 14D3.

red solid lines are the PEP vs. SNR for ETs that dominate at high SNR. The blue dashed curves are the PEP vs. SNR for ETs that dominate at medium SNR. The curves for uncorrelated channels are labeled by Δ -marker, the curves for correlated channels (14D3) and optimal precoding are labeled by (o-marker) and the curves for correlated channels (14D3) without precoding are labeled by (+-marker). In Fig. 4.22, it can be seen that the dominating ET at high SNR (red curve) with optimal precoding is almost equal with the corresponding ET for the i.i.d. case. Thus, with respect to high SNR the improvement due to precoding is quite substantial. The improvement of the ET dominating at low SNR is not that large, but nevertheless a remarkable improvement of the overall BER performance due to precoding is visible. As stated above, for practical systems it would be better to optimize for low SNR, i.e., to weight the $L_P^{(16)}(\mathbf{F}_{opt})$ more. I have shown here the principle way of finding optimal precoding filters for general space time block coded systems, but finding solutions for special SNR domains is beyond the scope of the current thesis.

4.3 Lower Bound for the BER in case of STB coded MIMO System

In Sec. 4.2 a tight union bound for the BER for space-time block coded transmission is calculated. Inspired by the so-called Nearest Neighbor Approximation (NNA) [27] used for the BER calculation in Additive White Gaussian Noise (AWGN) and Single Input Single Output (SISO) channels, we derive now a Minimum Distance Lower Bound (MDLB) for the case of space-time coded MIMO systems.

4.3.1 Nearest Neighbor Approximation

In the following we discuss the properties of the NNA for the SISO-AWGN case [27]. In the remaining sections the generalization for the space time block coded transmission in MIMO systems is presented.

Let's assume a very simple system model using an AWGN channel ($h = 1$):

$$y = s + n, \quad (4.94)$$

where y is the receive symbol, s is the transmit symbol and n is the complex Gaussian distributed channel noise with zero mean and variance σ_n^2 .

The best way of clarifying important BER-properties is to consider an illustrative example. To do so, we focus on a quite general, complex modulation format, namely 16QAM. The modulation signal constellation is shown in Fig. 4.23 (bit to symbol mapping is done by a Gray code).

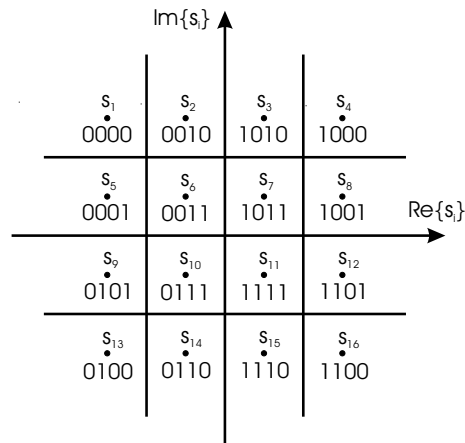


Figure 4.23: Signal constellation map of a 16QAM modulation format.

The exact Symbol Error Probability (SEP) can be written as:

$$P_{\mathcal{E}_S} = \sum_{i=1}^{|\mathcal{A}|} \sum_{\substack{j=1 \\ j \neq i}}^{|\mathcal{A}|} P(s_i \rightarrow s_j) P(s_i). \quad (4.95)$$

$|\mathcal{A}|$ is the size of the modulation alphabet, $P(s_i \rightarrow s_j)$ is the exact crossover probability and $P(s_i)$ is the probability of transmitting s_i . In contrast, the NNA can be calculated in a much simpler way:

$$P_{\mathcal{E}_S} \leq \bar{n}_{NN} \text{PEP}(d_{min}). \quad (4.96)$$

\bar{n}_{NN} denotes the average number of nearest neighboring symbols, d_{min} is the distance between the nearest neighbors and PEP is the pairwise error probability. Note that the PEP is not the exact crossover

probability, since it neglects the influence of the other symbols and thus only two remaining symbols are considered. This approximate crossover probability is calculated as if we would have BPSK modulation, i.e., integrating over the entire opposite half plane.

Let's focus on one specific symbol of the 16QAM map in order to show that the NNA is an upper bound for the SEP $P_{\mathcal{E}_s}$. For the symbol s_6 shown in Fig. 4.24 the exact symbol error probability is calculated by taking into account all decision regions excluding the decision region for s_6 .

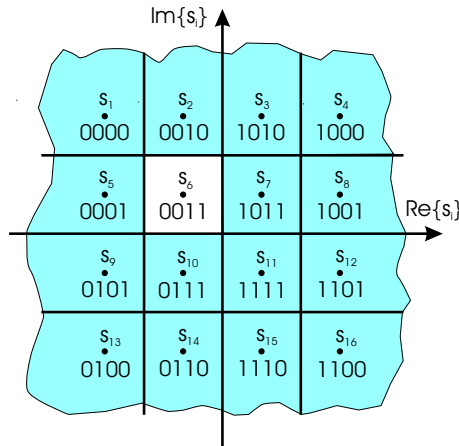


Figure 4.24: Decision regions for calculating the exact SEP.

In Fig. 4.25.a.) we can see the overlapping integration areas (decision regions) of the 16QAM modulation and in Fig. 4.25.b.) the areas that are counted twice and the corresponding number of bit errors are shown. In the course of calculating NNA for the symbol s_6 the integration areas are overlapping as shown in Fig. 4.25.a.) and therefore some error probabilities are counted twice as shown in Fig. 4.25.b.). For this reason the approximated SEP for the symbol s_6 is always larger than the exact symbol error probability. This holds in a similar manner for all symbols s_i ($i=1, \dots, 16$) and therefore the NNA in fact is an upper bound for the SEP. The simulated SEP vs. SNR performance and the NNA for an uncoded transmission

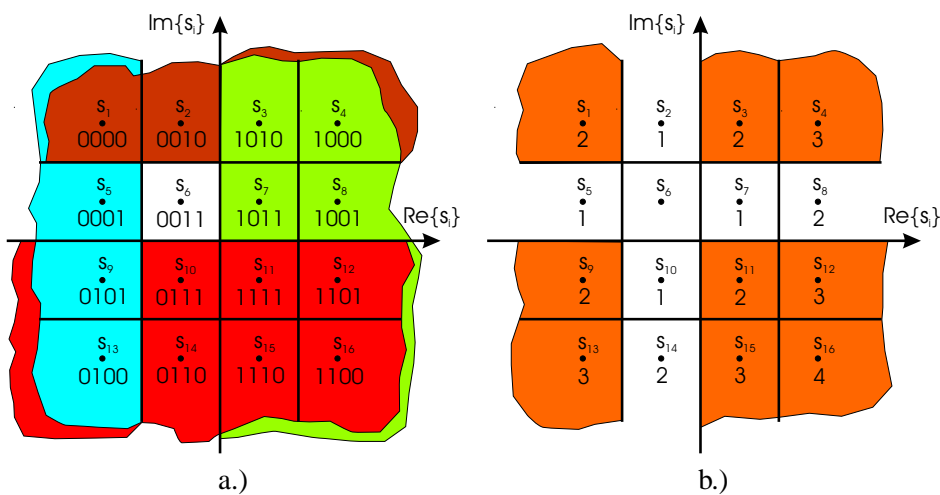


Figure 4.25: Overlapping integration areas for a 16QAM modulation.

over an AWGN channel using 16QAM are compared in Fig. 4.26. In Fig. 4.26 we can see that the NNA is indeed an upper bound for the SEP for the entire SNR range for the example of 16QAM modulation.

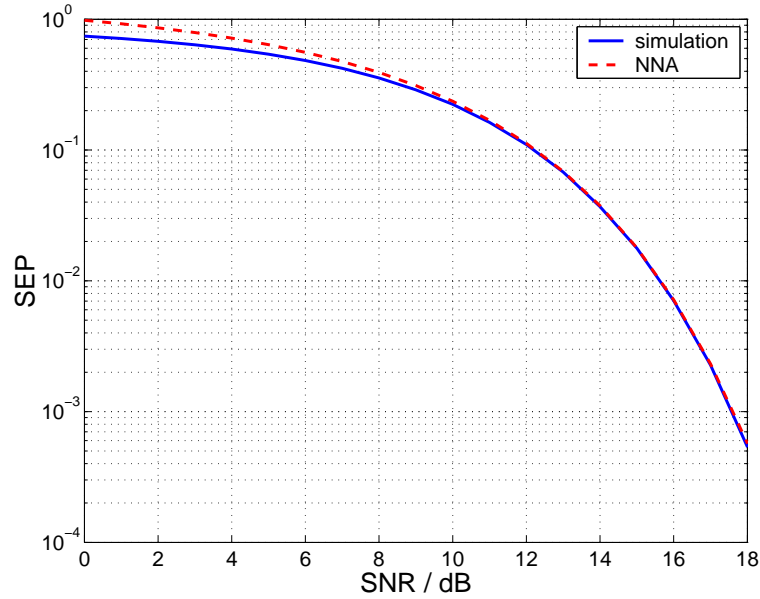


Figure 4.26: SEP vs. SNR performance for uncoded transmission. AWGN channel; 16QAM modulation.

Now let's focus on BERs. The exact BER can be calculated as:

$$\text{BER} = \sum_{i=1}^{|\mathcal{A}|} \sum_{\substack{j=1 \\ j \neq i}}^{|\mathcal{A}|} \frac{n_{BEi,j}}{\log_2(|\mathcal{A}|)} P(s_i \rightarrow s_j) P(s_i) . \quad (4.97)$$

$n_{BEi,j}$ is the number of bit errors corresponding to the crossover event $s_i \rightarrow s_j$. The NNA for the BER is:

$$\text{BER} \geq \bar{n}_{NN} \frac{1}{\log_2(|\mathcal{A}|)} \text{PEP}(d_{min}) . \quad (4.98)$$

Due to the Gray mapping the number of bit errors corresponding to nearest neighbor symbols is one and thus we have 1 over $\log_2(|\mathcal{A}|)$ in the above equation. Consider once again Fig. 4.25.b). Some decision regions are counted twice. Keeping in mind that for the exact calculation some regions have to be weighted by 2, 3 or 4, due to the distinct numbers of bit errors, the NNA, which counts some regions twice underestimates the BER in the case of more than 2 bit errors per symbol error. The region corresponding to s_1 is counted twice by the NNA, which is also done using the exact calculation, because of the two bit errors. The region corresponding to s_4 is counted twice by the NNA, but is weighted by the factor 3 using the exact calculation, because of three bit errors. This underestimation holds for all regions and for all symbols s_i ($i=1, \dots, 16$). Therefore the NNA is a lower bound for the BER. The simulated BER vs. SNR performance and the NNA for an uncoded transmission over a AWGN channel using 16QAM are compared in Fig. 4.27. In Fig. 4.27 we can see that the NNA is indeed a lower bound for the BER for the entire SNR range for the example of 16QAM modulation.

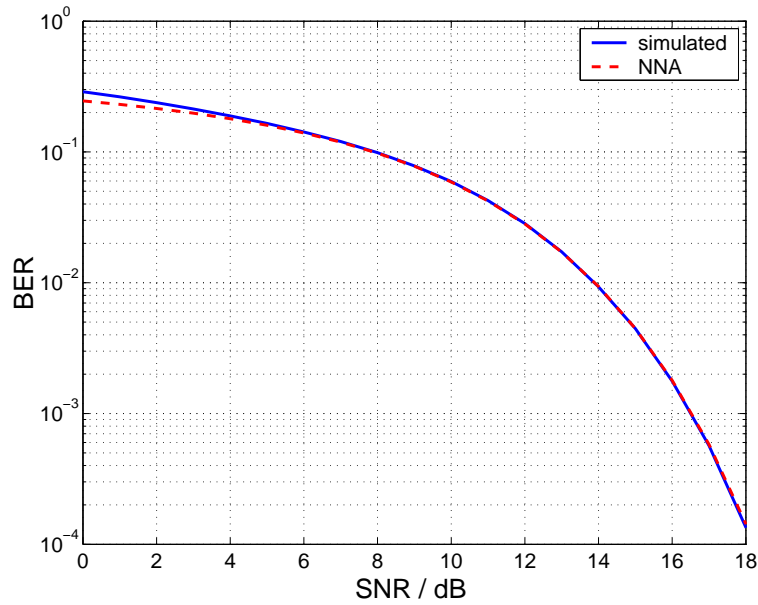


Figure 4.27: BER vs. SNR performance for uncoded transmission. AWGN channel; 16QAM modulation.

Summary:

-) Nearest Neighbor Approximation is an upper bound for the symbol error probability.
-) Nearest Neighbor Approximation is a lower bound for the bit error ratio.

4.3.2 Minimum Distance Lower Bound of the BER

4.3.2.1 Fundamentals

In this section I will generalize the NNA for the AWGN channel, discussed in Sec. 4.3.1, to the case of space-time block coded transmission. Remember Eqn. (4.98), where we can see, which entities are necessary to calculate the NNA. These entities are \bar{n}_{NN} , $1/\log_2(|\mathcal{A}|)$ (which represents the number of erroneous bits divided by the number of transmitted bits per symbol) and d_{min} .

First, I will focus on the principle of calculating the MDLB and afterwards I will show a simple example to illustrate the general theory. By applying this concept to MIMO systems, the following problem comes up: The distances between space time block code words change due to the distortion introduced by the MIMO channel matrix. More details of MIMO distance properties have been discussed in Sec. 4.1.3.1. The main point of Sec. 4.1.3.1 is that the smallest / largest distance at the transmitter (without channel influence) is **not** necessarily the smallest / largest distance at the receiver (with channel influence). I.e., the *Distance Proportion Preservation Property* does not hold. For this reason we do not know the nearest neighbors at the receiver beforehand. Therefore, we have to find the minimum distance at the receiver out of all crossover events. For this minimum distance crossover event, the error probability is calculated. This error probability is weighted with the corresponding number of crossover events, which have this minimum distance (equivalent to the number of nearest neighbors) and the corresponding number of bit errors.

To concretize these ideas about finding a generalization of the NNA of the AWGN channel to a space-time block coded MIMO system, we have to refresh the Error Type (ET) concept introduced in Def. 3.1. We know that there are several ETs contributing to the BER performance. An ET is specified by the distance, the number of bit errors and the frequency of these crossover events corresponding to the number of nearest neighbors. For the generalization of the NNA we have to find the minimum distance d_{min}^2 out of the n_{ET} (number of error types) distances d_k^2 . Actually, we want to know the PDF $p_{d_k^2|d_k^2=d_{min}^2}$ of the minimum distance resulting from a certain ET, in order to calculate an average error probability $P_{\mathcal{E}_k}$. Additionally, we have to know, which ET leads to the minimum distance (in order to do the accurate weighting) and the probability $P_{d_k^2=d_{min}^2}$ of the case that the minimum distance results from a certain ET with number k . According to the above explanations the MDLB for the BER can be calculated as:

$$\text{BER} \geq \sum_{k=1}^{n_{ET}} w_k P_{\mathcal{E}_k} P_{d_k^2=d_{min}^2} \quad \text{with} \quad w_k = \frac{f_k}{|\mathcal{A}|^{n_{IS}}} \frac{n_{BEk}}{\text{ld}(|\mathcal{A}|) n_{IS}}. \quad (4.99)$$

Remember that f_k is the frequency of crossover events, which correspond to ET k , n_{BEk} is the corresponding number of bit errors, n_{IS} is the number of independent symbols contained in a space-time block code word and $|\mathcal{A}|$ denotes the size of the modulation format.

The corresponding average error probability $P_{\mathcal{E}_k}$ can be calculated by averaging over all distances d_k^2 that are equal to d_{min}^2 :

$$P_{\mathcal{E}_k} = \int_0^\infty Q\left(\sqrt{\frac{\xi}{2\sigma_n^2}}\right) p_{d_k^2|d_k^2=d_{min}^2}(\xi) d\xi. \quad (4.100)$$

The probability of having $d_k^2 = d_{min}^2$ can be calculated as

$$P_{d_k^2=d_{min}^2} = \int_0^\infty p_{d_k^2|d_k^2=d_{min}^2}(\xi) d\xi, \quad (4.101)$$

where

$$p_{d_k^2|d_k^2=d_{min}^2} = \frac{p_{d_k^2, d_k^2=d_{min}^2}}{P_{d_k^2=d_{min}^2}}, \quad (4.102)$$

In this way we can adapt the NNA to the MDLB for space-time block coded transmission.

Next, I want to present an illustrative way back from the MDLB for MIMO systems to the NNA for SISO systems. Remember that we know beforehand, that in the SISO the nearest neighbors always have the same minimum distance and that the number of different bits corresponding to the nearest neighbors is one (due to Gray mapping). Equivalently, we can say that always the same ET corresponding to the nearest neighbor crossover event leads to the minimum distance, i.e., the distances of other crossover events corresponding to other ETs are always larger. Therefore, the probability that the minimum distance comes from the ET corresponding to nearest neighbor crossover events is 1 and thus the BER is equal to the NNA of Eqn. (4.98):

$$\text{BER} \geq \sum_{k=1}^{n_{ET}} w_k P_{\mathcal{E}_k} P_{d_k^2 = d_{min}^2} = w_k P_{\mathcal{E}_k} = \bar{n}_{NN} \frac{1}{\log_2(|\mathcal{A}|)} \text{PEP}(d_{min}). \quad (4.103)$$

Example: Cyclic Code

The strategy how to calculate the MDLB according to Eqn. (4.99) presented above is probably not quite obvious. Therefore I want to explain the essential steps to calculate the MDLB in more detail by means of an example in a slightly different way. Note that for the calculation of the MDLB for this example we go an alternative way compared to the strategy explained above and do not apply the results obtained above. Going this alternative way, it becomes more clear that the MDLB defined above is a generalization of the NNA. Additionally the alternative strategy allows us to verify the general expression in Eqn. (4.99). To keep matters as simple as possible the cyclic STBC with 2 transmit antennas and one receive antenna using BPSK modulation is considered in the following example.

The code words of this cyclic STBC are defined as:

$$\mathbf{S} = \begin{pmatrix} s_1 & s_2 \\ s_2 & s_1 \end{pmatrix}. \quad (4.104)$$

For the different code word matrices $\mathbf{S}_i, \mathbf{S}_j$ we can calculate the difference matrices \mathbf{B}_{ij} and the distance matrices \mathbf{A}_{ij} (Eqn. (4.1)). As already mentioned in Sec. 4.2 the eigenvalues of the distance matrices \mathbf{A}_{ij} determine the BER performance. Therefore, we analyze all 16 possible distance matrices \mathbf{A}_{ij} to find the error type table. Due to the specific structure of the code and the modulation format, there are only 3 different Error Types (ET). The corresponding key-parameters are listed in Tab.4.5. Note that the number of different information bits is denoted by n_{BEk} and the number of crossover events leading to a certain ET is denoted by f_k . Note that in contrast to the union bound calculation in Sec. 4.2 the order

ET k	$\lambda_1^{(k)}$	$\lambda_2^{(k)}$	f_k	n_{BEk}
k	0	0	4	0
1	4	4	8	1
2	16	0	2	2
3	0	16	2	2

Table 4.5: ET table for the cyclic STBC. BPSK modulation; $n_T = 2$.

of the eigenvalues is now in general of importance for the calculation of the PDFs of the distances and therefore we have to distinguish between ET2 and ET3. The reason why we have to distinguish ET2 and ET3 becomes more clear following the explanation regarding the distance calculation (Eqn. (4.120)). For the union bound ET2 and ET3 in Tab.4.5 would be summarized to one ET with the sum frequency $f' = f_2 + f_3$.

Using this code \mathbf{S} , defined in Eqn. (4.104), the receive vector \mathbf{y} can be calculated with:

$$\underbrace{\begin{pmatrix} y_1 & y_2 \end{pmatrix}}_{\mathbf{y}^T} = \underbrace{\begin{pmatrix} h_{11} & h_{12} \end{pmatrix}}_{\mathbf{h}^T} \underbrace{\begin{pmatrix} s_1 & s_2 \\ s_2 & s_1 \end{pmatrix}}_{\mathbf{S}} + \underbrace{\begin{pmatrix} n_1 & n_2 \end{pmatrix}}_{\mathbf{n}^T}. \quad (4.105)$$

An equivalent description is:

$$\underbrace{\begin{pmatrix} y_1 \\ y_2 \end{pmatrix}}_{\mathbf{y}} = \underbrace{\begin{pmatrix} h_{11} & h_{12} \\ h_{12} & h_{11} \end{pmatrix}}_{\mathbf{H}_v} \underbrace{\begin{pmatrix} s_1 \\ s_2 \end{pmatrix}}_{\mathbf{s}} + \underbrace{\begin{pmatrix} n_1 \\ n_2 \end{pmatrix}}_{\mathbf{n}}. \quad (4.106)$$

In vector-matrix notation the above equations can be written as:

$$\mathbf{y} = \mathbf{H}_v \mathbf{s} + \mathbf{n}, \quad (4.107)$$

where \mathbf{H}_v is called the virtual channel matrix, which depends on the channel and on the code! Eqn. (4.107) essentially describes an equivalent virtual MIMO system with a highly structured (2×2) MIMO channel.

As already shown in Sec. 3 it is possible to visualize the symbol constellation at the transmitter $\mathbf{s}^{(i)}$ and at the receiver with $\mathbf{s}_R^{(i)} = \mathbf{H}_v \mathbf{s}^{(i)}$ by using real valued channel matrix entries. This simplification is only introduced for reasons of visualizing. The calculations performed in the following (beginning with Eqn. (4.108)) are obviously also valid for complex valued channel matrix entries. Fig. 4.28 shows all 4 possible code words of the example code \mathbf{S} from Eqn. (4.104). Where the four possible symbol

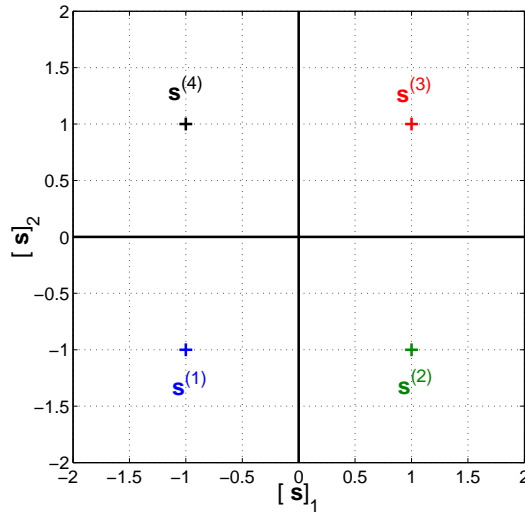


Figure 4.28: Signal constellation at the transmitter $\mathbf{s}^{(i)}$. cyclic STBC; BPSK modulation;

vectors are $\mathbf{s}^{(1)} = (-1 \ -1)^T$, $\mathbf{s}^{(2)} = (1 \ -1)^T$, $\mathbf{s}^{(3)} = (1 \ 1)^T$ and $\mathbf{s}^{(4)} = (-1 \ 1)^T$. $[\mathbf{s}]_i$ means the i -th component of vector \mathbf{s} . Therefore, the horizontal axis in Fig. 4.28 corresponds to the binary symbol s_1 and the vertical axis in Fig. 4.28 to the binary symbol s_2 .

Due to the multiplication of the symbol vectors $\mathbf{s}^{(i)}$ with the virtual channel matrix \mathbf{H}_v the symbol constellation is distorted by the transmission. An example for a symbol constellation at the receiver can be seen in Fig. 4.29. In this example the symbols are strongly distorted by a specific channel matrix. The symbols labeled by “+” are the symbols at the transmitter $\mathbf{s}^{(i)}$ and the corresponding symbols labeled by “o” are the symbols at the receiver $\mathbf{s}_R^{(i)}$. The colors denote the relationship, i.e., for example the red symbol labeled by “+” belongs to the red symbol labeled by “o”.

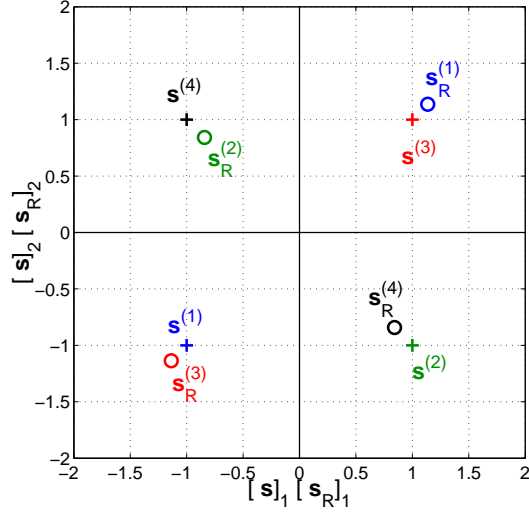


Figure 4.29: Signal distortion according to $\mathbf{H}_{v1}: \mathbf{s}_R^{(i)} = \mathbf{H}_{v1}\mathbf{s}^{(i)}$. cyclic STBC; BPSK modulation.

Note that we already distinguished 3 different ETs. Focusing on this symbol constellation it is also possible to identify 3 different ETs, which correspond to three different distances. These three distances are shown in Fig. 4.30. As it has already been explained in the general part of this section, we are

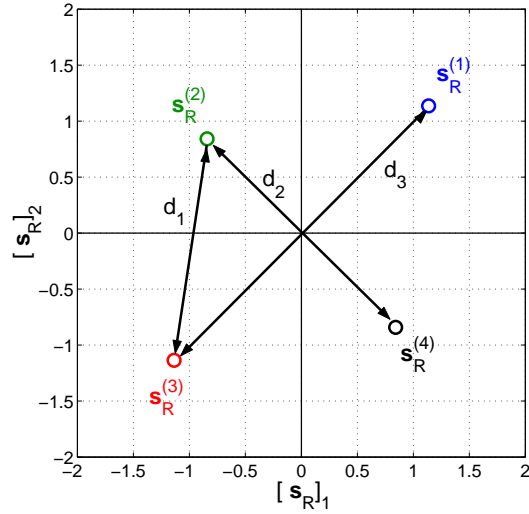


Figure 4.30: Three relevant symbol distances at the receiver. cyclic STBC; BPSK modulation; \mathbf{H}_{v1} .

only interested in the minimum distance d_{min} crossover event. Due to the channel distortion all, out of the three distances can become the minimum distance depending on the specific channel realization. Therefore it is necessary to distinguish three different cases, namely: $d_1 = d_{min}$, $d_2 = d_{min}$ or $d_3 = d_{min}$.

In the following we derive lower bounds for the conditional BERs for the three different cases. Then the BERs conditioned on the channel matrix are averaged with respect to all channels, which fulfill the condition $d_i = d_{min}$. Afterwards, the total probability theorem is used to merge the three average lower bounds for the BER together to get one overall lower bound for the average BER.

Starting with the first case, namely $d_1 = d_{min}$, this is the case for a certain channel vector \mathbf{h}_1 or equivalently a certain virtual channel matrix \mathbf{H}_{v1} . The symbol constellation for this case can be seen in

Fig.4.31.a.). Now let's derive a modified version of the NNA explained in Sec. 4.3.1. The modification

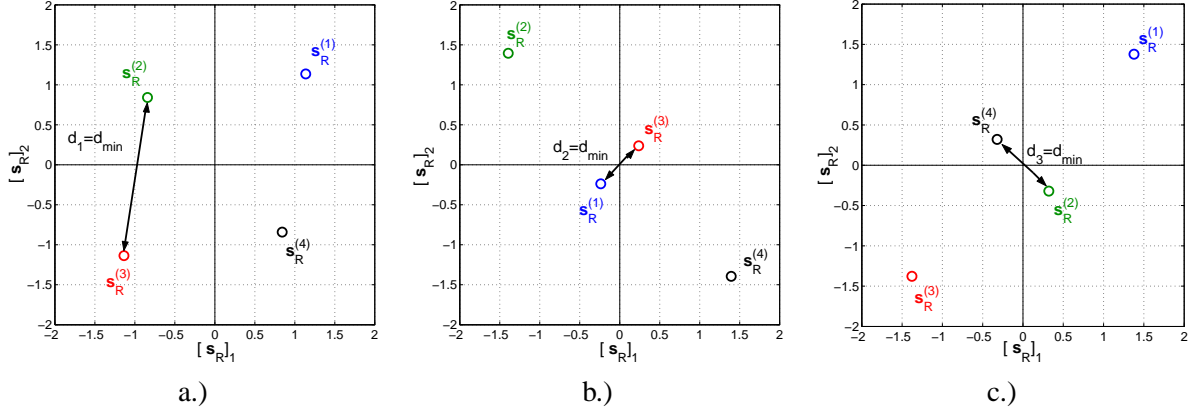


Figure 4.31: Minimum distance d_{min} for three different channel realization; a.) $d_1 = d_{min}$ for \mathbf{H}_{v1} , b.) $d_2 = d_{min}$ for \mathbf{H}_{v2} , c.) $d_3 = d_{min}$ for \mathbf{H}_{v3} ; cyclic STBC; BPSK modulation;

is, that not all nearest neighbors are considered, but only those nearest neighbors with the minimum distance. Keeping this in mind we start calculating the lower bound for the BER (conditioned on \mathbf{h}):

$$\text{BER}_1^{LB}(\mathbf{h}) = \bar{n}_{NN} \frac{n_{BE}}{\log_2(|\mathcal{A}|)} \text{PEP}(d_{min}) . \quad (4.108)$$

At this point we have to determine the values for the unknown variables d_{min} and \bar{n}_{NN} in the above equation. Obviously, d_{min} is d_1 in this case. The second unknown variable, the average number of nearest neighbors \bar{n}_{NN} , is also very easy to determine. Focusing on the symbol constellation shown in Fig.4.31.a.), we can see that all symbols have 2 nearest neighbors with minimum distance, therefore $\bar{n}_{NN} = 2$. The number of bit errors is 1 for this cross over event. Hence, we get:

$$\text{BER}_1^{LB}(\mathbf{h}) = 2 \frac{1}{2} \text{PEP}(d_1) = \text{Q} \left(\sqrt{\frac{d_1^2(\mathbf{h})}{2\sigma_n^2}} \right) . \quad (4.109)$$

This method is repeated for the case, when $d_2 = d_{min}$ holds. Once again the modified NNA is used to calculate the lower bound for the BER, where the unknown variables are determined with the aid of Fig.4.31.b.). Obviously, d_{min} is in this case d_2 . Focusing on $\mathbf{s}_R^{(1)}$ we can see only one nearest neighbor with minimum distance. This nearest neighbor has two different bits. The same holds for the symbol $\mathbf{s}_R^{(3)}$. For the symbols $\mathbf{s}_R^{(2)}$ and $\mathbf{s}_R^{(4)}$ all nearest neighbors appear at distances larger than the minimum distance d_2 . Therefore, $\bar{n}_{NN} = 1/4(1 + 0 + 0 + 1) = 1/2$ and $n_{BE} = 2$. Thus we finally get:

$$\text{BER}_2^{LB}(\mathbf{h}) = \frac{1}{2} \frac{2}{2} \text{PEP}(d_2) = \frac{1}{2} \text{Q} \left(\sqrt{\frac{d_2^2(\mathbf{h})}{2\sigma_n^2}} \right) . \quad (4.110)$$

For the third and the last case, with $d_3 = d_{min}$, matters are quite similar to the second case and we get:

$$\text{BER}_3^{LB}(\mathbf{h}) = \frac{1}{2} \text{Q} \left(\sqrt{\frac{d_3^2(\mathbf{h})}{2\sigma_n^2}} \right) . \quad (4.111)$$

As explained some paragraphs above, the lower bounds for the conditioned BERs are averaged over all channel realizations \mathbf{h} for that $d_i = d_{min}$:

$$\overline{\text{BER}}_k^{LB} = E_{\mathbf{h}|(d_k=d_{min})} \{ \text{BER}_k^{LB}(\mathbf{h}) \} = w_k \int_0^\infty \text{Q} \left(\sqrt{\frac{\xi}{2\sigma_n^2}} \right) p_{d_k^2|d_k^2=d_{min}^2}(\xi) d\xi , \quad (4.112)$$

where $w_1 = 1$, $w_2 = 1/2$ and $w_3 = 1/2$. The last step for the calculation of the total lower bound, the so-called MDLB, is to use the total probability theorem:

$$\text{BER}_{\text{MDLB}} = \overline{\text{BER}}_1^{LB} P_{d_1^2=d_{min}^2} + \overline{\text{BER}}_2^{LB} P_{d_2^2=d_{min}^2} + \overline{\text{BER}}_3^{LB} P_{d_3^2=d_{min}^2}, \quad (4.113)$$

where $P_{d_k^2=d_{min}^2}$ is the probability that $d_k^2 = d_{min}^2$ with respect to all channel realizations. The final result can be written as:

$$\text{BER}_{\text{MDLB}} = \sum_{k=1}^3 w_k \left[\int_0^\infty Q \left(\sqrt{\frac{\xi}{2\sigma_n^2}} \right) p_{d_k^2|d_k^2=d_{min}^2}(\xi) d\xi \right] P_{d_k^2=d_{min}^2}, \quad (4.114)$$

Inserting the key-parameters of Tab. 4.5 in Eqn. (4.99), we come to the same result as above with the same weights w_k , therefore this specific example verifies the general result given in Eqn. (4.99). With this simple example it becomes clear, that the MDLB is only a generalization of the well known NNA and that in principle it is not too difficult to be found.

So far matters are fairly simple, but calculating the corresponding PDFs of the distances is quite challenging. As in Sec. 4.2, the distances and their statistic strongly depend on the channel model and thus in the following spatially uncorrelated and correlated channel are considered separately. The corresponding calculations and explanations can be found in the following sections.

In general, for the calculation of the MDLB it is not necessary to investigate the symbol constellation as shown in the example above. The essential points for calculating the MDLB can be summarized as follows:

-) Find the ET table (ETs plus key-parameters).
-) Calculate the PDF of the distances: $p_{d_k^2|d_k^2=d_{min}^2}$.
-) Calculate the corresponding probabilities: $P_{d_k^2=d_{min}^2}$.
-) Apply the total probability theorem: Eqn. (4.99).

4.3.2.2 Spatially Uncorrelated Channels

In order to calculate the distances corresponding to different ETs, we have to adapt Eqn. (4.19) to end up with Eqn. (4.115). Here, we are no longer interested in crossover events but in ETs. Thus, the distance corresponding to the i -th ET can be calculated as:

$$\begin{aligned} d_i^2 &= \sum_{k=1}^{n_R} \mathbf{h}_k \underbrace{\mathbf{B}_i \mathbf{B}_i^H}_{\mathbf{A}_i} \mathbf{h}_k^H = \sum_{k=1}^{n_R} \mathbf{h}_k \underbrace{\mathbf{A}_i}_{\mathbf{U}_i \mathbf{D}_i \mathbf{U}_i^H} \mathbf{h}_k^H = \sum_{k=1}^{n_R} \underbrace{\mathbf{h}_k \mathbf{U}_i}_{\mathbf{h}_k^{(i)}} \mathbf{D}_i \underbrace{\mathbf{U}_i^H \mathbf{h}_k^H}_{\mathbf{h}_k^{(i)H}} \\ &= \sum_{k=1}^{n_R} \mathbf{h}_k^{(i)} \mathbf{D}_i \mathbf{h}_k^{(i)H} = \sum_{l=1}^{r_i} \underbrace{\sum_{k=1}^{n_R} |h_{k,l}^{(i)}|^2}_{\alpha_l^{(i)}} \lambda_l^{(i)} = \sum_{l=1}^{r_i} \alpha_l^{(i)} \lambda_l^{(i)}, \end{aligned} \quad (4.115)$$

At this point the set of STBCs can be subdivided into two sets.

Code Set 1: STBCs corresponding to Code Set (CS) 1 are codes with the following property: The eigenbases \mathbf{U}_i of the code word distance matrices \mathbf{A}_i for different ETs is the same. Consequently, the random variables $\alpha_l^{(i)}$ are also independent of the ETs and thus $\alpha_l^{(i)} = \alpha_l$ holds. Representatives of CS1 are for example: orthogonal codes (for example the code defined in Eqn. (4.8)), the Extended Alamouti code defined in Eqn. (4.10) and the cyclic code defined in Eqn. (4.9).

Code Set 2: STBCs corresponding to CS2 are all codes that do not belong to CS1, i.e., they do not have this advantageous property explained in the paragraph about CS1. A representative of CS2 is for example the D-STTD code Eqn. (4.11).

In the following, I will show the calculation of the necessary PDFs of the random variables d_i^2 for the general case and afterwards I will concentrate on the cyclic code as a simple example. For the general derivation the following is assumed: Regardless, which STBC is considered, always the property of CS1 is assumed, i.e., it is assumed that the random variables $\alpha_l^{(i)}$ are independent of the ET and thus $\alpha_l^{(i)} = \alpha_l$ holds. Because of this assumption no error is made for codes belonging to CS1. For codes belonging to CS2 this assumption causes an error in the resulting PDF. In spite of the error in the PDF, the resulting BER approximation is still a lower bound. This holds, because although in this case the random variables for different ETs are different and thus the resulting minimum distance will be smaller than with the assumption of CS1. Therefore, the BER in reality is higher than using this assumption. Hence, the BER in reality is larger than the calculated one and thus the resulting BER performance approximation is still a lower bound.

Calculating the PDF of the distances d_k^2 with $d_k^2 = d_{min}^2$:

As shown in Eqn. (4.115), the distance of the k -th ET is a weighted function (a linear function of α_l) of the random variables α_l . In the following we introduce the short notation for the weighted sum (linear function of α_l) given in Eqn. (4.115): $d_k^2 = f_k(\alpha_1, \alpha_2, \dots, \alpha_{n_T})$. We know that the random variables α_l are independently χ^2 distributed with $2 n_R$ degrees of freedom. Hence, the joint PDF of the random variables α_1 to α_{n_T} results in:

$$p_{\alpha_1, \alpha_2, \dots, \alpha_{n_T}}(\xi_1, \xi_2, \dots, \xi_{n_T}) = p_{\alpha_1}(\xi_1) p_{\alpha_2}(\xi_2) \dots p_{\alpha_{n_T}}(\xi_{n_T}) \quad (4.116)$$

In order to calculate the PDF of the distance d_k^2 from the joint PDF of the random variables α_1 to α_{n_T} , we have to bring the distance d_k^2 into play. The conditional PDF of the distance d_k^2 can be calculated by the aid of a linear PDF transformation according to the linear function f_k and the PDF of α_1 ¹¹:

$$p_{d_k^2 | \alpha_2, \dots, \alpha_{n_T}}(\eta | \xi_2, \dots, \xi_{n_T}) = \mathcal{T}_{f_k} \{ p_{\alpha_1}(\xi_1) \}, \quad (4.117)$$

¹¹It is not important, which random variable α_l is used for the transformation. α_1 is only an arbitrary choice

Due to the independency of the random variables α_l the joint PDF of the random variables d_k^2, α_2 to α_{n_T} reads as

$$\begin{aligned} p_{d_k^2, \alpha_2, \dots, \alpha_{n_T}}(\eta, \xi_2, \dots, \xi_{n_T}) &= p_{d_k^2 | \alpha_2, \dots, \alpha_{n_T}}(\eta | \xi_2, \dots, \xi_{n_T}) p_{\alpha_2}(\xi_2) \dots p_{\alpha_{n_T}}(\xi_{n_T}) \quad (4.118) \\ &= \mathcal{T}_{f_k} \{p_{\alpha_1}(\xi_1)\} p_{\alpha_2}(\xi_2) \dots p_{\alpha_{n_T}}(\xi_{n_T}), \end{aligned}$$

The desired PDF is obtained by averaging over the remaining random variables α_l ($l \neq 1$). Note that the integral is not over the entire domain of valid values for α_2 to α_{n_T} ($(\alpha_2, \dots, \alpha_{n_T})$ plane), but only over the region \mathcal{R}_k of the $(\alpha_2, \dots, \alpha_{n_T})$ plane where $d_k^2 = d_{min}^2$. The region \mathcal{R}_k is determined by using the other linear functions $d_i^2 = f_i(\alpha_1, \alpha_2, \dots, \alpha_{n_T})$ with $i \neq k$, which are the distances corresponding to the remaining ETs. Obviously, if there are n_{ET} different ETs, there are also n_{ET} different distances and n_{ET} different linear functions defining these distances. Hence the PDF can be calculated as:

$$p_{d_k^2, d_k^2 = d_{min}^2}(\eta) = \int_{\mathcal{R}_k} p_{d_k^2, \alpha_2, \dots, \alpha_{n_T}}(\eta, \xi_2, \dots, \xi_{n_T}) d\xi_2, \dots, d\xi_{n_T}. \quad (4.119)$$

After showing the principal way of calculating the PDFs of the distances d_k^2 with $d_k^2 = d_{min}^2$, I want to concretize this algorithm for the cyclic code **S** defined in Eqn. (4.104) with two transmit antennas and one receive antenna using BPSK modulation:

Example: Cyclic Code for two transmit antennas

Remember the ETs (Tab. 4.5) and the distance calculation in Eqn. (4.115). Accordingly, we can find three distances corresponding to the three different ETs:

$$\begin{aligned} d_1^2 &= \lambda_1^{(1)} \alpha_1 + \lambda_2^{(1)} \alpha_2 = 4 \alpha_1 + 4 \alpha_2 = f_1(\alpha_1, \alpha_2) \\ d_2^2 &= \lambda_1^{(1)} \alpha_1 = 16 \alpha_1 = f_2(\alpha_1, \alpha_2) \\ d_3^2 &= \lambda_2^{(1)} \alpha_2 = 16 \alpha_2 = f_3(\alpha_1, \alpha_2) \end{aligned} \quad (4.120)$$

Note that due to only one receive antenna, the random variables α_l are χ^2 distributed with 2 degrees of freedom:

$$p_{\alpha_l}(\xi_l) = e^{-\xi_l} \sigma(\xi_l), \quad (4.121)$$

where $\sigma(\xi_l)$ denotes the Heaviside step function.

Starting with the calculation of $p_{d_1^2, d_1^2 = d_{min}^2}(\eta)$, the joint PDF reads as:

$$p_{d_1^2, \alpha_2}(\eta, \xi_2) = \mathcal{T}_{f_1} \{p_{\alpha_1}(\xi_1)\} p_{\alpha_2}(\xi_2), \quad (4.122)$$

The PDF transform according to f_1 (Eqn. (4.120)) is a simple affine transformation:

$$d_1^2 = 4 \alpha_1 + 4 \xi_2, \quad (4.123)$$

therefore the conditional PDF of the distance d_1^2 can be expressed as PDF of α_1 as:

$$p_{d_1^2 | \alpha_2}(\eta | \xi_2) = \frac{1}{4} p_{\alpha_1} \left(\frac{\eta}{4} - \xi_2 \right), \quad (4.124)$$

Accordingly the joint PDF reads as:

$$p_{d_1^2, \alpha_2}(\eta, \xi_2) = \frac{1}{4} p_{\alpha_1} \left(\frac{\eta}{4} - \xi_2 \right) p_{\alpha_2}(\xi_2) = \frac{1}{4} e^{-(\eta/4 - \xi_2)} \sigma(\eta/4 - \xi_2) e^{-\xi_2} \sigma(\xi_2), \quad (4.125)$$

Before evaluating the integral in Eqn. (4.119), we have to find the corresponding region \mathcal{R}_1 for that $d_1^2 = d_{min}^2$ is fulfilled.

For $p_{d_1^2|d_1^2=d_{min}^2}$, the realizations of d_1^2 and d_2^2 must fulfill the condition $d_1^2 < d_2^2$ and thus we get:

$$\begin{aligned} 4\xi_1 + 4\xi_2 &< 16\xi_1 \\ \xi_2 &< 3\xi_1 \end{aligned} \quad (4.126)$$

At this point the distance equation f_1 is inserted in Eqn. (4.126). Note that we focus on the realizations of the random variables (instead of the random variables). Therefore, the function f_1 (regarding realizations) is $\eta = 4\xi_1 + 4\xi_2$ instead of $d_1^2 = 4\alpha_1 + 4\alpha_2$. More concrete, we insert $\xi_1 = \frac{\eta}{4} - \xi_2$ in Eqn. (4.126):

$$\begin{aligned} \xi_2 &< 3\left(\frac{\eta}{4} - \xi_2\right) \\ 4\xi_2 &< \frac{3\eta}{4} \\ \xi_2 &< \frac{3\eta}{16} \end{aligned} \quad (4.127)$$

From the second condition $d_1^2 < d_3^2$ we get in the same way:

$$\xi_2 > \frac{\eta}{16} \quad (4.128)$$

Therefore the desired PDF $p_{d_1^2|d_1^2=d_{min}^2}(\eta)$

$$p_{d_1^2|d_1^2=d_{min}^2}(\eta) = \int_{\mathcal{R}_1} p_{d_1^2,\alpha_2}(\eta, \xi_2) d\xi_2 = \frac{1}{4}e^{-\eta/4} \int_{\eta/16}^{3\eta/16} \sigma(\eta/4 - \xi_2)\sigma(\xi_2) d\xi_2 = \frac{\eta}{32}e^{-\eta/4} \sigma(\eta). \quad (4.129)$$

For the remaining two distance-PDFs: $p_{d_2^2|d_2^2=d_{min}^2}(\eta)$ and $p_{d_3^2|d_3^2=d_{min}^2}(\eta)$, the calculation is very similar. Therefore, the results of the two PDFs are shown in Eqn. (4.130) and Eqn. (4.131) without going into details.

The PDF $p_{d_2^2|d_2^2=d_{min}^2}(\eta)$ results in:

$$p_{d_2^2|d_2^2=d_{min}^2}(\eta) = \int_{\mathcal{R}_2} p_{d_2^2,\alpha_2}(\eta, \xi_2) d\xi_2 = \frac{1}{16}e^{-\eta/16} \int_{3\eta/16}^{\infty} e^{-\xi_2} \sigma(\eta/16)\sigma(\xi_2) d\xi_2 = \frac{1}{16}e^{-\eta/4} \sigma(\eta), \quad (4.130)$$

and

$$p_{d_3^2|d_3^2=d_{min}^2}(\eta) = \int_{\mathcal{R}_3} p_{\alpha_1,d_3^2}(\xi_1, \eta) d\xi_1 = \frac{1}{16}e^{-\eta/16} \int_{3\eta/16}^{\infty} e^{-\xi_1} \sigma(\eta/16)\sigma(\xi_1) d\xi_1 = \frac{1}{16}e^{-\eta/4} \sigma(\eta). \quad (4.131)$$

Having calculated these PDFs, we proceed with the calculation of the probabilities $P_{d_k^2=d_{min}^2}$ according to Eqn. (4.101):

$$P_{d_1^2=d_{min}^2} = \int_0^{\infty} p_{d_1^2,d_k^2=d_{min}^2}(\eta) d\eta = \int_0^{\infty} \frac{\eta}{32}e^{-\eta/4} \sigma(\eta) d\eta = \frac{1}{2}, \quad (4.132)$$

$$P_{d_2^2=d_{min}^2} = \int_0^{\infty} p_{d_2^2,d_k^2=d_{min}^2}(\eta) d\eta = \int_0^{\infty} \frac{1}{16}e^{-\eta/4} \sigma(\eta) d\eta = \frac{1}{4}, \quad (4.133)$$

$$P_{d_3^2=d_{min}^2} = \int_0^{\infty} p_{d_3^2,d_k^2=d_{min}^2}(\eta) d\eta = \int_0^{\infty} \frac{1}{16}e^{-\eta/4} \sigma(\eta) d\eta = \frac{1}{4}. \quad (4.134)$$

With these probabilities the desired PDFs according to Eqn. (4.102) result in:

$$p_{d_1^2|d_1^2=d_{min}^2} = \frac{p_{d_1^2,d_1^2=d_{min}^2}}{P_{d_1^2=d_{min}^2}} = \frac{\eta}{16}e^{-\eta/4} \sigma(\eta), \quad (4.135)$$

$$P_{d_2^2|d_2^2=d_{min}^2} = \frac{P_{d_2^2, d_2^2=d_{min}^2}}{P_{d_2^2=d_{min}^2}} = \frac{1}{4} e^{-\eta/4} \sigma(\eta), \quad (4.136)$$

$$P_{d_3^2|d_3^2=d_{min}^2} = \frac{P_{d_3^2, d_3^2=d_{min}^2}}{P_{d_3^2=d_{min}^2}} = \frac{1}{4} e^{-\eta/4} \sigma(\eta), \quad (4.137)$$

Knowing these PDFs we can calculate the average error probabilities of the three ETs according to Eqn. (4.100):

$$\begin{aligned} P_{\mathcal{E}_1} &= \int_0^\infty Q\left(\sqrt{\frac{\eta}{2\sigma_n^2}}\right) P_{d_1^2|d_1^2=d_{min}^2}(\eta) d\eta = \int_0^\infty Q\left(\sqrt{\frac{\eta}{2\sigma_n^2}}\right) \frac{\eta}{16} e^{-\eta/4} \sigma(\eta) \\ &= \left(\frac{1-\mu}{2}\right)^2 \left[1 + 2\left(\frac{1+\mu}{2}\right)\right], \\ P_{\mathcal{E}_2} &= \int_0^\infty Q\left(\sqrt{\frac{\eta}{2\sigma_n^2}}\right) \frac{1}{4} e^{-\eta/4} \sigma(\eta) d\eta = \left(\frac{1-\mu}{2}\right), \end{aligned} \quad (4.138)$$

$$P_{\mathcal{E}_3} = \int_0^\infty Q\left(\sqrt{\frac{\eta}{2\sigma_n^2}}\right) \frac{1}{4} e^{-\eta/4} \sigma(\eta) d\eta = \left(\frac{1-\mu}{2}\right), \quad (4.139)$$

with

$$\mu = \sqrt{\frac{1}{\sigma_n^2 + 1}}. \quad (4.140)$$

Now we are almost done. By applying the total probability theorem Eqn. (4.114) we obtain the final results:

$$\begin{aligned} \text{BER}_{\text{MDLB}} &= \sum_{k=1}^3 w_k \left[\int_0^\infty Q\left(\sqrt{\frac{\xi}{2\sigma_n^2}}\right) P_{d_k^2|d_k^2=d_{min}^2}(\xi) d\xi \right] P_{d_k^2=d_{min}^2} \\ &= 1 \left\{ \left(\frac{1-\mu}{2}\right)^2 \left[1 + 2\left(\frac{1+\mu}{2}\right)\right] \right\} \frac{1}{2} + \frac{1}{2} \left\{ \left(\frac{1-\mu}{2}\right) \right\} \frac{1}{4} + \frac{1}{2} \left\{ \left(\frac{1-\mu}{2}\right) \right\} \frac{1}{4} \\ &= \frac{1}{2} \left(\frac{1-\mu}{2}\right)^2 \left[1 + 2\left(\frac{1+\mu}{2}\right)\right] + \frac{1}{4} \left(\frac{1-\mu}{2}\right). \end{aligned} \quad (4.141)$$

In Fig. (4.32) the calculated MDLB is compared to simulation results and the union bound calculated according to the approach described in Sec. 4.2. As we can see, the MDLB underestimates the BER vs. SNR performance compared to the simulation result, which is considered here as the exact or true BER-performance. The union bound for this example is tighter than the MDLB. For other examples, shown in Sec. 4.3.2.5, the MDLB becomes tighter or similar tight to the simulation results as the union bound. With the MDLB and the previously calculated union bound Eqn. (4.48), a two-sided bounding of the true BER vs. SNR performance is possible. For the special case that both bounds are tight, as for most examples analyzed in this thesis, we can even specify the exact performance, at least in the high SNR domain.

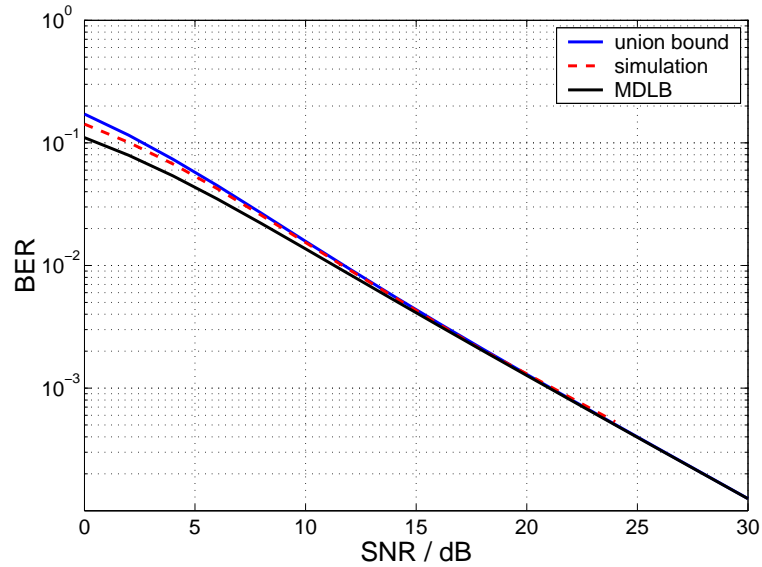


Figure 4.32: BER vs. SNR performance of the cyclic STBC. BPSK modulation; $n_T = 2$, $n_R = 1$; uncorrelated channels.

4.3.2.3 Spatially Correlated Channels

For spatially correlated channels the MDLB-calculation in principle is performed in the same way, but distance calculations are slightly different compared to the case of spatially uncorrelated channels. In order to calculate the distances corresponding to different ETs, we have to start with Eqn. (4.55). Again, we are no longer interested in crossover events but in ETs. Thus, the distance corresponding to the i -th ET can be calculated according to Eqn. (4.55) as

$$d_i^2 = \mathbf{g} \tilde{\mathbf{R}}_H^{1/2} \tilde{\mathbf{A}}_i \tilde{\mathbf{R}}_H^{1/2 H} \mathbf{g}^H = \mathbf{g} \mathbf{U}_{\tilde{\mathbf{R}}_H}^* \underbrace{\mathbf{D}_{\tilde{\mathbf{R}}_H}^{1/2} \mathbf{U}_{\tilde{\mathbf{R}}_H}^T \tilde{\mathbf{A}}_i \mathbf{U}_{\tilde{\mathbf{R}}_H}^* \mathbf{D}_{\tilde{\mathbf{R}}_H}^{1/2}}_{\mathbf{Z}_i} \mathbf{U}_{\tilde{\mathbf{R}}_H}^T \mathbf{g}^H. \quad (4.142)$$

Taking into account that multiplying a Gaussian random vector by a unitary matrix does not change the Gaussian statistic, we get:

$$d_i^2 = \sum_{m=1}^{n_{NZ}} \underbrace{|g_m^{(i)}|^2}_{\alpha_m^{(i)}} \lambda_{\mathbf{Z}_i}^{(m)}, \quad (4.143)$$

where $g_m^{(i)}$ are complex Gaussian random variables with zero mean and unit variance. For correlated channels the eigenbases for different ET is different regardless of the specific code. The only exception are orthogonal codes, which always have specific properties. For this reason an exact calculation of the the distances and the corresponding PDFs in general is not possible. In order to make the calculation of the MDLB feasible, the same assumption as for CS2 for uncorrelated channels is made, namely it is assumed that the eigenbasis is the same for all ETs and therefore the realizations $g_m^{(i)} = g_m$ are independent from the specific ET.

In principle all steps to calculate the necessary PDFs of all relevant distances are the same as for uncorrelated channels. The difference in deriving the PDFs lies in some detail and therefore I will now show the PDF-derivation for a specific example.

Example: Cyclic Code for two transmit antennas

In this example, I will show some details of the PDF calculation for the cyclic code with two transmit antennas and one receive antenna using BPSK modulation. For this correlated channel, scenario 14D3 with strong spatial correlation has been chosen. The ET table is now different compared to the uncorrelated case, because now we have different ET-key-parameters. For the **uncorrelated** case the key-parameters are essentially the eigenvalues of the distance matrix \mathbf{A}_i and for the **correlated** case the key-parameters are the eigenvalues of the matrix \mathbf{Z}_i . We start by investigating all 16 crossover events to find the modified ET table. Again, there are 3 different ETs and the corresponding key-parameters are listed in Tab. 4.6. Note that the key-parameters for each channel correlation type are different! The number of crossover events leading to a certain ET is denoted by f_k and the number of different information bits is n_{BEk} .

The model parameters extracted from measurements performed in scenario 14D3 are:

$$\mathbf{U}_{TX} = \begin{pmatrix} 0.7076 & -0.6790 + j0.1956 \\ 0.6790 + j0.1956 & 0.7076 \end{pmatrix}, \quad (4.144)$$

$$\mathbf{\Omega} = \begin{pmatrix} 0.1516 & 1.8484 \end{pmatrix}. \quad (4.145)$$

\mathbf{U}_{RX} degenerates to 1, because only one receive antenna is used.

ET k	$\lambda_{\mathbf{Z}_k}^{(1)}$	$\lambda_{\mathbf{Z}_k}^{(2)}$	f_k	n_{BEk}
k	0	0	4	0
1	0.6064	7.3936	8	1
2	2.9560	0.0000	2	2
3	0.0000	29.0439	2	2

Table 4.6: ET table for the cyclic STBC. BPSK modulation; $n_T = 2$; correlation scenario 14D3.

Accordingly, we can find 3 distances corresponding to the 3 different ETs:

$$\begin{aligned} d_1^2 &= 0.6064 \alpha_1 + 7.3936 \alpha_2 = f_1(\alpha_1, \alpha_2) \\ d_2^2 &= 2.9560 \alpha_1 = f_2(\alpha_1, \alpha_2) \\ d_3^2 &= 29.0439 \alpha_2 = f_3(\alpha_1, \alpha_2) \end{aligned} \quad (4.146)$$

It is assumed that $\alpha_1^{(i)} = \alpha_1$ and $\alpha_2^{(i)} = \alpha_2$ as explained above. The random variables α_l are χ^2 distributed with 2 degrees of freedom:

$$p_{\alpha_l}(\xi_l) = e^{-\xi_l} \sigma(\xi_l), \quad (4.147)$$

where $\sigma(\xi_l)$ denotes the Heaviside step function.

Starting with the calculation of $p_{d_1^2, d_1^2=d_{min}^2}(\eta)$, the joint PDF results in:

$$p_{d_1^2, \alpha_2}(\eta, \xi_2) = \mathcal{T}_{f_1} \{p_{\alpha_1}(\xi_1)\} p_{\alpha_2}(\xi_2), \quad (4.148)$$

The PDF transform according to f_1 (Eqn. (4.146)) is a simple affine transformation:

$$d_1^2 = 0.6064 \alpha_1 + 7.3936 \xi_2, \quad (4.149)$$

therefore the conditional PDF of the distance d_1^2 can be expressed by means of the PDF of α_1 resulting in:

$$p_{d_1^2|\alpha_2}(\eta|\xi_2) = \frac{1}{0.6064} p_{\alpha_1} \left(\frac{\eta}{0.6064} - 12.1926 \xi_2 \right), \quad (4.150)$$

Accordingly the joint PDF results in:

$$\begin{aligned} p_{d_1^2, \alpha_2}(\eta, \xi_2) &= \frac{1}{0.6064} p_{\alpha_1} \left(\frac{\eta}{0.6064} - 12.1926 \xi_2 \right) p_{\alpha_2}(\xi_2) \\ &= \frac{1}{0.6064} e^{-(\eta/0.6064 - 12.1926 \xi_2)} \sigma(\eta/0.6064 - 12.1926 \xi_2) e^{-\xi_2} \sigma(\xi_2), \end{aligned} \quad (4.151)$$

Before doing the integration according to Eqn. (4.119), we have to find the corresponding region \mathcal{R}_1 for that $d_1^2 = d_{min}^2$ is valid.

The realizations of d_1^2 and d_2^2 must fulfill the condition $d_1^2 < d_2^2$ and thus we get:

$$\begin{aligned} 0.6064 \xi_1 + 7.3936 \xi_2 &< 2.9560 \xi_1 \\ \xi_2 &< 0.3178 \xi_1 \end{aligned} \quad (4.152)$$

At this point the distance equation f_1 is inserted in Eqn. (4.152). Note that we focus on the realizations of the random variables (instead of the random variables). Therefore, the function f_1 (regarding realization) is $\eta = 0.6064 \xi_1 + 7.3936 \xi_2$ instead of $d_1^2 = 0.6064 \alpha_1 + 7.3936 \alpha_2$. More concrete, we insert $\xi_1 = \frac{\eta}{0.6064} - 12.1926 \xi_2$ in Eqn. (4.152):

$$\begin{aligned} \xi_2 &< 0.3178 \left(\frac{\eta}{0.6064} - 12.1926 \xi_2 \right) \\ 4.8748 \xi_2 &< 0.5241 \eta \\ \xi_2 &< 0.1075 \eta \end{aligned} \quad (4.153)$$

From the second condition $d_1^2 < d_3^2$ we get in the same way:

$$\xi_2 > 0.0344 \eta \quad (4.154)$$

Therefore the desired PDF $p_{d_1^2 | d_1^2 = d_{min}^2}(\eta)$ results in

$$\begin{aligned} p_{d_1^2, d_1^2 = d_{min}^2}(\eta) &= \int_{\mathcal{R}_1} p_{d_1^2, \alpha_2}(\eta, \xi_2) d\xi_2 \\ &= \frac{1}{0.6064} e^{-\eta/0.6064} \int_{0.0344 \eta}^{0.1075 \eta} e^{12.1926 \xi_2} \sigma(\eta/0.6064 - 12.1926 \xi_2) \sigma(\xi_2) d\xi_2 \\ &= 0.1473 \left(e^{-0.4459 \eta} - e^{-1.2641 \eta} \right) \sigma(\eta). \end{aligned} \quad (4.155)$$

For the remaining two distance PDFs $p_{d_2^2 | d_2^2 = d_{min}^2}(\eta)$ and $p_{d_3^2 | d_3^2 = d_{min}^2}(\eta)$ the calculation is very similar. Therefore, the results of the two PDFs are shown in Eqn. (4.156) and Eqn. (4.157) without going into details.

The desired PDF $p_{d_2^2 | d_2^2 = d_{min}^2}(\eta)$ results in:

$$\begin{aligned} p_{d_2^2, d_2^2 = d_{min}^2}(\eta) &= \int_{\mathcal{R}_2} p_{d_2^2, \alpha_2}(\eta, \xi_2) d\xi_2 \\ &= \frac{1}{2.9560} e^{-\eta/2.9560} \int_{0.1075 \eta}^{\infty} e^{-\xi_2} \sigma(\eta/2.9560) \sigma(\xi_2) d\xi_2 = 0.3383 e^{-0.4459 \eta} \sigma(\eta), \end{aligned} \quad (4.156)$$

and

$$\begin{aligned} p_{d_3^2, d_3^2 = d_{min}^2}(\eta) &= \int_{\mathcal{R}_3} p_{\alpha_1, d_3^2}(\xi_1, \eta) d\xi_1 \\ &= \frac{1}{29.0439} e^{-\eta/29.0439} \int_{1.2293 \eta}^{\infty} e^{-\xi_1} \sigma(\eta/29.0439) \sigma(\xi_1) d\xi_1 = 0.0344 e^{-1.2641 \eta} \sigma(\eta). \end{aligned} \quad (4.157)$$

Having calculated the necessary PDFs of the minimum distances, we proceed with the calculation of the probabilities $P_{d_k^2=d_{min}^2}$ according to Eqn. (4.101):

$$P_{d_1^2=d_{min}^2} = \int_0^\infty p_{d_1^2, d_k^2=d_{min}^2}(\eta) d\eta = \int_0^\infty 0.1473 \left(e^{-0.4459\eta} - e^{-1.2641\eta} \right) \sigma(\eta) d\eta = 0.2138, \quad (4.158)$$

$$P_{d_2^2=d_{min}^2} = \int_0^\infty p_{d_2^2, d_k^2=d_{min}^2}(\eta) d\eta = \int_0^\infty 0.3383 e^{-0.4459\eta} \sigma(\eta) d\eta = 0.7561, \quad (4.159)$$

$$P_{d_3^2=d_{min}^2} = \int_0^\infty p_{d_3^2, d_k^2=d_{min}^2}(\eta) d\eta = \int_0^\infty 0.0344 e^{-1.2641\eta} \sigma(\eta) d\eta = 0.0272. \quad (4.160)$$

With these probabilities the desired PDFs according to Eqn. (4.102) result in:

$$p_{d_1^2|d_1^2=d_{min}^2} = \frac{p_{d_1^2, d_1^2=d_{min}^2}}{P_{d_1^2=d_{min}^2}} = 0.6890 \left(e^{-0.4459\eta} - e^{-1.2641\eta} \right) \sigma(\eta), \quad (4.161)$$

$$p_{d_2^2|d_2^2=d_{min}^2} = \frac{p_{d_2^2, d_2^2=d_{min}^2}}{P_{d_2^2=d_{min}^2}} = 0.4459 e^{-0.4459\eta} \sigma(\eta), \quad (4.162)$$

$$p_{d_3^2|d_3^2=d_{min}^2} = \frac{p_{d_3^2, d_3^2=d_{min}^2}}{P_{d_3^2=d_{min}^2}} = 1.2641 e^{-1.2641\eta} \sigma(\eta), \quad (4.163)$$

Knowing these PDFs we can calculate the average error probabilities of the three ETs according to Eqn. (4.100):

$$\begin{aligned} P_{\mathcal{E}_1} &= \int_0^\infty Q\left(\sqrt{\frac{\eta}{2\sigma_n^2}}\right) p_{d_1^2|d_1^2=d_{min}^2}(\eta) d\eta \\ &= \int_0^\infty Q\left(\sqrt{\frac{\eta}{2\sigma_n^2}}\right) 0.6890 \left(e^{-0.4459\eta} - e^{-1.2641\eta} \right) \sigma(\eta) d\eta \\ &= 1.5451 \left(\frac{1-\mu_1}{2} \right) - 0.5451 \left(\frac{1-\mu_2}{2} \right), \\ P_{\mathcal{E}_2} &= \int_0^\infty Q\left(\sqrt{\frac{\eta}{2\sigma_n^2}}\right) 0.4459 e^{-0.4459\eta} \sigma(\eta) d\eta = \left(\frac{1-\mu_1}{2} \right), \end{aligned} \quad (4.164)$$

$$P_{\mathcal{E}_3} = \int_0^\infty Q\left(\sqrt{\frac{\eta}{2\sigma_n^2}}\right) 1.2641 e^{-1.2641\eta} \sigma(\eta) d\eta = \left(\frac{1-\mu_2}{2} \right), \quad (4.165)$$

with

$$\mu_1 = \sqrt{\frac{1}{4\sigma_n^2 0.4459 + 1}} \quad \mu_2 = \sqrt{\frac{1}{4\sigma_n^2 1.2641 + 1}}. \quad (4.166)$$

Now we are almost done. By applying the total probability theorem (Eqn. (4.114)) we obtain the final result:

$$\begin{aligned} \text{BER}_{\text{MDLB}} &= \sum_{k=1}^3 w_k \left[\int_0^\infty Q\left(\sqrt{\frac{\xi}{2\sigma_n^2}}\right) p_{d_k^2|d_k^2=d_{min}^2}(\xi) d\xi \right] P_{d_k^2=d_{min}^2} \\ &= 1 \left\{ 1.5451 \left(\frac{1-\mu_1}{2} \right) - 0.5451 \left(\frac{1-\mu_2}{2} \right) \right\} 0.2138 \\ &\quad + \frac{1}{2} \left\{ \left(\frac{1-\mu_1}{2} \right) \right\} 0.7587 + \frac{1}{2} \left\{ \left(\frac{1-\mu_2}{2} \right) \right\} 0.0272 \\ &= 0.7097 \left(\frac{1-\mu_1}{2} \right) - 0.1029 \left(\frac{1-\mu_2}{2} \right), \end{aligned} \quad (4.167)$$

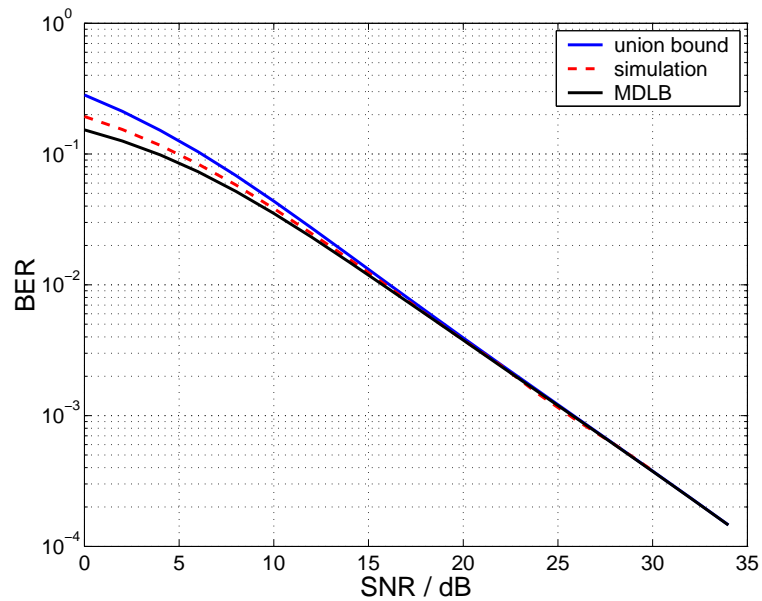


Figure 4.33: BER vs. SNR performance of the cyclic STBC. BPSK modulation; $n_T = 2$, $n_R = 1$; correlation scenario 14D3.

In Fig. (4.33) the calculated MDLB is compared to simulation results and a union bound calculated according to Sec. 4.2. As we can see, the MDLB underestimates the BER vs. SNR performance compared with the simulation results, which are considered as the exact or true BER curves. In contrast to the uncorrelated case, for the correlated case the MDLB is tighter than the union bound. Hence, with the MDLB and the previously calculated union bound, a two-sided bounding of the true BER vs. SNR performance is possible. For the special case that both bounds are tight, as for most examples analyzed in this thesis, we can predict the exact BER performance very precisely, at least in the high SNR domain.

4.3.2.4 Hybrid Method to calculate the MDLB

As it has been shown in Sec. 4.3.2.2 and Sec. 4.3.2.3, the calculations of the PDFs for the ET-distances, necessary to determine the MDLB, are rather complicated. The complexity of the calculation-algorithm increases with increasing system complexity, i.e., with the number of transmit and receive antennas and the modulation format. In order to circumvent lengthy derivations, I would like to propose a so-called *Hybrid Method*, which combines both, the analytical calculation and numerical evaluations. Instead of the conventional method of finding the BER by numerical simulations, where data are transmitted and at the receiver the bit errors are counted, the analytical approach for calculating the MDLB (explained in the previous section) is used. However, the tedious evaluations of the integrals are performed numerically.

The structure chart for the *Hybrid Method* is shown in Fig. 4.34.

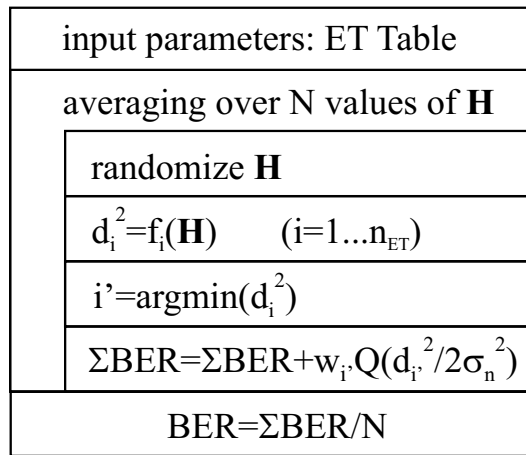


Figure 4.34: Structure chart for the MDLB determination.

With this approach we can easily get a very good approximation of the BER performance (MDLB), without performing difficult calculations. In some cases it is not necessary to get an analytical result, but we only want a BER vs. SNR curve. For such cases, the *Hybrid Method* is a very powerful technique to save a lot of computation time.

Obviously, the calculation of the union bound, which has been discussed in Sec. 4.2, is much easier compared with the calculation of the MDLB. Nevertheless, this union bound can also be calculated according to this hybrid method.

4.3.2.5 Examples and Discussion

Note that for the following examples the union bounds and the MDLBs are not calculated analytically, because of the huge calculation effort, especially for evaluating the MDLB. Instead, in this section the *Hybrid Method* is used to evaluate both bounds.

Cyclic Code:

The cyclic code for 4 transmit and 4 receive antennas using BPSK modulation, already discussed in Sec. 4.2, is analyzed at this point. The cyclic code belongs to Code Set (CS) 1. Therefore, the eigenbasis is the same for all ETs and a very accurate distance calculation is possible. The corresponding ETs are listed in Table 4.1. In Fig. 4.35 the simulated BER vs. SNR performance (dashed red curve), the tight union bound for the BER vs. SNR performance (solid blue curve) and the MDLB for the BER vs. SNR performance (solid black curve) for this cyclic code ($n_T = n_R = 4$) utilizing BPSK modulation for uncorrelated MIMO channels are compared. As we can see in Fig. 4.35 the MDLB is extremely tight. In this case and for all codes corresponding to CS1 the MDLB is tighter than the union bound. As we

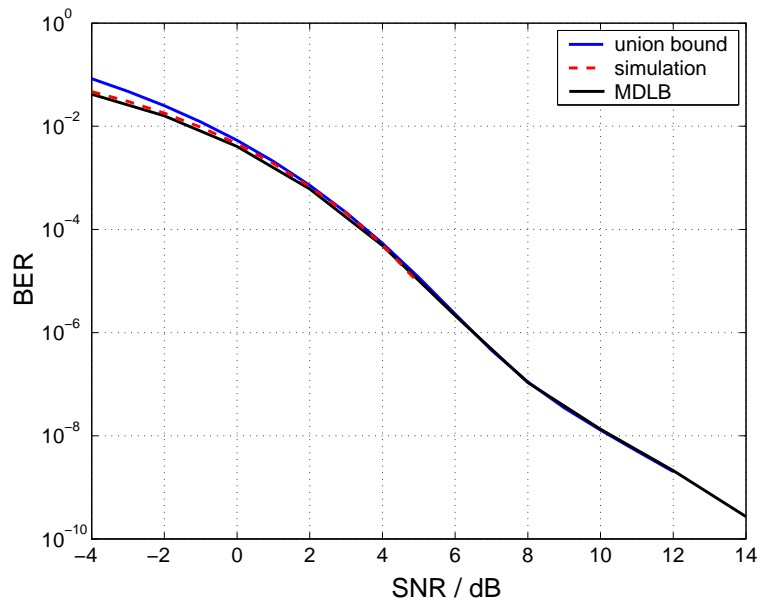


Figure 4.35: BER vs. SNR performance of the cyclic STBC. BPSK modulation; $n_T = n_R = 4$; uncorrelated channels.

can see, the lower bound and the union bound coincide for BER values of 10^{-3} and below. Obviously if a lower bound and a union bound coincide, both bounds are tight. This result is confirmed by the simulation results shown in Fig. 4.35.

In case of correlated fading all codes have distinct eigenbases for all ETs. Thus, an exact calculation of the distances and their PDFs is not possible. For this reason, the tightness of the MDLB is much worse compared with the case of uncorrelated fading. The simulated BER vs. SNR performance (dashed red curves), the tight union bounds for the BER vs. SNR performance (solid blue curves) and the MDLB for the BER vs. SNR performance (solid black curves) for this cyclic code ($n_T = n_R = 4$) utilizing BPSK modulation are compared in Fig. 4.36 for several spatial correlation types: 1D3 (o-marker) and 14D3 (+-marker). As it can be seen in Fig. 4.36, for correlated channels the union bound is tighter than the lower bound. Only for the BER below 10^{-5} the lower bound and the union bound coincide. Nevertheless, the lower bound helps us to bound the BER from below and from above. Note that in this case the union bound is already tight for BER values below 10^{-3} in contrast to the lower bound.

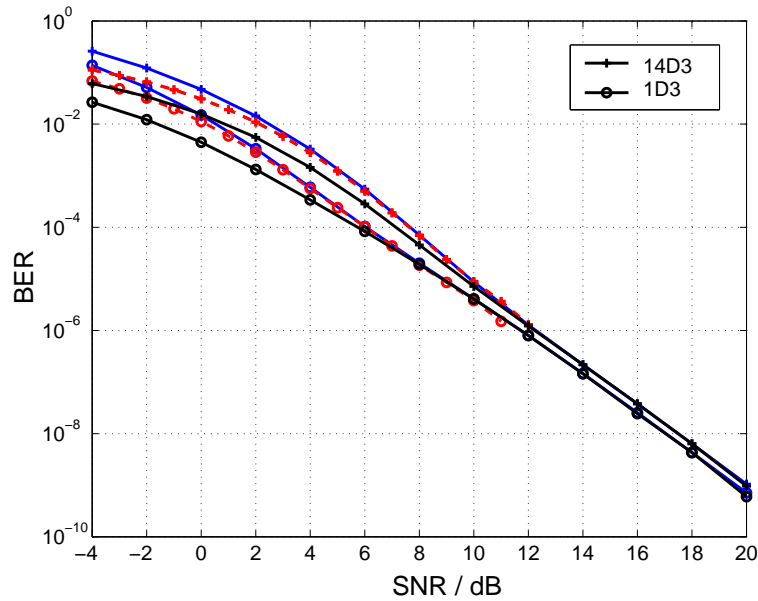


Figure 4.36: BER vs. SNR performance for the cyclic STBC. BPSK modulation; $n_T = n_R = 4$; several correlation types.

Extended Alamouti Code:

The EA code also belongs to CS1. The MDLB for this code is also an extraordinary tight performance approximation. In Fig. 4.37 the simulated BER vs. SNR performance (dashed red curves), the tight union bound for the BER vs. SNR performance (solid blue curves) and the MDLB for the BER vs. SNR performance (solid black curves) for the Extended Alamouti STBC ($n_T = n_R = 4$) utilizing QPSK modulation are compared for uncorrelated MIMO channels. It is essentially tighter than the union bound in the low SNR range. For BER values of 10^{-3} and below the union bound and the lower bound coincide.

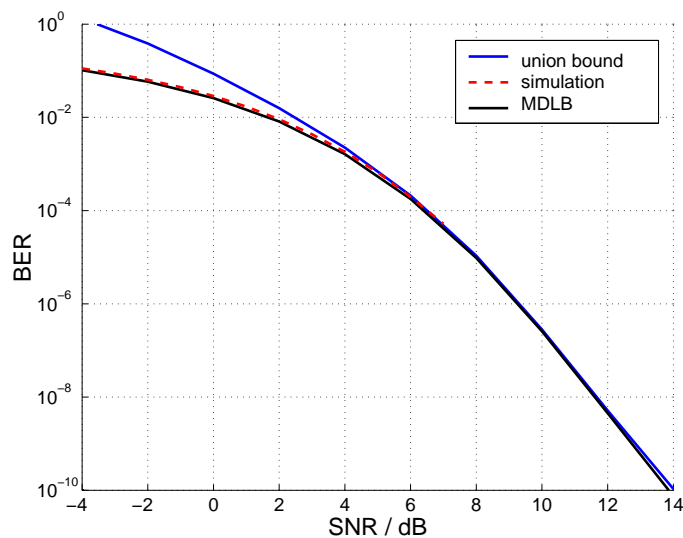


Figure 4.37: BER vs. SNR performance for the Extended Alamouti STBC. QPSK modulation; $n_T = n_R = 4$; uncorrelated channels.

In Fig. 4.38 the simulated BER vs. SNR performance (dashed red curves), the tight union bounds for the BER vs. SNR performance (solid blue curves) and the MDLB for the BER vs. SNR performance (solid black curves) for the Extended Alamouti code ($n_T = n_R = 4$) utilizing QPSK modulation are shown for several spatial correlation types: 1D3 (o-marker) and 14D3 (+-marker). In contrast to the cyclic code, the lower bound is also very tight in spatially correlated channels.

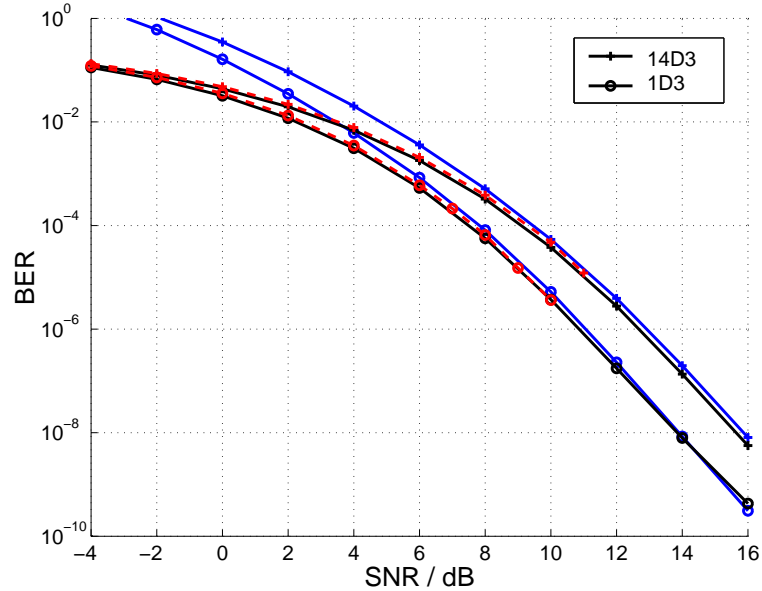


Figure 4.38: BER vs. SNR performance for the Extended Alamouti STBC. QPSK modulation; $n_T = n_R = 4$; several correlation types.

Orthogonal Code:

In Fig. 4.39 the simulated BER vs. SNR performance (dashed red curves), the tight union bounds for the BER vs. SNR performance (solid blue curves) and the high SNR approximation for the BER vs. SNR performance (solid black curves) for a specific orthogonal STBC ($n_T = n_R = 4$) utilizing QPSK modulation are compared for uncorrelated MIMO channels. In general, orthogonal codes belong to CS1. Orthogonal codes have an additional nice property, namely that the distance matrix \mathbf{A} is always a weighted identity matrix. For this reason, the eigenbasis for different ETs is the same and thus the performance approximation is very tight for correlated fading too. As already explained the performance of orthogonal codes can be calculated more easily in a different way, but in order to show that the more general framework developed in this thesis holds also for this special case, I want to show results for the orthogonal code defined in Eqn. (4.8) gained with this framework.

In Fig. 4.39 it can be seen that the MDLB is tighter than the union bound. The MDLB coincides with the simulated performance in the entire SNR range.

In Fig. 4.40 the simulated BER vs. SNR performance (dashed red curves), the tight union bounds for the BER vs. SNR performance (solid blue curves) and the MDLB for the BER vs. SNR performance (solid black curves) for a specific orthogonal code ($n_T = n_R = 4$) utilizing QPSK modulation are shown for several spatial correlation types: 1D3 (o-marker) and 14D3 (+-marker).

D-STTD Code:

The D-STTD code discussed in this paragraph belongs to CS2, i.e., it has not the nice property of the same eigenbasis for all ETs. In Fig. 4.41 the simulated BER vs. SNR performance (dashed red curves), the tight union bounds for the BER vs. SNR performance (solid blue curves) and the MDLB for the BER vs.

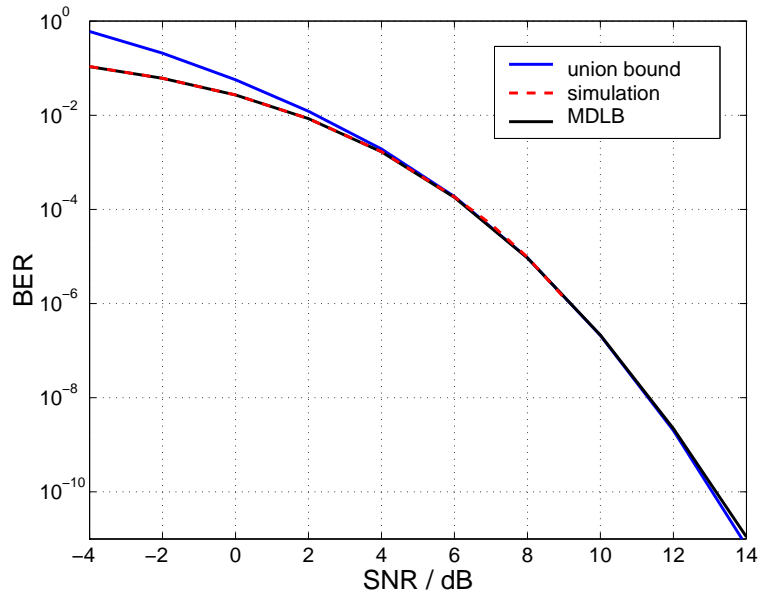


Figure 4.39: BER vs. SNR performance for a specific orthogonal STBC. QPSK modulation; $n_T = n_R = 4$; uncorrelated channels.

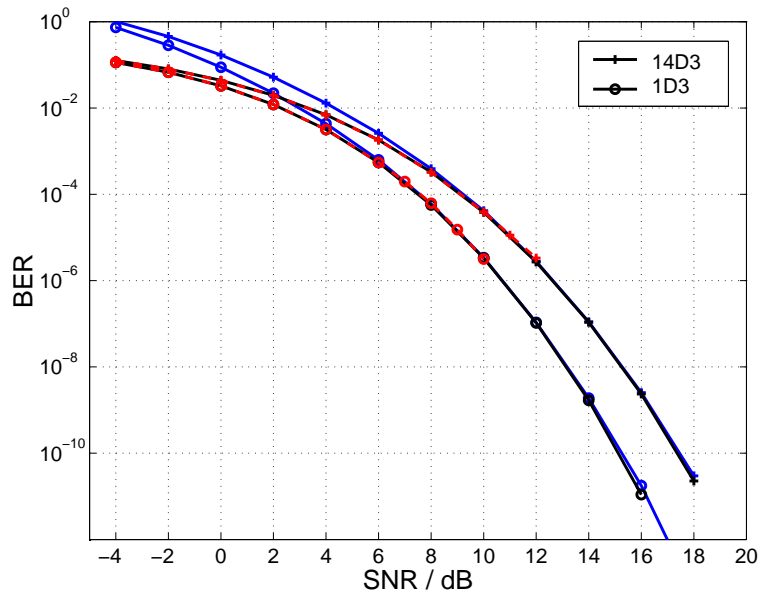


Figure 4.40: BER vs. SNR performance for a specific orthogonal STBC. QPSK modulation; $n_T = n_R = 4$; several correlation types.

SNR performance (solid black curves) for the D-STTD code ($n_T = n_R = 4$) utilizing QPSK modulation are compared for uncorrelated channels. In Fig. 4.42 the simulated BER vs. SNR performance (dashed red curves), the tight union bounds for the BER vs. SNR performance (solid blue curves) and the MDLB for the BER vs. SNR performance (solid black curves) for the D-STTD code ($n_T = n_R = 4$) utilizing QPSK modulation are compared for several spatial correlation types: 1D3 (o-marker) and 14D3 (+marker).

The lower bound for uncorrelated channels (Fig. 4.41) is quite tight compared to the results for correlated channels (Fig. 4.42).

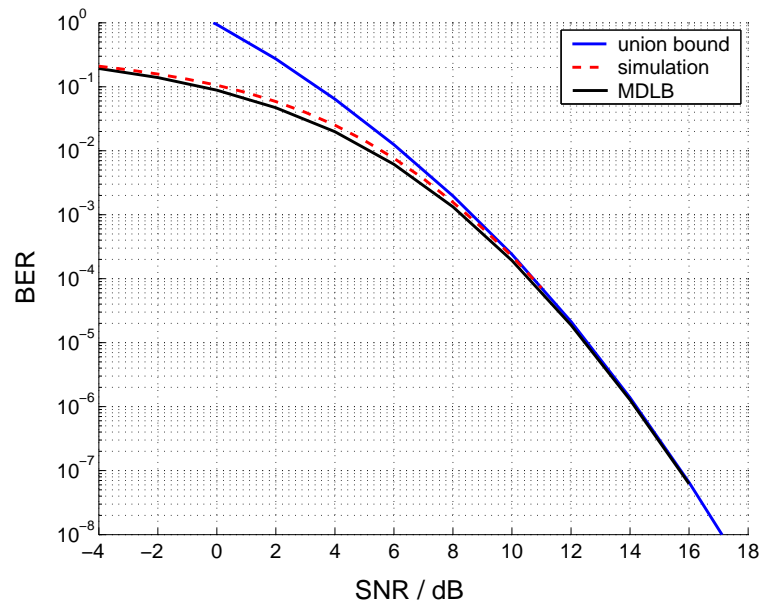


Figure 4.41: BER vs. SNR performance for the D-STTD code. QPSK modulation; $n_T = n_R = 4$, uncorrelated channels.

For the correlated scenarios the MDLB becomes tight for BER values below 10^{-8} . In the low SNR domain the lower bound is tighter than the union bound, but for BER values below 10^{-3} the union bound coincides with the simulated performance.

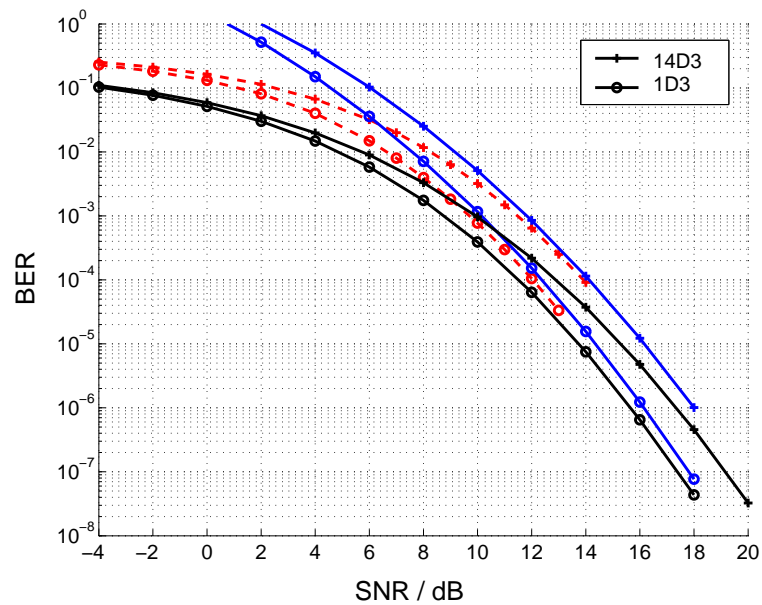


Figure 4.42: BER vs. SNR performance for the D-STTD code. QPSK modulation; $n_T = n_R = 4$; several correlation types.

Summarizing the results shown in this section, we can say that the MDLB is an extraordinary tight performance approximation for spatially uncorrelated channels. In case of correlated fading, the MDLB is in some cases very loose. The first reason for the looseness of this bound is that the calculated distance PDFs are no longer exact and the second reason is that for correlated channels not only the minimum

distance is of importance but also other crossover events should be considered. Due to the large number of similar ETs and thus similar distances, not only the minimum distance is of essential importance, but also distances that are not far away from the minimum distance contribute to the mean BER. Thus, for correlated scenarios the union bound is better suited to approximate the BER performance of STBCs. In spite of these deficiencies of the MDLB it is still a lower bound and together with the union bound it provides a bounding of the BER performance from below and from above.

Chapter 5

Summary and Conclusions

At last I want to summarize the main results and conclusions of this thesis. The main scope of this thesis was to find appropriate and tight performance measures for data transmission over MIMO systems that can be given in closed form. The motivation for this work was to avoid time consuming data transmission simulations and to get more insight into the error mechanism. The derived performance measures are calculated for frequency flat MIMO channels using ML receivers, where spatially uncorrelated and spatially correlated channels have been investigated. The so-called Weichselberger Model is used to simulate spatially correlated MIMO channels. The parameters for this model are extracted from actual MIMO channel measurement data.

In chapter 3, we start with the distance properties of uncoded MIMO systems. The essential difference between MIMO and SISO systems are elaborated: The signal distances in SISO systems behave “good-natured” in contrast to distances observed at the receiver of MIMO systems. For **SISO** systems we can summarize:

-) The smallest (largest) distance of signal pairs at the transmitter transforms to the smallest (largest) distance at the receiver.
-) The distance of a signal pair at the receiver is zero only, if either the distance of the signal pair at the transmitter is zero or the channel gain is zero, that is $|h|^2 = 0$.

These properties are essential in calculating the error performance of a SISO system. One very good and simple-to-calculate BER performance approximation is the so-called nearest neighbor approximation, which cannot be applied in a straightforward way to MIMO systems. In contrast, MIMO systems show a much more involved distance behavior. For **MIMO** systems the following properties hold:

-) The transmit signal constellation may be heavily distorted, due to the matrix multiplication of the transmit signal vector with the channel matrix **H**.
-) The largest distance at the transmitter may be transformed into the smallest distance at the receiver.
-) The distance at the receiver can be zero, even if every channel coefficient is far away from zero.

The most common possible approach to approximate the BER performance is a union bound. A union bound is simply the sum over all Pairwise Error Probabilities (PEPs). In the course of deriving this union bound, I discovered that the performance of a MIMO-system can fully and more easily be described by so-called Error Types (ETs). An ET is essentially the set of all crossover events that have the same key-parameters. The key-parameters depend on the case which channel correlation type is considered, i.e., whether the MIMO-channel is spatially uncorrelated or spatially correlated. This union bound is compared with simulation results for several uncoded MIMO systems, i.e., for different modulation schemes, different number of transmit and receive antennas and different correlation types. It turns out

that the union bound is tight for BER values of 10^{-3} and below. In the low SNR range, the overestimation of the BER by the union bound can be quite substantial.

In order to compare the results of different MIMO-systems or different correlation types it is helpful to find a high-SNR approximation, which specifies the position and the slope of the BER vs. SNR curve for infinitely high SNR. In this way the error performance of a system can be specified by two numbers, the system diversity and the coding advantage. Comparing error performance curves for different correlation types, this concept allows to specify a diversity loss and a power loss due to spatial correlation. Interestingly, the high SNR approximation for uncorrelated and correlated channels, according to the parameters extracted from measurement data, show that no diversity loss occurs due to spatial correlation. The influence of spatial correlation only shows up in a power loss, which can be quantified with the aid of the high SNR approximation.

Furthermore, a new precoding filter that minimizes the power loss is derived. This filter can be found analytically by Lagrange multiplier techniques, but due to the involved cost function, this optimization problem is solved numerically. The derived optimum precoding filter is tested in simulations. The surprising result of this investigation is that the performance of the precoded system in correlated fading is even better than the performance of the standard system (without precoding) in **uncorrelated** MIMO channels in the low SNR regime. For high SNR values the system without precoding operating in uncorrelated fading is only slightly better than the precoded transmission performed over spatially correlated channels.

The second main part of this thesis is the performance analysis of space-time block coded systems, described in Chapter 4. Starting with the investigation of the signal distances, I have found out that in MIMO systems multiple errors can dominate the BER performance! I call this specialty of MIMO systems "**The MIMO-Paradoxon**". This fact is in sharp contrast to block coded SISO systems, where only single symbol errors dominate the performance. This MIMO paradoxon can be confirmed by looking at the results of the union bound, where for some codes the ETs corresponding to multiple errors cause a flattening out of the BER vs. SNR curve (e.g.: Cyclic Code, Extended Alamouti Code).

The tightness of the derived union bound is checked again by comparing it with simulation results. The union bound is tight for BER values of 10^{-3} and below for all investigated codes and correlation types. Our results show, that for some codes a flattening out of the BER vs. SNR curve occurs at high SNR. This effect comes from rank deficient ETs corresponding to multiple errors. In most cases these rank deficiencies occur quite seldom and thus the flattening out can only be observed at very low BER values, so that it is practically not very relevant. In correlated fading it has been observed that the BER vs. SNR curves show this flattening out at quite low to medium SNR values.

A high SNR approximation of the union bound is derived that allows to specify the diversity order and the power loss of a system. As for uncoded systems, the analysis of the code performance, especially the high SNR approximation, shows that no diversity loss due to spatial correlation of the MIMO channels is observed, even though realistic parameters for the correlation model (extracted from measurement data) are used.

Next, an optimal precoder adapted to the spatially correlated channel is derived. Unfortunately, the optimization problem here is very complex and thus the optimization is solved numerically. Unfortunately, the numerical solution is not easy either, mainly because of the large number of local minima. Including the precoding filter in the coded data transmission simulations, some performance improvement can be achieved, but it is by far not that large as in the uncoded case.

The last main point discussed in this thesis is the so-called Minimum Distance Lower Bound (MDLB), where only that Error Type (ET) is considered that suffers from the minimum distance out of all possible distances. This bounding principle is easy to understand and the results are very tight (tighter than the union bound), but the calculation complexity is very high. Therefore, sometimes a so-called hybrid

method is used to perform the nasty analytical calculations numerically. In the derivation of the MDLB the entire set of STBCs is subdivided into two sets. For Code Set (CS) 1 (cyclic code, Extended Alamouti code, orthogonal codes) an exact calculation of the distances and thus an extraordinary tight BER performance approximation is achieved. For codes not belonging to CS1 (CS2) the resulting approximations are not that tight. It is also possible to calculate the MDLB for correlated channels, but the results show that, for this case, the MDLB is very loose for some codes and therefore the union bound is better suited to characterize the BER performance of a MIMO-system than the MDLB (the union bound is tighter and is easier to calculate). However, together with the union bound the MDLB allows a two-sided bounding of the BER performance from above and from below, which may be valuable in certain applications.

For practical applications we can say that in order to obtain a BER-performance characteristic of a MIMO-system without performing time consuming data transmission simulations, the union bound is the more appropriate means than the MDLB. This suggestion is based on the fact that the union bound is a lot easier to calculate and nevertheless it is quite tight.

Appendix A

Notation

H	a boldface capital letter denotes a matrix
n	a boldface lower case letter denotes a vector
$\mathcal{N}_C^{r \times s}(\mu, \sigma^2)$	matrix with independent identically distributed complex Gaussian entries with mean μ and variance σ^2 consisting of r rows and s columns
$(\cdot)^T$	transpose operator
$(\cdot)^H$	complex conjugate transpose operator (Hermitian operator)
$(\cdot)^*$	complex conjugate operator
$\text{tr}(\cdot)$	trace operator applicable on matrices
$\det(\cdot)$	determinant operator applicable on matrices
$\mathbf{E}_{\mathbf{H}}\{\cdot\}$	expectation with respect to H
$\ \cdot\ _F$	Frobenius norm operator
$ \cdot _2$	l2-norm operator
\mathcal{A}	symbol alphabet of the modulation format
$ \mathcal{A} $	size of the symbol alphabet
$\text{ld}(\cdot)$	base 2 logarithm
$\text{Re}\{\cdot\}$	real part operator
I	denotes an identity matrix
\otimes	Kronecker matrix product
\odot	element-wise matrix product
$[\cdot]_i$	i -th element of a vector
$\mathbf{Q}(\cdot)$	Gaussian Q-function
$\delta(\cdot)$	Dirac impulse
$\sigma(\cdot)$	Heaviside step function

Appendix B

Acronyms

BLAST	bell layered space time
UMTS	universal mobile telecommunication system
BS	base station
BER	bit error ratio
SNR	signal to noise ratio
MIMO	multiple input multiple output
SISO	single input single output
CLS	closed loop scheme
i.i.d.	independently identical distributed
ULA	uniform linear array
ML	maximum likelihood
ZF	zero forcing
MMSE	minimum mean square error
STC	space time coding
STTC(s)	space time trellis code(s)
STBC(s)	space time block code(s)
O-STBC(s)	orthogonal space time block code(s)
NO-STBC(s)	non-orthogonal space time block code(s)
STB	space time block
MDLB	minimum distance lower bound
ET	error type
EA	extended Alamouti
D-STTD	double space time transmit diversity
BPSK	binary phase shift keying
QPSK	quadrature phase shift keying
16QAM	16 quadrature amplitude modulation
RX	receive
TX	transmit
PDF	probability density function
NNA	nearest neighbor approximation
PEP	pairwise error probability
SEP	symbol error probability
CF	characteristic function

Appendix C

Important Variables

Ω	power coupling matrix
\mathbf{H}	channel matrix
\mathbf{H}_v	virtual channel matrix
n_T	number of transmit antennas
n_R	number of receive antennas
n_{OTS}	number of occupied time slots
n_{IS}	number of information symbols
σ_n^2	noise variance
\mathbf{b}	difference vector
\mathbf{B}	code word difference matrix
\mathbf{A}	code word distance matrix
r	rank of the distance matrix \mathbf{A}
d_T^2	squared distance at the transmitter
d_R^2	squared distance at the receiver
n_{BE}	number of bit errors
f_k	frequency of crossover events leading to the k -th error type
n_{ET}	number of error types
n_{NZ}	number of non zero eigenvalues
D	diversity order
L_D	diversity loss due to spatial correlation
L_P	power loss due to spatial correlation
\mathbf{S}	code word matrix
R_S	information symbol rate

Appendix D

Model Parameters

Here, the model parameters for the W-model of two measured MIMO channels with 4 transmit and 4 receive antennas are shown.

Scenario 1D3 (moderate correlation):

$$\begin{aligned}
 \mathbf{U}_R &= \begin{pmatrix} -0.1801 + j0.5078 & -0.6267 + j0.1581 & -0.1156 - j0.3503 & +0.3917 + j0.0495 \\ +0.5883 & -0.0400 - j0.0876 & +0.6734 & +0.4332 + j0.0589 \\ -0.1449 - j0.3855 & +0.0066 - j0.1041 & -0.3578 + j0.3938 & +0.7324 \\ -0.2784 + j0.3412 & +0.7498 & +0.0710 - j0.3497 & +0.3405 - j0.0252 \end{pmatrix} \\
 \mathbf{\Omega} &= \begin{pmatrix} 4.6077 & 3.1241 & 2.2073 & 0.5668 \\ 1.1409 & 1.0368 & 0.5792 & 0.1384 \\ 0.3107 & 0.2949 & 0.1678 & 0.0501 \\ 0.7222 & 0.6310 & 0.3523 & 0.0806 \end{pmatrix} \\
 \mathbf{U}_T &= \begin{pmatrix} +0.1658 - j0.1171 & +0.6186 & +0.6378 & -0.4089 - j0.0457i \\ +0.5037 - j0.1540 & +0.4797 + j0.1452 & -0.2410 - j0.2361 & +0.5980 \\ +0.6891 & -0.1513 - j0.1072 & -0.3965 + j0.0494 & -0.5733 + j0.0482 \\ +0.4483 + j0.0737 & -0.4204 - j0.3937 & +0.5316 + j0.1928 & +0.3645 - j0.0959 \end{pmatrix}
 \end{aligned} \tag{D.1}$$

Scenario 14D3 (strong correlation):

$$\begin{aligned}
 \mathbf{U}_R &= \begin{pmatrix} +0.0856 + j0.3895 & +0.7500 & -0.3496 - j0.3387 & -0.0303 + j0.2013 \\ +0.3635 + j0.3481 & +0.1558 - j0.2166 & +0.5582 & -0.3493 - j0.4919 \\ +0.5252 + j0.1216 & -0.1838 + j0.2130 & +0.1511 - j0.3523 & +0.6952 \\ +0.5449 & +0.0462 + j0.5338 & -0.1422 + j0.5332 & -0.2620 + j0.2068 \end{pmatrix} \\
 \mathbf{\Omega} &= \begin{pmatrix} 9.3684 & 1.5098 & 0.7868 & 0.3238 \\ 1.8690 & 0.3816 & 0.3365 & 0.0868 \\ 0.4698 & 0.2008 & 0.2451 & 0.0636 \\ 0.1341 & 0.0496 & 0.0630 & 0.0417 \end{pmatrix} \\
 \mathbf{U}_T &= \begin{pmatrix} +0.4399 - j0.1712 & +0.6255 & +0.5631 & +0.1218 - j0.2326 \\ -0.4977 + j0.0977 & -0.1957 - j0.3155 & +0.3838 + j0.2954 & +0.4979 - j0.3498 \\ +0.5180 & -0.3487 - j0.0714 & -0.1628 - j0.3559 & +0.6722 \\ -0.4935 - j0.0898 & +0.2282 + j0.5406 & +0.0996 - j0.5341 & +0.2973 + j0.1433 \end{pmatrix}
 \end{aligned} \tag{D.2}$$

Appendix E

Error Types for Uncoded MIMO Systems

In this section the Error Types (ETs) for a 4×4 MIMO system in spatially correlated fading with BPSK modulation are tabulated. For every correlation type the corresponding ET table is different. Tab. E.1 and Tab. E.2 correspond to scenario 1D3 and 14D3.

ET	$\lambda_1^{(k)}$	$\lambda_2^{(k)}$	$\lambda_3^{(k)}$	$\lambda_4^{(k)}$	n_{BEk}	f_k	d_{Wk}^2	d_{Tk}^2
0	0.000	0.000	0.000	0.000	0	16	0	0
1	11.0960	3.1376	0.8910	1.9300	1	16	2.7816	4
2	11.3431	2.8631	0.8042	1.7903	1	16	2.6150	4
3	10.0675	2.7693	0.7891	1.7109	1	16	2.4769	4
4	9.5168	2.8113	0.8096	1.7126	1	16	2.4679	4
5	31.9519	8.5297	2.3572	5.3349	2	8	7.6514	8
6	20.5239	5.1545	1.4568	3.2249	2	8	4.7216	8
7	31.9301	8.0789	2.2234	5.0772	2	8	7.3460	8
8	21.8655	5.8023	1.6475	3.5716	2	8	5.2271	8
9	19.3190	5.0258	1.4304	3.1275	2	8	4.5652	8
10	26.9198	7.9856	2.2468	4.9171	2	8	6.9809	8
11	12.9264	3.4716	1.0333	2.1059	2	8	3.1435	8
12	21.8032	6.6593	1.9034	4.0571	2	8	5.7866	8
13	19.3600	6.0955	1.7537	3.7137	2	8	5.2653	8
14	10.8913	3.1860	0.9632	1.9253	2	8	2.8323	8
15	22.4008	6.3230	1.7972	3.8785	2	8	5.6055	8
16	12.2489	3.1757	0.9505	1.9300	2	8	2.9064	8
17	51.8992	12.9931	3.5531	8.2057	3	4	11.8413	12
18	41.1804	10.5459	2.9303	6.6010	3	4	9.5736	12
19	38.6289	10.2241	2.8614	6.3600	3	4	9.2075	12
20	47.2414	12.6465	3.4977	7.9079	3	4	11.3379	12
21	34.1530	9.4398	2.6758	5.8088	3	4	8.4136	12
22	19.6495	5.7809	1.7126	3.5140	3	4	5.1133	12
23	37.4027	12.0221	3.4142	7.3343	3	4	10.3011	12
24	11.8349	3.0421	0.9689	1.8248	3	4	2.8246	12
25	25.2368	6.7849	1.9732	4.1230	3	4	6.1093	12
26	29.2844	9.0509	2.6043	5.5070	3	4	7.8521	12
27	32.1396	9.6051	2.7395	5.8860	3	4	8.3996	12
28	41.7568	12.1362	3.4033	7.4940	3	4	10.6624	12
29	25.2372	6.9191	2.0118	4.2051	3	4	6.1996	12
30	11.5317	2.9438	0.9413	1.7689	3	4	2.7419	12
31	21.4525	5.7074	1.6713	3.5149	3	4	5.1787	12
32	35.6524	9.1338	2.5683	5.6718	3	4	8.2990	12
33	68.4632	17.4141	4.7743	10.9653	4	2	15.8060	16
34	48.2116	14.1540	4.0032	8.7105	4	2	12.4200	16
35	31.4808	8.7604	2.5569	5.3354	4	2	7.8318	16
36	49.2800	15.6165	4.4337	9.5387	4	2	13.4316	16
37	34.0327	9.2163	2.6645	5.6585	4	2	8.2926	16
38	11.2226	2.9465	1.0001	1.7393	4	2	2.7539	16
39	39.1280	10.3482	2.9675	6.3324	4	2	9.3396	16
40	54.3687	14.1946	3.9510	8.8712	4	2	12.8245	16

Table E.1: ET table for a 4×4 MIMO system in correlated fading for BPSK modulation (scenario 1D3).

ET	$\lambda_1^{(k)}$	$\lambda_2^{(k)}$	$\lambda_3^{(k)}$	$\lambda_4^{(k)}$	n_{BEk}	f_k	d_{Wk}^2	d_{Tk}^2
0	0.000	0.000	0.000	0.000	0	16	0	0
1	12.5765	2.8414	1.0663	0.2959	1	16	1.8324	4
2	11.8874	2.5624	0.8710	0.2830	1	16	1.6553	4
3	11.6918	2.5782	0.9183	0.2862	1	16	1.6777	4
4	11.7996	2.7136	1.0613	0.2886	1	16	1.7696	4
5	5.4916	1.8279	1.2295	0.4120	2	8	1.5017	8
6	38.9203	8.0499	2.3444	0.7230	2	8	4.8005	8
7	5.1637	1.3438	0.8076	0.3557	2	8	1.1882	8
8	11.3435	3.1279	1.7102	0.4540	2	8	2.2910	8
9	37.7662	7.8275	2.3002	0.7105	2	8	4.6883	8
10	6.0771	2.0744	1.3932	0.4297	2	8	1.6575	8
11	43.4362	8.9797	2.6451	0.7456	2	8	5.2664	8
12	9.6163	2.7892	1.6249	0.4411	2	8	2.0939	8
13	37.4087	7.9822	2.5449	0.7149	2	8	4.8278	8
14	41.9947	8.9374	2.7710	0.7827	2	8	5.3415	8
15	9.6079	2.7246	1.5643	0.4327	2	8	2.0517	8
16	40.9057	8.5092	2.5659	0.7199	2	8	5.0355	8
17	13.4199	3.2397	1.5259	0.6257	3	4	2.5383	12
18	18.3378	4.6659	2.2414	0.7091	3	4	3.4149	12
19	20.2730	5.1190	2.4020	0.7360	3	4	3.6803	12
20	13.6282	3.3915	1.6505	0.6381	3	4	2.6414	12
21	22.0605	5.1307	2.2220	0.6774	3	4	3.6128	12
22	82.3476	16.6719	4.4917	1.3035	3	4	9.4687	12
23	17.0342	4.7126	2.5171	0.7150	3	4	3.4669	12
24	88.1955	17.9850	4.9049	1.3863	3	4	10.1909	12
25	28.1241	6.7147	2.9210	0.7649	3	4	4.5322	12
26	22.3009	5.8822	2.8779	0.7873	3	4	4.1521	12
27	20.9469	5.5726	2.7698	0.7708	3	4	3.9732	12
28	16.2446	4.4173	2.3402	0.6922	3	4	3.2835	12
29	25.7976	6.2931	2.8552	0.7444	3	4	4.3099	12
30	85.2878	17.4199	4.7866	1.3553	3	4	9.9083	12
31	81.1668	16.4082	4.4094	1.2871	3	4	9.3241	12
32	20.2984	4.7234	2.0872	0.6505	3	4	3.3778	12
33	8.8518	2.8602	1.9514	0.7776	4	2	2.4896	16
34	43.5575	9.6055	3.4822	1.0902	4	2	6.3130	16
35	55.4691	12.5026	4.5945	1.2604	4	2	7.9607	16
36	14.2856	4.9445	3.2941	0.9058	4	2	3.8102	16
37	51.2074	11.6279	4.3681	1.2130	4	2	7.4946	16
38	144.5212	28.8946	7.3379	2.0893	4	2	15.9067	16
39	24.1627	6.0832	3.0843	0.8418	4	2	4.4199	16
40	41.5872	9.0465	3.2229	1.0509	4	2	5.9746	16

Table E.2: ET table for a 4×4 MIMO system in correlated fading for BPSK modulation (scenario 14D3).

Appendix F

Error Types for the Cyclic STBC

In this section, I show the ETs and the corresponding key-parameters for the cyclic code utilizing a 4×4 MIMO system and BPSK modulation in spatially correlated fading. For each correlation type the ET table is different. Tab. C.1 and Tab. C.2 correspond to the scenario 1D3 and 14D3.

ET	$\lambda_{\mathbf{z}_k}^{(1)}$	$\lambda_{\mathbf{z}_k}^{(2)}$	$\lambda_{\mathbf{z}_k}^{(3)}$	$\lambda_{\mathbf{z}_k}^{(4)}$	$\lambda_{\mathbf{z}_k}^{(5)}$	$\lambda_{\mathbf{z}_k}^{(6)}$	$\lambda_{\mathbf{z}_k}^{(7)}$	$\lambda_{\mathbf{z}_k}^{(8)}$	$\lambda_{\mathbf{z}_k}^{(9)}$	$\lambda_{\mathbf{z}_k}^{(10)}$	$\lambda_{\mathbf{z}_k}^{(11)}$	$\lambda_{\mathbf{z}_k}^{(12)}$	$\lambda_{\mathbf{z}_k}^{(13)}$	$\lambda_{\mathbf{z}_k}^{(14)}$	$\lambda_{\mathbf{z}_k}^{(15)}$	$\lambda_{\mathbf{z}_k}^{(16)}$	$n_{BE\ k}$	f_k	$d_{W\ k}^2$	$d_{T\ k}^2$
0	0.000	0.000	0.000	0.000	0.000	0.000	0.000	0.000	0.000	0.000	0.000	0.000	0.000	0.000	0.000	0.000	0	16	0	0
1	18.431	12.496	8.829	4.563	4.147	2.888	2.523	2.317	2.267	1.409	1.242	1.179	0.671	0.553	0.322	0.200	1	64	2.01	4.00
2	69.941	24.676	18.048	17.638	11.123	8.020	4.895	4.826	4.737	2.882	2.276	1.371	0.000	0.000	0.000	0.000	2	32	7.78	10.08
3	27.901	18.834	8.851	8.690	5.409	4.950	3.024	2.512	2.126	1.424	1.240	0.763	0.000	0.000	0.000	0.000	2	32	4.12	10.08
4	68.513	17.434	11.172	10.977	4.780	2.925	1.727	0.994	0.000	0.000	0.000	0.000	0.000	0.000	0.000	0.000	2	16	6.58	16.00
5	50.853	37.554	16.081	9.883	9.833	6.037	4.558	2.843	0.000	0.000	0.000	0.000	0.000	0.000	0.000	0.000	2	16	11.12	16.00
6	64.482	47.604	20.262	15.998	12.552	12.395	7.685	5.738	4.157	3.598	2.599	2.346	1.150	0.573	0.334	0.207	3	32	4.50	8.94
7	154.602	39.271	24.734	12.954	10.763	9.121	4.188	2.558	2.395	2.271	1.458	1.186	0.692	0.554	0.322	0.200	3	16	3.49	6.93
8	28.415	18.015	9.553	8.484	8.014	4.803	4.539	2.865	2.683	2.541	2.237	1.602	1.350	1.239	0.852	0.660	3	16	3.49	6.93
9	73.723	49.985	35.316	18.254	16.589	11.554	10.095	9.268	9.068	5.636	4.971	4.718	2.684	2.213	1.289	0.801	4	8	8.05	64.00
10	101.707	75.108	32.162	19.766	19.666	12.075	9.116	5.686	0.000	0.000	0.000	0.000	0.000	0.000	0.000	0.000	4	4	22.24	32.00
11	273.852	69.656	43.861	19.097	0.000	0.000	0.000	0.000	0.000	0.000	0.000	0.000	0.000	0.000	0.000	0.000	4	2	63.22	64.00
12	44.890	11.786	6.957	4.000	0.000	0.000	0.000	0.000	0.000	0.000	0.000	0.000	0.000	0.000	0.000	0.000	4	2	11.02	16.00

Table F.1: ET table for a 4×4 MIMO system utilizing the cyclic code defined in Eqn. (4.9) in correlated fading for BPSK modulation (scenario 1D3).

ET	$\lambda_{\mathbf{z}_k}^{(1)}$	$\lambda_{\mathbf{z}_k}^{(2)}$	$\lambda_{\mathbf{z}_k}^{(3)}$	$\lambda_{\mathbf{z}_k}^{(4)}$	$\lambda_{\mathbf{z}_k}^{(5)}$	$\lambda_{\mathbf{z}_k}^{(6)}$	$\lambda_{\mathbf{z}_k}^{(7)}$	$\lambda_{\mathbf{z}_k}^{(8)}$	$\lambda_{\mathbf{z}_k}^{(9)}$	$\lambda_{\mathbf{z}_k}^{(10)}$	$\lambda_{\mathbf{z}_k}^{(11)}$	$\lambda_{\mathbf{z}_k}^{(12)}$	$\lambda_{\mathbf{z}_k}^{(13)}$	$\lambda_{\mathbf{z}_k}^{(14)}$	$\lambda_{\mathbf{z}_k}^{(15)}$	$\lambda_{\mathbf{z}_k}^{(16)}$	$n_{BE\ k}$	f_k	$d_{W\ k}^2$	$d_{T\ k}^2$
0	0.000	0.000	0.000	0.000	0.000	0.000	0.000	0.000	0.000	0.000	0.000	0.000	0.000	0.000	0.000	0.000	0	16	0	0
1	37.473	7.476	6.039	3.147	1.879	1.526	1.345	1.295	0.980	0.803	0.536	0.347	0.254	0.252	0.198	0.166	1	64	1.14	4.00
2	15.860	8.594	4.238	3.620	3.128	2.710	1.693	1.007	0.813	0.736	0.432	0.405	0.000	0.000	0.000	0.000	2	32	1.96	10.08
3	146.535	29.261	12.010	7.390	5.199	3.065	2.107	2.081	1.686	1.450	0.456	0.399	0.000	0.000	0.000	0.000	2	32	3.89	10.08
4	145.390	29.050	7.982	7.360	2.704	2.097	1.929	0.769	0.000	0.000	0.000	0.000	0.000	0.000	0.000	0.000	2	16	6.17	16.00
5	27.694	10.753	6.766	4.261	3.426	2.951	0.914	0.833	0.000	0.000	0.000	0.000	0.000	0.000	0.000	0.000	2	16	4.00	16.00
6	48.413	23.445	12.979	10.349	6.092	4.844	4.337	3.889	1.749	1.565	1.150	1.076	0.489	0.436	0.318	0.184	3	32	2.55	8.94
7	326.327	65.217	16.536	6.214	4.709	3.160	1.569	1.350	1.295	0.983	0.819	0.347	0.254	0.252	0.202	0.166	3	16	1.98	6.93
8	40.984	16.923	8.789	5.621	5.454	4.681	2.129	1.839	1.764	1.507	0.818	0.663	0.528	0.480	0.220	0.196	3	16	1.98	6.93
9	35.407	11.440	7.805	3.110	0.000	0.000	0.000	0.000	0.000	0.000	0.000	0.000	0.000	0.000	0.000	0.000	4	2	9.96	64.00
10	55.389	21.507	13.533	8.522	6.853	5.903	1.828	1.666	0.000	0.000	0.000	0.000	0.000	0.000	0.000	0.000	4	4	8.01	32.00
11	578.084	115.578	29.351	8.357	0.000	0.000	0.000	0.000	0.000	0.000	0.000	0.000	0.000	0.000	0.000	0.000	4	2	63.63	64.00
12	149.894	29.904	24.156	12.589	7.516	6.106	5.383	5.180	3.922	3.212	2.145	1.388	1.017	1.008	0.794	0.666	4	8	4.56	16.00

Table F.2: ET table for a 4×4 MIMO system utilizing the cyclic code defined in Eqn. (4.9) in correlated fading for BPSK modulation (scenario 14D3).

Bibliography

- [1] G.J.Foschini, M.J.Gans, "On Limits of Wireless Communications in Fading Environments when Using Multiple Antennas", *Wireless Personal Communications* 1998, vol.6, pp. 311-335.
- [2] I.E.Telatar, "Capacity of Multi-Antenna Gaussian Channels", AT&T Bell Labs, <http://mars.belllabs.com/cm/ms/what/mars/papers/proof>, 1995.
- [3] S.Verdú, "Multiuser Detection", Cambridge University Press, New York, 1998.
- [4] G.J.Foschini, "Layered space-time architecture for wireless communications in a fading environment when using multi-element antennas", *Bell Labs Tech. J.*, vol. 1, no. 2, pp. 41-59, 1996.
- [5] Z.Chen, J.Yuan, B.Vucetic, "An improved space time trellis coded modulation scheme on slow Rayleigh fading channels", *ICC 2001*, vol.4, pp.1110-1116, 2001.
- [6] Z.Chen, B.Vucetic, J.Yuan, K.L.Lo, "Space-time trellis codes with two three and four transmit antennas in quasi-static flat channels", *ICC 2002*, vol.3, pp. 1589-1595, 2002.
- [7] M.Rupp, H.Weinrichter, G.Gritsch, "Approximate ML Detection for MIMO Systems with Very Low Complexity", *ICASSP'04*, Montreal, Canada, pp. 809-812, May 2004.
- [8] H.Artés, D.Seethaler, F.Hlawatsch, "Efficient Detection Algorithms for MIMO Channels: A geometrical Approach to Approximate ML Detection", *IEEE Transactions on Signal Processing*, Special Issue on MIMO communications Systems, vol. 51, no. 11, pp. 2808-2820, Nov. 2003.
- [9] U.Fincke, M.Phost, "Improved methods for calculating vectors of short length in a lattice, including a complexity analysis", *Math. of Comp.*, vol. 44, pp. 463-471, April 1985.
- [10] J.H.Winters, J.Salz, R.D.Gitlin, "The impact of antenna diversity on the capacity of wireless communication systems", *IEEE Transactions on Communications*, vol. 42, pp. 1740-1750, Feb. 1994.
- [11] W.Weichselberger, "Spatial Structure of Multiple Antenna Radio Channels - A Signal Processor Viewpoint", Ph.D. Thesis, Vienna University of Technology, December 2003.
- [12] M.Herdin, "Non-Stationary Indoor MIMO Radio Channels", Ph.D. Thesis, Vienna University of Technology, August 2004.
- [13] H.Özcelik, "Indoor MIMO Channel Models", Ph.D. Thesis, Vienna University of Technology, October 2004.
- [14] Kai Yu, M.Bengtsson, B.Ottersten, D.McNamara, P.Karlsson, M.Beach, "Second Order Statistics of NLOS Indoor MIMO Channels Based on 5.2 GHz Measurements", *Globecom 2001*, San Antonio, Texas, Vol. 1, pp. 156-160, November 2001.

- [15] Da-Shan Shiu, G.J.Foschini, M.J.Gans, J.M.Kahn, "Fading Correlation and Its Effect on the Capacity of Multielement Antenna Systems", *IEEE Transactions on Communications*, Vol. 48, No. 3, pp. 502-513, March 2000.
- [16] Chen-Nee Chuah, J.M.Kahn, D.Tse, "Capacity of Multi-Antenna Array Systems in Indoor Wireless Environment", *Globecom*, Sydney, Australia, Vol. 4, pp. 1894-1899, 1998.
- [17] D.Chizhik, F.Rashid-Farrokhi, J.Ling, A.Lozano, "Effect of Antenna Separation on the Capacity of BLAST in Correlated Channels", *IEEE Communications Letters*, Vol. 4, No. 11, pp. 337-339, Nov.2000.
- [18] A.Hottinen, O.Tirkkonen, R.Wichman, "Multi-Antenna Transceiver Techniques for 3G and Beyond", John Wiley & Sons, Chichester, England, 2003.
- [19] J.P.Kermoal, L.Schumacher, K.I.Pedersen, P.E.Mogensen, F.Frederiksen, "A Stochastic MIMO Radio Channel Model With Experimental Validation", *IEEE Journal on Selected Areas in Communications*, Vol. 20, No. 6, pp. 1211-1226, August 2002.
- [20] J.Fuhl, A.F.Molisch, E.Bonek, "Unified Channel Model for Mobile Radio Systems with Smart Antennas", *IEE Proceedings Pt.F.(Radar, Sonar and Navigation)*, Vol. 145, No. 1, pp. 32-41, Feb. 1998.
- [21] H.Özcelik, M.Herdin, W.Weichselberger, J.Wallace, E.Bonek, "Deficiencies of the Kronecker MIMO radio channel model", *Electronics Letters*, vol.39, pp.1209-1210, 2003.
- [22] B.Badic, M.Rupp, H.Weinrichter, "Adaptive Channel Dependent Extended Alamouti Space Time Code using minimum Feedback", *CIC*, Seoul, Korea, Oct. 2003.
- [23] B.Badic, M.Rupp, H.Weinrichter, "Quasi-Orthogonal Space-Time Block Codes for Data Transmission over Four and Eight Transmit Antennas with Very Low Feedback Rate", *5.th ITG Conference on Source and Channel Coding*, Erlangen, Deutschland, pp.157-164, Jan. 2004.
- [24] H.Özcelik, M.Herdin, R.Prestros, E.Bonek, "How MIMO capacity is linked with single element fading statistics", *International Conference on Electromagnetics in Advanced Applications*, Torino, Italy, pp. 775-778, 8. - 12. Sept. 2003.
- [25] G.Gritsch, H.Weinrichter, "Adaptive Subspace Modulation in Spatially Correlated MIMO Systems", *PIMRC*, vol. 4, pp. 1772-1776, Sep. 2002.
- [26] G.Gritsch, H.Weinrichter, M.Rupp, "Two Adaptive Space-Time Block Coded MIMO Systems Exploiting Partial Channel Knowledge at the Transmitter", *5.th ITG Conference on Source and Channel Coding*, Erlangen, Deutschland, pp. 31-38, Jan. 2004.
- [27] John G. Proakis, "Digital Communications", 3rd ed. McGraw-Hill, Inc. 1995.
- [28] W.Weichselberger, M.Herdin, H.Özcelik, E.Bonek, "A Novel Stochastic MIMO Channel Model and its Physical Interpretation", *International Symposium on Wireless Personal Multimedia Communications*, Yokosuka, Japan, 19. - 22. Oktober 2003.
- [29] V.Tarokh, N.Seshadri, A.R.Calderbank, "Space-time codes for high data rate wireless communication: Performance criterion and code construction", *IEEE Trans. Inform. Theory*, vol. 44, no. 2, pp. 744-765, March 1998.
- [30] M.T.Ivrlac, T.P.Kurpjuhn, C.Brunner, W.Utschick, "Efficient use of fading correlation in MIMO systems", *54th VTC*, Atlantic City, USA, vol. 4, pp. 2763-2767, 2001

- [31] M.Herdin, G.Gritsch, B.Badic, E.Bonek, "The influence of channel models on simulated MIMO performance", VTC'04, Milan, Italy, May 2004.
- [32] M.Kiessling, J.Speidel, N.Geng, M.Reinhardt, "Performance Analysis of MIMO Maximum Likelihood Receivers with Channel Correlation, Colored Gaussian Noise, and Linear Prefiltering", ICC 2003, vol.5, pp. 3026-3030.
- [33] X.Zhu, R.D.Murch, "Performance Analysis of Maximum Likelihood Detection in a MIMO Antenna System", IEEE Transactions on Communications, vol. 50, No. 2, pp. 187-191, Feb. 2002.
- [34] G.Gritsch, H.Weinrichter, M.Rupp, "Understanding the BER-Performance of Space-Time Block Codes", SPAWC, Rome, June 2003.
- [35] G.Gritsch, H.Weinrichter, M.Rupp, "A Union Bound of the Bit Error Ratio for Data Transmission over Correlated Wireless MIMO Channels", ICASSP'04, Montreal, Canada, pp. 405-408, May 2004.
- [36] Hsiao-feng Lu, Y.Wang, P.V.Kumar, K.M.Chuggi, "On the Performance of Space-Time Codes", Information Theory Workshop 2002, Bangalore, India, pp. 49-52, October 2002
- [37] A.Papoulis, "Probabilities, Random Variables and Stochastic Processes", McGraw-Hill, 2.Ed., 1984.
- [38] B.Hassibi, B.M.Hochwald, "How much training is needed in multiple-antenna wireless links?", IEEE Transactions on Information Theory, vol. 49, No. 4, pp. 951-963, April 2003.
- [39] M.Dong, L.Tong, "Optimal design and placement of pilot symbols for channel estimation", IEEE Transactions on Acoustics, Speech, and Signal Processing, vol. 50, No. 12, pp. 3055-3069, Dec. 2002.
- [40] D.Schafhuber, G.Matz, F.Hlawatsch, "Adaptive Wiener Filters for Time-Varying Channel Estimation in Wireless OFDM Systems", ICASSP, vol. 4, pp. 688-691, April 2003.
- [41] D.Schafhuber, M.Rupp, G.Matz, F.Hlawatsch, "Adaptive Identification and Tracking of Doubly Selective Fading Channels for Wireless MIMO-OFDM Systems", SPAWC, Rome, June 2003.
- [42] M.R.Spiegel, "Theory and Problems of Probability and Statistics", McGraw-Hill, New York, 1992.
- [43] T.K.Moon, "Mathematical Methods and Algorithms for Signal Processing", Prentice Hall, New Jersey, 2000.
- [44] M.Kiessling, J.Speidel, I.Viering, M.Reinhardt, "Statistical Prefiltering for MMSE and ML Receivers with Correlated MIMO Channels", WCNC, vol.2, pp. 919-924.March 2003
- [45] Texas Instruments, "Double-STTD scheme for HSDPA systems with four transmit antennas: Link Level Simulation Results", Temporary document 21(01)-0701, Release 5 Ad hoc, 3GPP TSG RAN WG1, June 2001.
- [46] M.Rupp, C.F.Mecklenbräuker, "On Extended Alamouti Schemes for Space-Time Coding", WPMC, Honolulu, pp. 115-118, Oct. 2002.
- [47] T.H.Liew, L.Hanzo, "Space-Time Codes and Concatenated Channel Codes for Wireless Communications", Proceeding of the IEEE, vol.90, no.2, pp. 187-219, 2002.
- [48] S.Vishwanath, W.Yu, R.Negi,A.Goldsmith, "Space-time turbo codes: decorrelation properties and performance analysis for fading channels", GLOBECOM, vol.2, pp. 1016-1020, Nov. 2000.

-
- [49] S.Alamouti, "A Simple Transmitter Diversity Technique for wireless communications", *IEEE Journal on Selected Areas of Communications, Special Issue on Signal Processing for Wireless Communications*, vol.16, No.8, pp.1451-1458, 1998.
- [50] R.Zurmühl, "Matrizen", Springer-Verlag, Berlin, Deutschland, 2.Auflage, 1958.
- [51] V.Tarokh, N.Seshadri, A.R.Calderbank, "Space-time codes for high data rate wireless communication: Performance criterion and code construction", *IEEE Trans. Inform. Theory*, vol. 44, no. 2, pp. 744-765, March 1998.
- [52] O.Tirkkonen, A.Hottinen, "Complex Space-Time Block Codes for four TX antennas", *Globecom 2000*, vol. 2, pp. 1005-1009, Dec. 2000.
- [53] Z.Wang, G.B.Giannakis, "A Simple and General Parameterization Quantifying Performance in Fading Channels", *IEEE Transactions on Communications*, vol. 51, no.8, pp. 1389-1398, Aug. 2003.
- [54] G.Gritsch, H.Weinrichter, M.Rupp, "A Tight Lower Bound for the Bit Error Ratio of Space-Time Block Codes", *VTC'04, Milan, Italy*, May 2004.
- [55] H.Sampath, A.Paulraj, "Linear Precoding for Space-Time Coded Systems with known Fading Correlation", *Communications Letters*, vol. 6, no. 6, pp. 239-241, June 2002.
- [56] B.Vucetic, J.Yuan, "Space-Time Coding", John Wiley & Sons, England, 2003.
- [57] E.G.Larsson, P.Stoica, "Space-Time Block Coding for Wireless Communications", Cambridge University Press, Cambridge UK, 2003.
- [58] A.Paulraj, R.Nabar, D.Gore, "Introduction to Space-Time Wireless Communication", Cambridge University Press, Cambridge UK, 2003.